

Binding-induced DNA assembly for detection of proteins and nucleic acids

by

Yanwen Lin

A thesis submitted in partial fulfillment of the requirements for the degree of

Doctor of Philosophy

Department of Chemistry
University of Alberta

© Yanwen Lin, 2018

ABSTRACT

The major research goal of my thesis is to design and develop the binding-induced assembly for the detection of specific proteins and nucleic acid sequences. My research builds on fundamentals of DNA chemistry and incorporates the recent advances in nanotechnology and signal amplification.

I have studied the formation of binding-induced DNA three-way junctions (TWJs). By combining a TWJ with DNA strand displacement, I have developed a fluorescence turn-on assay and applied this assay to the detection of prostate specific antigen (PSA) and human α -thrombin.

I used the binding-induced DNA TWJ to construct a molecular translator that converted the input target information into a pre-designed output DNA. The output DNA was hybridized to the oligonucleotides that functionalized on gold nanoparticles (AuNPs), each AuNP consisting of approximately 10^5 Au atoms. Detection of Au in the AuNPs using inductively coupled plasma mass spectrometry (ICP-MS) provided amplified and quantitative detection of the target molecules, such as human α -thrombin, microRNA 10b and microRNA 128.

I further developed a binding-induced molecular amplifier (BIMA) technique, achieving improved sensitivity. AuNPs were used as the scaffold to conjugate multiple oligonucleotide sequences. Binding of a single target molecule to two affinity probes, one conjugated on the AuNPs and the other free in solution, induced the formation of a DNA structure with a recognizable nicking site. A nicking endonuclease enzyme cleaved off multiple DNA barcode molecules from each AuNP. The output DNA barcodes subsequently triggered the toehold-mediated strand displacement reactions that turned on fluorescence of

molecular beacons. Detection of the amplified fluorescence signals enabled highly sensitive detection of the target molecules, including specific DNA sequences, PSA, platelet-derived growth factor (PDGF-BB), and the interaction between PDGF and its receptor β .

The binding-induced DNA nanotechnologies described in this thesis have shown feasibility for the detection of several target proteins and nucleic acids. They have the promising potential for the detection of various biomolecules and applications to disease diagnostics.

PREFACE

This thesis is original work by Yanwen Lin. A portion of Chapter 1 has been published as Deng, B.; Lin, Y.; Wang, C.; Li, F.; Wang, Z.; Zhang, H.; Li, X.-F.; Le, X. C. “Aptamer Binding Assays for Proteins: The Thrombin Example--A Review.” *Analytica Chimica Acta* **2014**, 837, 1-15. I was responsible for the manuscript composition and figures. Deng, B., Wang, C., Li, F., Wang, Z., Zhang, H., Li, X.-F., Le, X. C. were involved with the manuscript composition and editing.

Chapter 2 has been published as Li, F.; Lin, Y.; Le, X. C., “Binding-Induced Formation of DNA Three-Way Junctions and Its Application to Protein Detection and DNA Strand Displacement.” *Analytical Chemistry* **2013**, 85 (22), 10835-10841. I was responsible for the data collection and analysis as well as the manuscript editing. F. Li contributed to the data collection and analysis, manuscript composition, and concept formation. X. C. Le, the supervisory and corresponding author, was involved with concept formation and manuscript composition.

Chapter 4 has been published as Li, F.; Lin, Y.; Lau, A.; Tang, Y.; Chen, J.; Le, X. C., “Binding-Induced Molecular Amplifier as a Universal Detection Platform for Biomolecules and Biomolecular Interaction.” *Analytical Chemistry* **2018**, 90 (14), 8651-8657. I was responsible for the data collection and analysis as well as the manuscript editing. F. Li contributed to the data collection and analysis, manuscript composition, and concept formation. Lau, A., Tang, Y., Chen, J. aided with manuscript editing. X. C. Le, the supervisory and corresponding author, was involved with concept formation and manuscript composition.

Acknowledgments

First, I would like to thank my supervisor, Dr. X. Chris Le, for all his great support not only in the lab but also in my life. Chris knows what is best for his students, he gave me a lot of freedom and opportunities to design my own projects, and when I came into trouble, he was always there to provide guidance. He taught me how to stay curious and creative even when there are many difficulties. When faced with seemingly impossible problems, he taught me to stay calm, be patient, and tackle it step-by-step. I learned through Chris that there is no shortcut to success, but if you work hard enough, your efforts will pay off. It is my pleasure to have a supervisor like him. I would like to thank Dr. Xing-Fang Li as well, for her caring about my professional and personal life.

I would also like to thank to my supervisory committee, Dr. Hongquan Zhang and Julianne Gibbs, as well as my examining committee, Dr. Daniel Figeys, Dr. Yunjie Xu and Dr. Andrei Drabovich, for giving me so many insightful suggestions and comments.

I also appreciate the support from Katerina Carastathis, Dianne Sergy and Anita Weiler, you helped much in organization and logistics during my stressful graduate school life. Thank you to Dr. Anna Jordan for being exceptionally patient and continuing to encourage me.

Thank you to all the dear friends I made during the PhD program. Wenwen, Aleks, Rebecca and Mike, as well as everyone in AET. A special thanks to Feng, Zhixin, and Xiufen, who patiently guided me when I first came to the lab. Thank you so much for your company, I could not have finished the whole PhD program alone and will always miss you.

A great thanks to my mom and dad, they have given me almost everything that parents could offer to their child, I would never have achieved this without them; thanks to my sister

Ranran, whom I love from the bottom of my heart. This is also for my aisuru aikata beloved bee, for the bright blue burning scorpion fire, for the wonderful summer miracle happened to me seven years ago, for seasons and oceans in the southern hemisphere, for Na and Au, for my only magician, for those people who shared their passion and love with me, for the shining gleam of my misspent youth and all the joy and pain we go through together, and for my dearest, bittersweet fatal uncertainty: you can, I can.

Finally, a special thanks to Luis Cernuda, my favorite Spanish poet, for his poems and “La eternidad identifica al poeta”, which gives me the necessary calm and courage to face the difficulties from past to future.

Table of Contents

Chapter One: Introduction	1
1.1 DNA Nanotechnology.....	1
1.2 Dynamic DNA Strand Displacement	3
1.2.1 Toehold-mediated DNA strand displacement	4
1.3 Binding-induced DNA Assembly Nanostructures	7
1.3.1 DNA Three-way junction structure.....	8
1.3.2 Binding-induced DNA annealing technology	10
1.3.3 Proximity ligation assays	13
1.3.4 Binding-induced DNA assembly technology.....	14
1.4 Nanomaterial-assisted Signal Detection and Amplification for DNA Nanotechnology	19
1.4.1 Colorimetric assays using oligonucleotides functionalized AuNPs	19
1.4.2 Fluorescence-based assays.....	23
1.4.3 Inductively coupled plasma mass spectrometry	26
1.5 Affinity Separation.....	28
1.5.1 Affinity separation using magnetic beads	28
1.6 Rationale and Objective.....	32
Chapter Two: Binding-Induced Formation of DNA Three-Way Junctions and Its Application to Protein Detection and DNA Strand Displacement.....	35

2.1 Introduction.....	35
2.2 Experimental.....	37
2.2.1 Materials and reagents	37
2.2.2 Probe preparation for the binding-induced DNA three-way junction.....	39
2.2.3 Real-time monitoring of the toehold-mediated DNA strand displacement	40
2.2.4 Binding-induced TWJ probes for prostate specific antigen and human α -thrombin	40
2.2.5 Detection of PSA and thrombin using binding-induced TWJ	41
2.2.6 Monitoring the formation of binding-induced TWJ using gel electrophoresis	42
2.2.7 Real-time detection of streptavidin using binding-induced TWJ	42
2.2.8 Monitoring the kinetics of DNA strand displacement mediated by associative DNA toehold.....	43
2.2.9 Monitoring the kinetics of binding-induced DNA strand displacement	44
2.3 Results and Discussion	45
2.3.1 Assay for prostate specific antigen and streptavidin.....	45
2.3.2 Assay for human α -thrombin	49
2.3.3. Key design parameters influencing the kinetics	51
2.3.4. Comparison with DNA strand-displacement strategies	59
2.4 Conclusions.....	61

Chapter Three: Protein and MicroRNA Detection Using a Binding-Induced DNA

Three-Way Junction and Gold Nanoparticle Amplification by ICP-MS.....	62
3.1 Introduction.....	62
3.2 Experimental.....	65
3.2.1 Materials and reagents	65
3.2.2 Preparation of DNA linker functionalized AuNPs.....	69
3.2.3 Preparation of DNA linker functionalized MBs	69
3.2.4 Preparation of probes and beacons for binding-induced three-way junctions.	70
3.2.5 Monitoring the salt effects on TWJ formation and output DNA displacement using fluorescence.....	71
3.2.6 Detection of output DNA using AuNP amplification by ICP-MS	72
3.2.7 Detection of human α -thrombin and streptavidin using the TWJ and AuNP amplification by ICP-MS.....	74
3.2.8 Detection of miRNA using the TWJ and AuNP amplification by ICP-MS.....	75
3.3 Results and Discussion	76
3.3.1 Key design parameters influencing TWJs formation and displacement.....	76
3.3.2 Output DNA detection using AuNPs amplification by ICP-MS.....	85
3.3.3 Assay for human α -thrombin and streptavidin.....	88
3.3.4 Assay for miRNA 10b and miRNA 128.....	91
3.4 Conclusion	97

Chapter Four: Binding-Induced Molecular Amplifier as a Universal Detection

Platform for Biomolecules and Biomolecular Interaction	98
4.1 Introduction.....	98
4.2 Experimental.....	102
4.2.1 Materials and reagents	102
4.2.2 Preparation of BIMA	105
4.2.3 Molecular translation using BIMA	106
4.2.4 BIMA for probing the interaction between PDGF-BB and PDGFR- β	107
4.3 Results and Discussion	108
4.3.1 Designing and screening the hairpin probes for the SNA track.....	108
4.3.2 Real-time characterization of BIMA using fluorescently labeled HPs.....	111
4.3.3 Characterizing BIMA using a strand displacement beacon	114
4.3.4 BIMA as a versatile and amplifiable platform for translating a broad range of targets	118
4.3.5 Application of BIMA to probing the protein-protein interaction.....	122
4.4 Conclusions.....	124
 Chapter Five: DNA Assembly-Enhanced Binding-Induced Molecular Amplifier as Applied to the Detection of Thrombin	 125
5.1 Introduction.....	125
5.2 Experimental.....	129
5.2.1 Materials and reagents	129

5.2.2 Preparation of DNA molecular amplifier on AuNPs	131
5.2.3 Characterization of ssDNA-AuNP and dsDNA-AuNP molecular amplifier.	131
5.2.4 Target detection using a DNA-AuNP molecular amplifier	133
5.3 Results and Discussion	134
5.3.1 Biotin labeled DNA-AuNP binding-induced molecular amplifier for streptavidin	134
5.3.2 Reduction of background signal for dsDNA-AuNP amplifier.....	138
5.3.3 Effect of spacer on the generation of output DNA from dsDNA-AuNP	141
5.3.4 Effect of AuNP size on dsDNA assembly-enhanced binding-induced molecular amplifier.....	143
5.3.5 Application of the DNA binding-induced molecular amplifier to the detection of thrombin.....	147
5.4 Conclusions.....	152
Chapter Six: Conclusions and Future Work	153
Reference	157
Appendix A: List of publications from the PhD program.....	182

List of Tables

Table 2-1. DNA sequences and modifications for binding-induced DNA TWJ	38
Table 3-1. DNA sequences and modifications for binding-induced DNA TWJ molecular translator	66
Table 3-2. Operating parameters of ICP-MS.....	73
Table 4-1. DNA sequences and modifications for BIMA	103
Table 5-1. DNA sequences and modifications for dsDNA functionalized BIMA	130
Table 5-2. DNA loading amount on 20 nm size AuNPs.....	132
Table 5-3. Loading amount of dsDNA on different size AuNPs.....	143

List of Figures

Figure 1-1. Design of DNA origami	2
Figure 1-2. Schematic illustrations of toehold-mediated strand displacement assays	6
Figure 1-3. Formation of (A) a DNA TWJ triggers the associative toehold-mediated DNA strand displacement and (B) a binding-induced DNA TWJs	9
Figure 1-4. Binding-induced DNA annealing technologies built on the binding of two aptamers to the thrombin molecule	13
Figure 1-5. Schematic illustration of proximity ligation assay.	14
Figure 1-6. Schematic illustrations of (A) the binding-induced DNA assembly (BINDA), (B) a binding-induced DNA strand displacement molecular translator, (C) a binding-induced DNA nanomachine triggered by a biomolecular target	18
Figure 1-7. Schematic illustrations of (A) a AuNP colorimetric oligonucleotide detection; (B) protein detection assay based on cyclic enzymatic signal amplification (CESA)	22
Figure 1-8. Strategies for fluorescence-based assays	24
Figure 1-9. Schematic diagram showing the detection of two distinct target miRNAs by the multiplexed NanoFlare	26
Figure 1-10. Magnetic beads (MBs) used in affinity separations that make use of specific interactions between aptamer and thrombin	31
Figure 2-1. Schematic showing the principle of the binding-induced formation of DNA TWJ	36
Figure 2-2. Detection of PSA using binding-induced TWJ	47
Figure 2-3. (A) Schematic showing the formation of TWJ and the displacement of the	

fluorescence quencher C; (B) Real-time monitoring of the fluorescence increase due to the binding-induced TWJ; (C) Increases in fluorescence signals as a function of the concentration of streptavidin.....	48
Figure 2-4. Detection of human α -thrombin using binding-induced TWJ.	50
Figure 2-5. Monitoring the toehold-mediated DNA strand displacement	53
Figure 2-6. Characterization of the oligonucleotides involved in the formation of binding-induced TWJ and strand displacement	54
Figure 2-7. (A) Schematic showing the design for real-time monitoring of the formation of binding-induced TWJ; (B-C) Optimizing the kinetics of binding-induced TWJ by using different designs of motif TB and in the absence of streptavidin.....	56
Figure 2-8. Effect of incubation temperature (37 and 25 °C) on the formation kinetics of binding-induced TWJ.....	58
Figure 2-9. Comparison of four different DNA strand-displacement strategies and their kinetic profiles.....	60
Figure 3-1. Schematic diagram showing the design for target protein detection using a DNA TWJ and AuNP amplification by ICP-MS.....	64
Figure 3-2. Schematic illustration of the streptavidin-biotin responsive binding-induced TWJ displaced output DNA detection	77
Figure 3-3. Salt effects of Mg^{2+} and Na^+ ions in the reaction buffer	80
Figure 3-4. Optimization of the binding-induced TWJs by using different designs of TWJ1 probes.....	81
Figure 3-5. (A) Optimization of the two probe ratios for prehybridizing the output beacon; (B) Optimization of the ratio between output beacon and the TWJ probes.....	84

Figure 3-6. (A) Schematic showing the design of output DNA detection using AuNP amplification by ICP-MS. (B) Increases in Au metal signal intensity by ICP-MS as a function of concentration of output DNA.....	87
Figure 3-7. Comparison of different TBA modified TWJ1 and TWJ2 pair.....	89
Figure 3-8. Detection of proteins (thrombin and streptavidin) using binding-induced TWJ and AuNP amplification by ICP-MS	90
Figure 3-9. Schematic showing the design of miRNA detection using the TWJ and AuNP amplification by ICP-MS.....	91
Figure 3-10. Detection of miRNA 10b and miRNA 128 using fluorescence	93
Figure 3-11. Detection of miRNA 10b and miRNA 128 using ICP-MS.....	96
Figure 4-1. Schematic illustration of the principle of BIMA.....	101
Figure 4-2. (A) Schematic illustration of the design of hairpin probes; (B) Schematic illustration of the fluorescence turn-on assay for determining the optimal HP design. (C) Fluorescence readout as a function of stem length varying from 5 to 12 bp	109
Figure 4-3. Schematic illustration of the possible source of the target-independent opening of the HP and the nonspecific activation of the strand displacement beacon .	111
Figure 4-4. (A) Schematic illustration of a streptavidin-specific BIMA that releases FAM-labeled DNA barcodes in response to streptavidin; (B) Real-time monitoring fluorescence increases of BIMA.....	112
Figure 4-5. (A) Optimization of DW concentration for BIMA; (B) Concentration dependency of BIMA to the input streptavidin.....	113
Figure 4-6. (A) Schematic illustration of a streptavidin-specific BIMA that releases multiple	

DNA barcode molecules in response to a single streptavidin; (B) Real-time monitoring fluorescence increases of BIMA; (C) Amplification efficiencies (AE) of BIMA as a function of concentrations of the input streptavidin.....	115
Figure 4-7. (A) Schematic illustration of the principle of toehold-mediated strand displacement beacon (FQ) that quantifies the DNA barcode generated from BIMA; (B) Real-time characterization of strand displacement beacon; (C) Standard external calibration curve	116
Figure 4-8. The impact of target concentration on the amplification efficiency of BIMA	117
Figure 4-9. The BIMA assay for amplifying prostate specific antigen (PSA) and platelet-derived growth factor BB (PDGF-BB).....	121
Figure 4-10. The BIMA assay to probe the interaction between PDGF-BB and PDGF receptor β	123
Figure 5-1. Schematic illustration of a protein triggered BIMA.....	127
Figure 5-2. Schematic illustration of streptavidin–biotin dsDNA-AuNP molecular amplifier model system	135
Figure 5-3. Kinetics of the chemical dissociation of ssDNA-AuNP and dsDNA-AuNP induced by 20 μ M DTT over a period of 2 h at 37 $^{\circ}$ C.....	136
Figure 5-4. Characterization of using various lengths of NB probes.....	137
Figure 5-5. (A) Kinetic studies of different blockers on quencher-labeled dsDNA-AuNP; (B) Optimization of Blocker 4 (from 400 pM to 100 nM)	139
Figure 5-6. Kinetic studies comparing quencher labeled dsDNA-AuNP (Y1-FQB) to non-quencher labeled dsDNA-AuNP (Y1-FSB).....	141

Figure 5-7. Comparison of different lengths of output DNA using (A) dsDNA-AuNP without quencher labels (B) dsDNA-AuNP with quencher labels	142
Figure 5-8. Comparison of different diameters of AuNP (from 20 nm to 50 nm).....	144
Figure 5-9. Evaluation of the streptavidin–binding system using 30 nm AuNP.....	146
Figure 5-10. Schematic illustration of a thrombin-TBA binding-induced molecular amplifier.....	148
Figure 5-11. Potassium effects on the TBA reaction.....	149
Figure 5-12. Detection of thrombin dynamic range.....	150
Figure 5-13. Specificity of thrombin with other common serum proteins (human hemoglobin, cytochrome c, transferrin, and prothrombin).....	151

List of Abbreviations

A	adenine
AuNPs	gold nanoparticles
BIMA	binding-induced molecular amplifier
BINDA	binding-induced DNA assembly
BSA	bovine serum albumin
C	cytosine
DNA	deoxyribonucleic acid
DNA-AuNPs	DNA functionalized gold nanoparticles
dsDNA	double strand DNA
ssDNA	single strand DNA
ELISA	enzyme linked immunosorbent assay
FAM	carboxyfluorescein amidite
G	guanine
ICP-MS	Inductively coupled plasma mass spectrometry
MBs	magnetic beads
β -ME	β -mercaptoethanol
miRNA	microRNA
PAGE	polyacrylamide gel electrophoresis
PBS	phosphate buffered saline
PCR	polymerase chain reaction
PDGF	platelet derived growth factor
PLA	proximity ligation assay

RNA	ribonucleic acid
ROX	ROX reference dye
T	thymine
TBA	thrombin binding aptamer
TWJ	three-way junction

Chapter One: Introduction

1.1 DNA Nanotechnology

There has been a growing demand for biological studies and biomolecule detections on the nanometer scale, and nanotechnology has experienced advances in this field. Nucleic acids, especially DNA strands, are used widely for designing and building artificial nanostructures and nanodevices¹. Because of the discovery of Watson–Crick base pairing and the commercialization of oligonucleotide synthesis and modification²⁻³, DNA strands show their predictability, programmability, specificity, and affordability. DNA constructed nanostructures are applied widely as part of nano motors, nano machines, nano vehicles, and molecular computation⁴⁻⁵. The hybridization of complementary DNA strands enables them to be a powerful and versatile tool for engineering DNA nanotechnology in both structural and dynamic ways⁶.

Structural DNA nanotechnology focuses on the self-assembly of static structures⁷, including two-dimensional (2D) and three-dimensional (3D) DNA crystal lattices, construction of nanotubes, organization of periodic arrays, as well as other networks assembled through DNA junctions and hybridizations with nanomaterials, eg. gold nanoparticles, carbon nanotubes, and fullerene molecules. DNA origami is one of the most important breakthroughs for structural DNA nanotechnology development. This technology first introduces a long scaffold DNA strand that can fold into defined 2D shapes with the help of short ‘staple’ DNA strands, then the DNA origami construction is used to build 3D shapes.

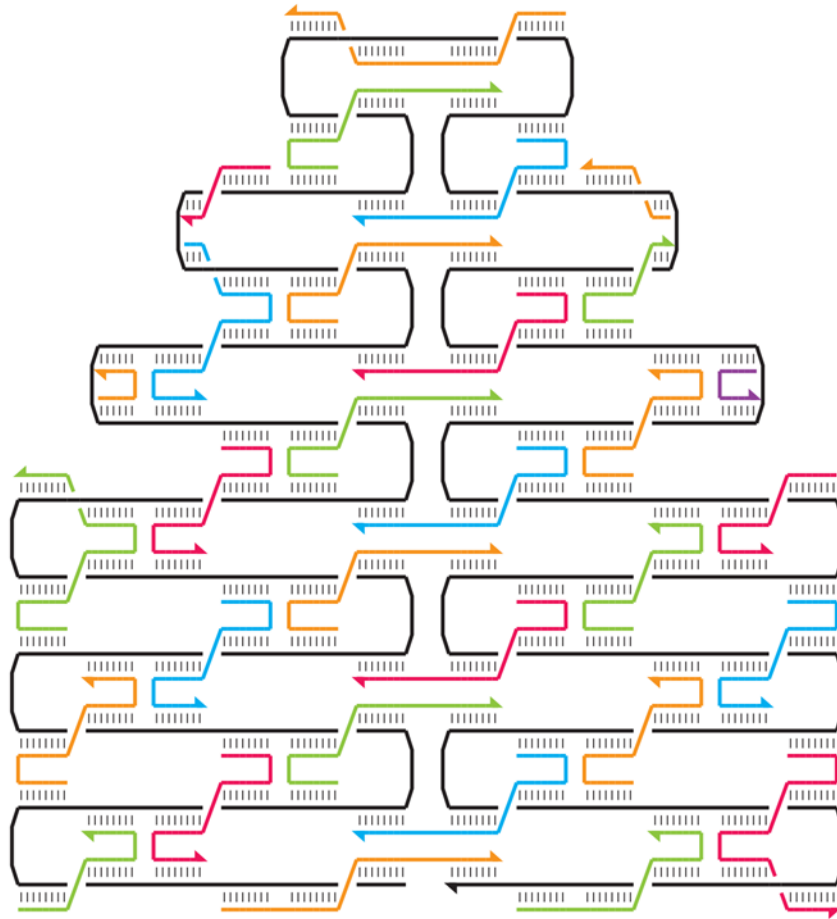


Figure 1-1. Design of DNA origami. Black line is a single-strand long scaffold DNA. All other colourful lines are short DNA strands that are utilized as ‘staples’ to shape and hold the scaffold DNA in place. Reprinted and adapted with permission⁸. Copyright 2006 Springer Nature.

While the development of static nanostructures concentrates on the equilibrium end-states, researchers also turn their interest to the study of engineering DNA nanotechnology systems with non-equilibrium dynamic properties⁹. By designing switchable DNA structures and devices, many dynamic DNA nanotechnologies have been inspired, such as DNA walkers, DNA motors, DNA robots, autonomous DNA machines, and DNA computers¹⁰.

Both structural and dynamic DNA nanotechnologies play an important and unique role for the detection of biomolecules and disease diagnostics by generating or amplifying detection signals. In this Chapter, recent developments of dynamic DNA nanotechnology will be reviewed, mainly focusing on programming binding-induced DNA strategies for high sensitivity detection of biomolecules, including nucleic acids and proteins. These DNA strategies can work as a molecular translator and convey various input targets to a unified output molecule for the subsequent signal transduction and quantification. Nanomaterials, especially DNA functionalized AuNPs, are applied as a vital scaffold to construct the nanostructures and as a signal indicator or amplifier for target detection. Other dynamic DNA assembly assays also are introduced to draw comparisons. These aspects about binding-induced DNA nanotechnologies form the basis of the subject in this thesis.

1.2 Dynamic DNA Strand Displacement

As a promising design medium for dynamic functions, DNA strand displacement reaction is used widely to manipulate the nanodevices and circuits because there are no covalent bonds modified, only non-covalent interactions between DNA strands, such as hydrogen bonds in A - T and C - G base pairs. It is a simple but robust mechanism, in which two DNA strands hybridize together, while one or more pre-hybridized DNA strands are displaced in this process. There is no requirement for protein enzymes or temperature change during the strand displacement reactions. The applications of dynamic DNA strand displacement are summarized in the following Section.

1.2.1 Toehold-mediated DNA strand displacement and its application

To initiate the DNA strand displacement, an overhang, single-stranded domain (referred to as toehold) and a branch migration process are necessary. In Figure 1-1A, A toehold (yellow) is a short, nonhybridized overhang sequence in a double-stranded DNA (dsDNA), normally 4–10 nucleotides. Toehold is called the “sticky end”, which triggers the displacement. The toehold is exposed in the pre-hybridized dsDNA, and in the presence of a single strand that can hybridize with the toehold domain, strand displacement is induced by branch migration, and a new complex is formed. Often, the reactants that initiate the reactions are called inputs (blue-yellow), and the DNA strands that are released finally from the complex are referred to as outputs (blue). By varying the length of toeholds from short to long, the melting temperature of the toehold domain increases. The complex that formed by input strand and toehold is more stable, and the DNA strand displacement reaction rate can increase over a factor of 10^6 .

Li and his coworkers applied the toehold-mediated strand displacement technology for nucleic acid detection (Figure 1-1B)¹¹. First, they prehybridized a dsDNA beacon, with one longer strand fluorophore labeled and the other shorter strand quencher labeled. A few nucleotides were left unhybridized as the toehold domain for strand displacement. In the absence of target nucleic acids, the fluorophore label was brought in close proximity to the quencher label on the dsDNA beacon, and no fluorescent signal came from the duplex. In the presence of the target nucleic acids, they hybridized with the toehold domain, triggered the toehold-mediated displacement, and displaced the shorter strand with the quencher label from the prehybridized beacon, leaving the newly-formed complex fluorescent. It was a fluorescence turn-on assay with high sensitivity and high specificity between the full

complementary and the single mismatch nucleic acid target detection.

To study the kinetics of DNA strand displacement, Winfree and coworkers developed a toehold exchange reaction¹²⁻¹³. As shown in Figure 1-1C, for one DNA strand, both 3'- and 5'- ends have a toehold domain separately (green and yellow). Two different strands with partial complementary to this DNA strand share one common domain (blue) in the middle. Branch migration could happen in both directions, and the kinetics mainly depend on the ΔG of initial toehold and new formed toehold. Quantitative estimations of strand displacement rate constants were able to be predicted from the lengths and sequences of the toehold domains involved. A further study of the thermodynamic properties was carried out by Zhang and Yin using toehold exchange reactions to mimic the hybridization of the DNA strands close to its melting temperature¹⁴. They used a near-optimal assay to discriminate the single-base changes, including replacements, deletions, and insertions, from the fully matched target nucleic acids. Five different DNA targets and 55 single-based mismatched spurious analogues produced discrimination factors between three and more than 100 under a wide range of temperatures, salinities, and probe concentrations. Effective discrimination also applied to the RNA target experiments.

Multiple toehold-mediated strand displacement reactions were improved for isothermal, PCR-independent nanostrategies¹⁵. Ghadiri and coworkers designed a universal translator for the detection of nucleic acids by using consecutive toehold-mediated strand displacement reactions, in which any input target strand was able to convert into a unique output DNA¹⁶. Shown in Figure 1-1D, an intermediate predesigned DNA was displaced by the target nucleic acid through the first toehold-mediated strand displacement reaction, then the intermediate DNA triggered a second toehold-mediated strand displacement, and a universal output DNA

was released in the solution. To detect the output DNA, a strand displacement beacon was prehybridized with fluorescein amidite (FAM) and Dabcyl black quencher (Dab) labeled probes. In the presence of output DNA, the displacement beacon released the FAM labeled strand, and a fluorescent signal was generated. This also worked for label-free input DNA and small-molecule targets.

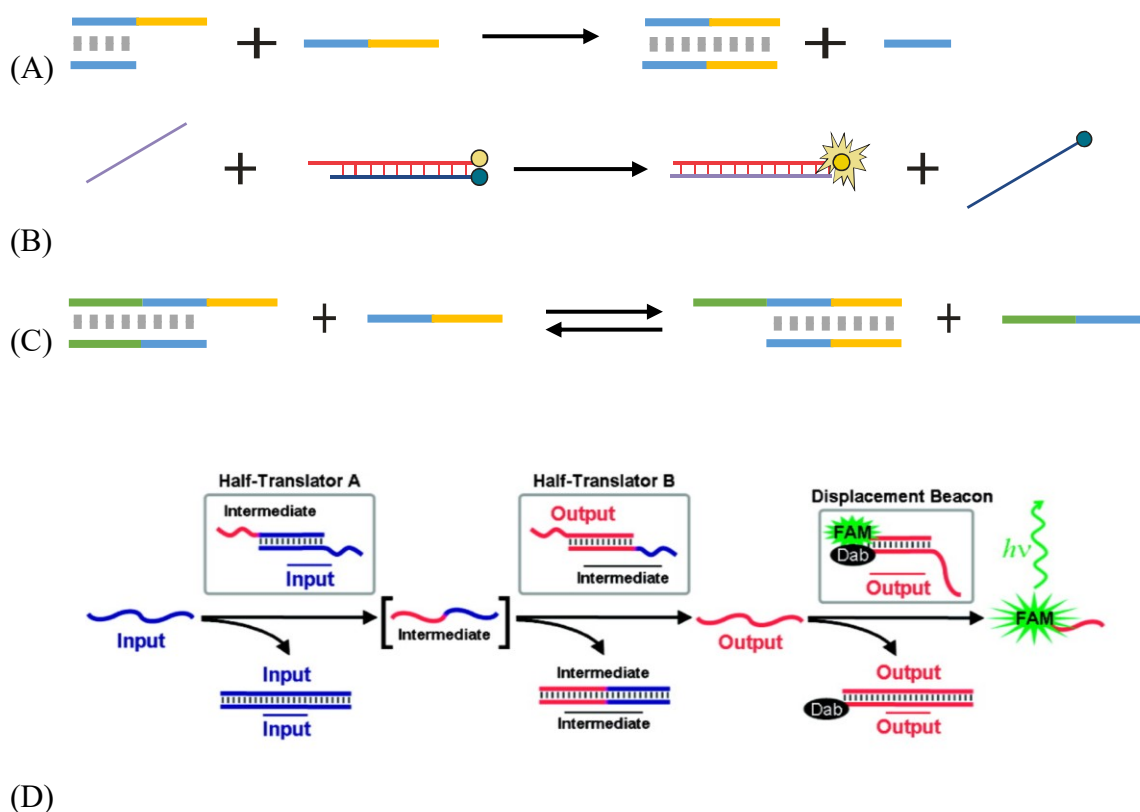


Figure 1-2. Schematic illustrations of toehold-mediated strand displacement assays. (A) Toehold-mediated DNA strand displacement. (B) Target nucleic acid detection using a fluorescence and quencher labeled strand displacement beacon. (C) Toehold exchange reactions for DNA displacement kinetic studies and single-base mismatch discrimination. (D) Multiple strand displacement based universal translator. Reprinted and adapted with permission¹⁶. Copyright 2009 American Chemical Society.

1.3 Binding-induced DNA Assembly Nanostructures

Recently, DNA assembly through affinity binding has been developed as an important strategy to construct dynamic DNA nanostructures for detection of biomolecules. Unlike nucleic acids, proteins are difficult to amplify directly, therefore, the binding-induced DNA assembly (BINDA) can accomplish the detection of trace levels of target proteins by transferring the detection target to the amplifiable DNA. As a non-covalent interaction, affinity binding is a main feature that occurs in the process of DNA assembly. Through affinity binding, two or more affinity ligand modified DNA probes react with one single target molecule. Because the signal generation requires simultaneous binding of multiple probes to the same target molecule, the background commonly encountered in the single-recognition approaches is reduced substantially. Thus, assays based on detection of binding-induced assembly can achieve better detection limits (lower background) compared to assays involving a single binding event.

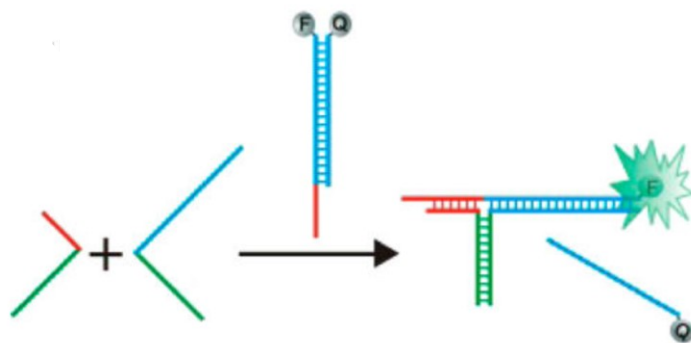
One of the commonly used affinity ligands is aptamer, an oligonucleotide that consists of a short DNA or RNA strand. Aptamer is selected specifically through an in vitro evolution, referred to as systematic evolution of ligands by exponential enrichment (SELEX)¹⁷⁻¹⁸. A high affinity strand sequence is obtained for the target molecule from a large oligonucleotide library after repeating selection circles. Protein-antibodies interactions, protein-aptamers interactions, and nucleic acids hybridizations are three main binding events that are used in the construction of binding-induced DNA nanotechnologies. Here, we illustrate the principle of binding-induced DNA assay for the detection of target molecules and its novel applications.

1.3.1 DNA Three-way junction structure

DNA three-way junctions (DNA TWJs) are one of the most popular fundamental building blocks to construct DNA architectures and dynamic assemblies¹⁹. Compared to the linear duplex formed by double-stranded nucleic acids, DNA TWJ has in an approximately Y-shaped geometry and consists of three extended and unstacked helices²⁰. Because of the multiple strands complex, the TWJ can be responsive to the single-stranded DNA or the RNA target that are partially complementary to each other and trigger the associative toehold-mediated DNA strand displacement²¹⁻²². As shown in Figure 1-2A, one of the TWJ formation probes is pre-hybridized to a double-stranded beacon. In the presence of target nucleic acids, the probe is displaced, and a TWJ can be formed with signal generation. This DNA TWJ structure also was applied for protein detections. Our group has developed a binding-induced DNA TWJs strategy that is able to convert protein bindings to the formation of DNA TWJ²³. The binding-induced DNA TWJ makes use of two DNA motifs, each conjugated to an affinity ligand (Figure 1-2B). Because the complementary region on the two DNA motifs is too short to hybridize stably at experimental temperature, in the absence of target protein, the target-independent reaction between two DNA motifs is minimized. The binding of two affinity ligands to the target molecule triggers an assembly of the DNA motifs and initiates the subsequent DNA strand displacement, resulting in a binding-induced TWJ. Real-time fluorescence monitoring of the binding-induced TWJ enables detection of the specific protein targets. A detection limit of 2.8 ng/mL was achieved for prostate-specific antigen. The binding-induced TWJ approach compares favorably with the toehold-mediated DNA strand displacement, the associative toehold-mediated DNA strand displacement, and the binding-induced DNA strand displacement. Importantly, the binding-induced TWJ

broadens the scope of dynamic DNA assemblies and provides a new strategy to design protein-responsive DNA devices and assemblies.

(A)



(B)

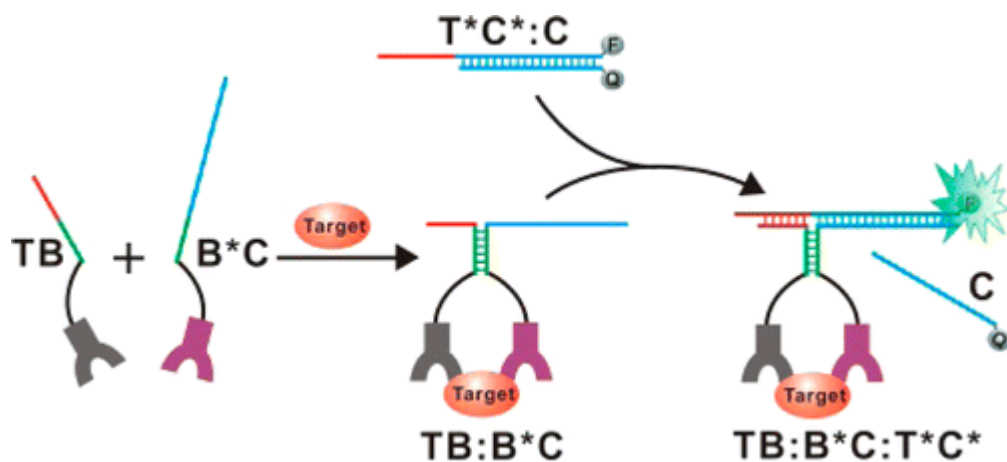


Figure 1-3. (A) Formation of a DNA TWJ triggers the associative toehold-mediated DNA strand displacement. (B) Principle of binding-induced formation of DNA TWJs. Reprinted with permission²³. Copyright 2013 American Chemical Society.

1.3.2 Binding-induced DNA annealing technology

Typically, effective binding-induced DNA annealing requires two DNA probes, each carrying an affinity ligand, to react with a single target molecule²⁴⁻²⁵. Both DNA probes contain a short complementary sequence, and the melting temperature (T_m) is lower than room temperature. The two DNA probes are designed in such a way that they do not hybridize on their own or self-assemble. After incubating and binding with one single target, the two DNA sequences are brought into close proximity, and the previous inter-molecular hybridization turns into an intra-molecular hybridization. The local effective concentration was increased as well as the T_m of the two DNA probes and promotes the assembly of a new DNA motif because of the enhanced stability. Therefore, this newly assembled DNA motif is detected as an indirect measure of the target. The background can be reduced significantly because the incidence of two non-specific binding events to the same target molecule is much lower than that of one non-specific binding event to the target molecule. Therefore, a much lower detection limit can be achieved by using the dual-recognition and binding-induced assembly approach.

Heyduk *et al.* developed an aptamer based fluorescence assay that uses the binding-induced DNA annealing concept²⁴. They used two fluorescently labeled aptamers to comprise a fluorescence resonance energy transfer (FRET) pair (Figure 1-3A). FRET often happens between two fluorophores, one is a single donor and the other is a single acceptor²⁶. Usually, the energy transfer is undetectable until the donor and acceptor are brought to a close proximity of around 1–10 nm, which is achieved by the annealing of two DNA strands. Then, the energy transfer efficiency is inversely proportional to the sixth power of the distance between the signal donor and acceptor. A 29-mer aptamer was labeled with

fluorescein as the fluorescence donor, and a 15-mer aptamer was labeled with dabcy1 as the fluorescence acceptor. Binding of the two aptamers to the same thrombin molecule brought the fluorescence donor and acceptor into close proximity, facilitating FRET. Detection of FRET signals provided quantification for thrombin. This assay did not have amplification capacity, and the detection limit of thrombin was 50 pM.

Guisto *et al.* used rolling circle amplification (RCA) to achieve sensitive detection²⁷. They linked one aptamer to a circular DNA sequence and added to another aptamer a short primer sequence that could hybridize with the circular DNA and initiate the RCA (Figure 1-3B). The primer sequence was designed to be short enough to ensure minimum hybridization to the circular DNA. Binding of both aptamers to a thrombin molecule brought the primer to close proximity with the circular DNA template, promoting the RCA reaction. Then, elongated RCA products were labeled with an intercalating fluorescent dye, and fluorescence was detected. RCA increased the signal intensity and enhanced the sensitivity of the assay. A detection limit of 30 pM was achieved. Because RCA is a linear amplification technique, the improvement of sensitivity by RCA is not as high as that by the exponential amplification of PCR.

Our group incorporated silver nanoclusters (AgNCs) into this strategy for thrombin analysis (Figure 1-3C)²⁸. The authors modified two aptamers by connecting an AgNCs nucleation sequence to one aptamer and a guanine-rich sequence to the second aptamer with linker complementary sequences. Binding of both aptamers to thrombin resulted in substantially increased local concentrations of the complementary sequences, facilitating the stable hybridization between them. The formation of the DNA duplex structure ensured the close proximity of AgNCs with the G-rich sequence. The G-rich sequence could enhance

the red fluorescence of AgNCs by up to 500-fold when at a proximate distance with AgNCs²⁹. Thus, the enhanced red fluorescence was used for thrombin quantification.

Sequence independent enzymes, such as exonuclease III (Exo III), also are used to amplify and enhance detection signals³⁰. Liu and coworkers applied the binding-induced self-assembly of the aptamer subunits and Exo III as an amplifying catalyst (Figure 1-3D)³¹. The system consists of two aptamers that enable the self-assembly of the thrombin–G quadruplex aptamer complex. One aptamer is modified at its 3'- and 5'- ends with the BHQ2 quencher and the Cy3 fluorophore, respectively. In the absence of thrombin and the Exo III, the two aptamers exist as single-stranded configurations, and the fluorescence of Cy3 is quenched by BHQ2. The addition of thrombin results in the assembly of the two aptamer subunits into the thrombin–G quadruplex aptamer complex, in which the 3'- and 5'- ends of the aptamers are stabilized cooperatively into a duplex domain that leads to Exo III-catalyzed digestion. The fluorescence of Cy3 is generated after the labeled aptamer is cleaved by Exo III. This reaction recycles the analyte, thereby achieving amplification. The detection limit for this analysis of thrombin corresponds to 89 pM.

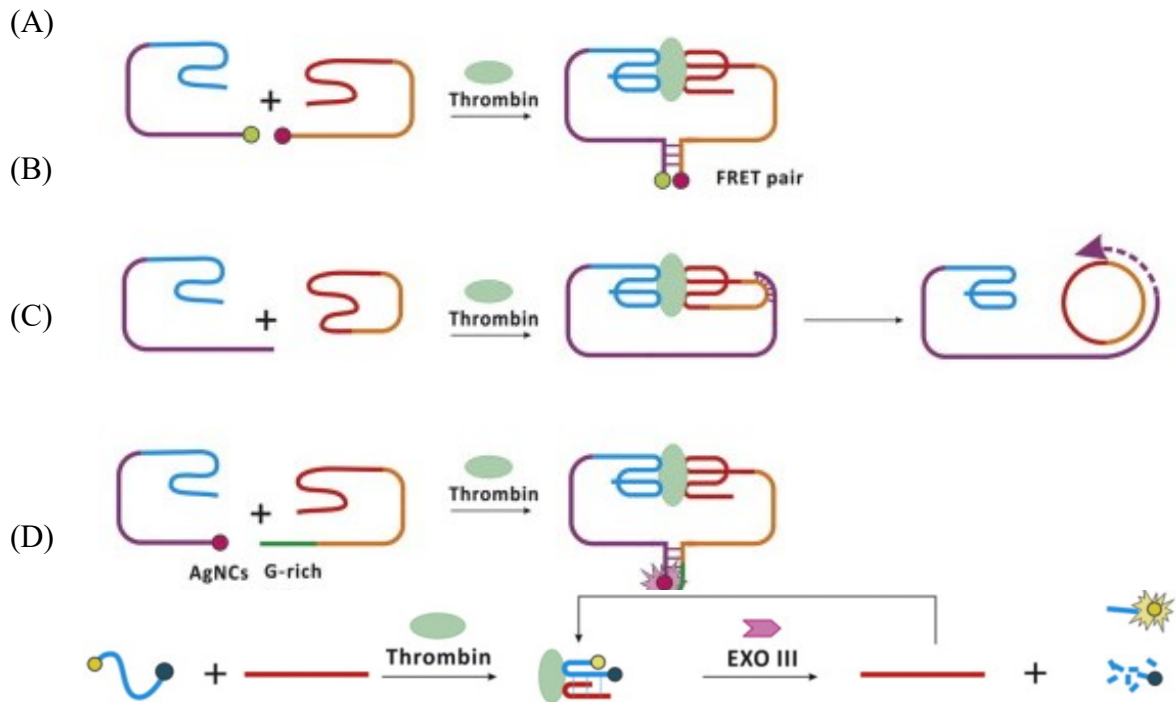


Figure 1-4. Binding-induced DNA annealing technologies built on the binding of two aptamers to the thrombin molecule. (A) Binding-induced proximity of two fluorophores generates a FRET signal for thrombin quantitation. (B) Binding of both aptamers leads to the close proximity of primer and circular DNA, promoting rolling circle amplification. (C) Binding-induced DNA assembly of the AgNCs nucleated aptamer and the G-rich aptamer enhances the red fluorescence of AgNCs. (D) Binding-induced aptamer assembly and cleavage by Exo III generate fluorescence signals for detection.

1.3.3 Proximity ligation assays

Fredriksson *et al.* first reported a “proximity ligation assay” (PLA) utilizing the dual-recognition of two aptamers for thrombin³². Two DNA probes were used, and each was conjugated to an aptamer that recognized a different epitope of thrombin. After the

incubation of the two probes with the target, two binding events brought the two DNA probes into close proximity. A “connector” oligonucleotide, with sequences complementary to the probes, was used to hybridize with the probes. Next, DNA ligase was used to join the 5’-end of one probe with the 3’-end of the second probe, forming a longer piece of DNA. The ligated piece of DNA was detected finally by real-time PCR (Figure 1-4). Using this strategy, the authors could improve the detection limit successfully by up to three orders of magnitude compared to the conventional enzyme linked immunosorbent assay (ELISA). The authors used more than 10,000-fold higher concentrations of the connector than the probes to drive the formation of the DNA assembly. Despite the high concentration of the connector oligonucleotide, the analytical background remained low because the ligation took place only when both affinity probes were bound to the same target molecule and were brought into close proximity.

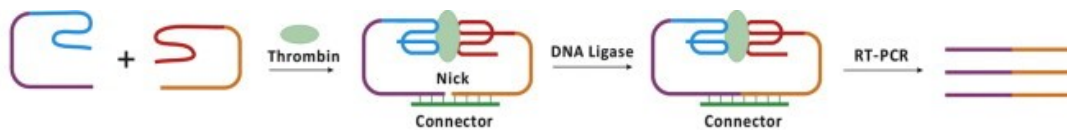


Figure 1-5. Two binding events bring DNA probes into close proximity, then hybridize with the connector and form a duplex, which is ligated and detected by real-time PCR.

1.3.4 Binding-induced DNA assembly technology

The BINDA strategy was studied by our group in 2009, when a patent application was filed³³. The strategy benefited from a more sophisticated DNA sequence design and enabled ultrasensitive detection for multiple biomolecules and construction of functional

nanostructures. We demonstrated a binding-induced hairpin system (Figure 1-5A) and applied it successfully for the detection of target proteins at the yoctomole level³⁴. Two DNA motifs were designed to have a short complementary sequence, but because the T_m is below the reaction temperature, the duplex is difficult to form in the absence of the target. One of the DNA motifs linked to a hairpin loop, and both of them had a blocker sequence to reduce the nonspecific binding and background signal further. When the two motifs were bound on the same molecule, the local effective concentration increased, and a stable hairpin motif was hybridized. An enzyme ligation step was added after the BINDA, the two DNA sequences that formed the hairpin motif were joined together, and the new sequence was detected by real-time PCR. Various target proteins, including streptavidin, platelet derived growth factor (PDGF), and prostate specific antigen (PSA), achieved a detection limit of yoctomole to zeptomole levels.

We applied the assembly of two DNA motifs on a AuNP to design a binding-induced DNA displacement molecular translator for the detection of biomolecules³⁵. As shown in Figure 1-5B, in the design of this molecular translator, the input target information was converted to a pre-designed output DNA by binding-induced DNA strand displacement. The AuNP was used as the scaffold and functionalized with affinity ligand modified DNA1 probes. A fluorophore labeled output DNA was pre-hybridized with the DNA1 probe, formed a stable duplex, and the fluorescence that was close to the surface of the AuNP was quenched. Another affinity ligand modified DNA2 probe was added in the solution to bind with the same target as the DNA1 probe. Because the length of the complementary region in the DNA2 probe was shorter than the length of the output DNA, in the absence of the target, it was difficult for the DNA2 probe to displace the pre-hybridized output DNA. The

binding triggered the DNA assembly, the DNA2 probe competed with the output DNA on the duplex, and the DNA2 probe displaced the output DNA from the AuNP scaffold, which generated a fluorescent signal. Streptavidin and PDGF BB were responsive to the molecular translator at sub nM levels.

A binding-induced DNA nanomachine that was triggered by proteins and nucleic acids was developed further³⁶ using the AuNP scaffold, distinct from the self-assembly DNA nanomachines. As shown in Figure 1-5C, hundreds of single-stranded anchorage probes (S1+C1) were functionalized on the surface of AuNPs; these fluorescence labeled probes were quenched because of the high quenching efficiency of AuNPs. Tens of affinity ligand DNA L1 probes also conjugated on the AuNP and were able to capture the target biomolecule. Another DNA probe, called the swing arm, also was modified with the affinity ligand; the swing arm contained a C1* sequence that was complementary to the C1 on the anchorage probe. Because the C1 and C1* only contained 7 nucleotides, their hybrid is not stable at room temperature, and the DNA nanomachine is not activated. However, in the presence of the target biomolecules, the affinity ligands that modified on both the anchorage probe and the swing arm probe are able to bind and form a complex, which brought the swing arm probe also on the AuNP scaffold. Consequently, the local concentration of C1 and C1* complementary region increased, and because of their close proximity, an intramolecular binding-induced assembly took place, the blocker on the swing arm probe was displaced, and C1:C1* hybridized stably. It should be noted that a nicking endonuclease can recognize the specific double-stranded DNA sequence, which is the C1:C1* duplex, but only C1 will be cleaved. After this cleavage, the fluorescence label on the C1 was released from the surface of AuNP, and this free oligonucleotide was no longer quenched and became

fluorescent. The swing arm probe was able to hybridize with another anchorage probe, and after moving around to cleave most of the reachable C1, the DNA nanomachine generated an amplified fluorescent signal. Therefore, by monitoring the increase of fluorescence in solution, the target biomolecule was detected, and the detection limit of platelet-derived growth factor-BB (PDGF-BB) was 5 pM. For the nucleic acids detection, the sequence of the anchorage probe contained a complementary region to one end of the target, and the swing arm probe contained a sequence that was complementary to the other end of the target. A Smallpox gene DNA target was detected at the 10 pM level. We have expanded this concept of DNA nanomachine on the AuNP scaffold to further applications, and a synthetic DNAzyme motor that can operate in living cells for biomolecule imaging was developed³⁷. Other constructions of binding-induced DNA assembly using double-stranded DNA probes or nanomaterials like quantum dots also have been studied.

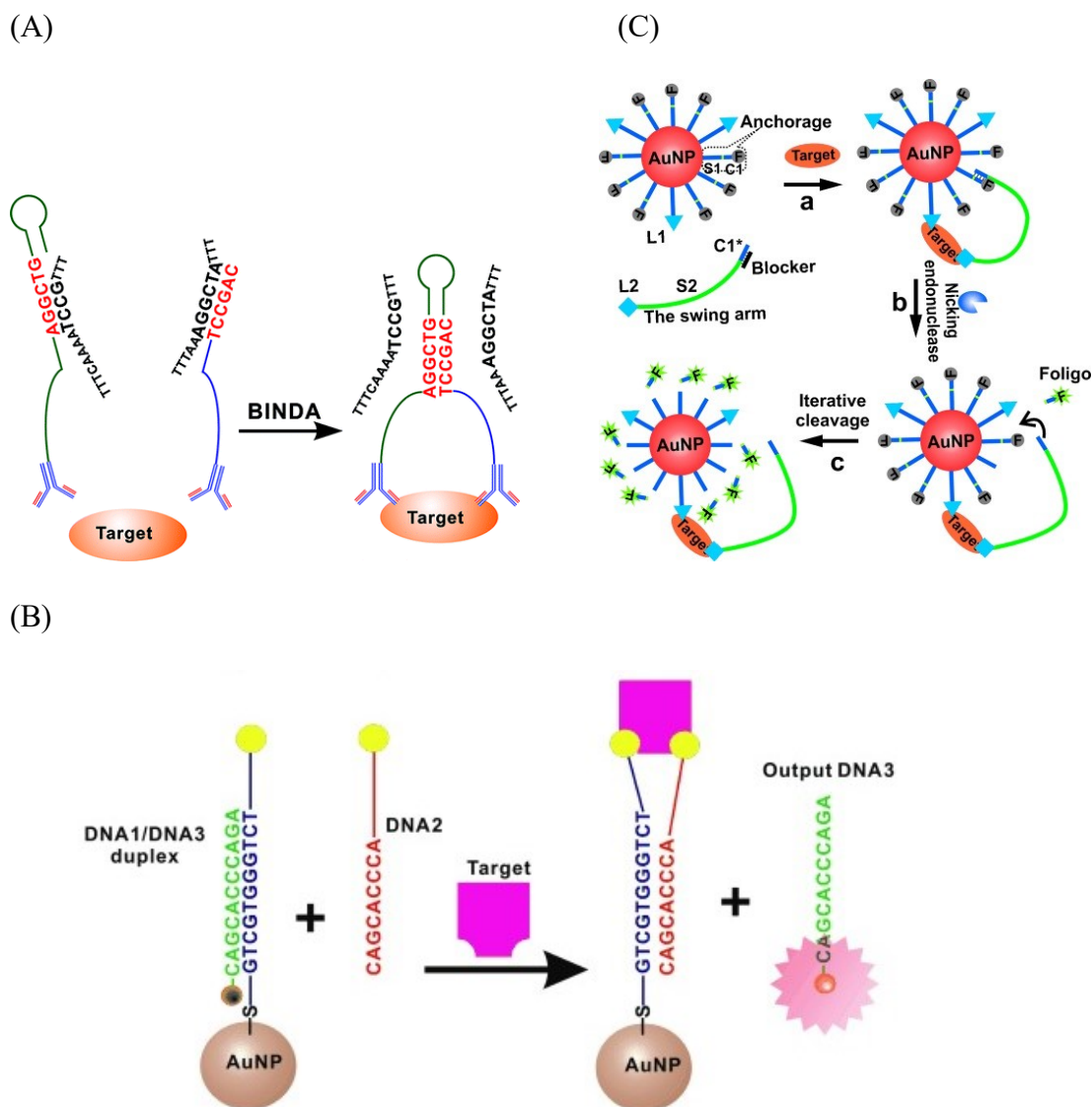


Figure 1-6. (A) Principle of binding-induced DNA assembly (BINDA). Reprinted with permission³⁴. Copyright 2012 American Chemical Society. (B) Schematic illustration of the binding-induced DNA strand displacement molecular translator. Reprinted with permission³⁸. Copyright 2012 WILEY-VCH Verlag GmbH & Co. KGaA. (C) Schematic illustration of the binding-induced DNA nanomachine triggered by a biomolecular target. Reprinted with permission³⁶. Copyright 2015 WILEY-VCH Verlag GmbH & Co. KGaA.

1.4 Nanomaterial-assisted Signal Detection and Amplification for DNA

Nanotechnology

Nanomaterials with extraordinary optical properties have been applied successfully in developing DNA nanotechnology for biomolecule detection. Wavelength dependence of the fluorescence quenching efficiency of nearby dyes by AuNPs and nanoparticles are the roles of spectral overlap and particle size. Examples of these nanomaterials include AuNPs, AgNPs, graphene, and Quantum dots. Among them, AuNP is one of the most widely applied nanomaterials because of the little size deviation from preparation, high fluorescent quenching efficacy, and electronic and catalytic properties. Robust synthetic procedures and a relatively stable state make it easy to control the size, shape, and solubility of AuNPs. With all these diverse features, AuNPs are an excellent scaffold for DNA nanotechnologies. With a high surface area per particle and perfect biocompatibility, multiple ligands can pack on one AuNP, and the functionalized AuNPs can be applied for the detection of proteins and nucleic acids in a complicated surrounding chemical environment both in vitro and in vivo.

1.4.1 Colorimetric assays using oligonucleotides functionalized AuNPs

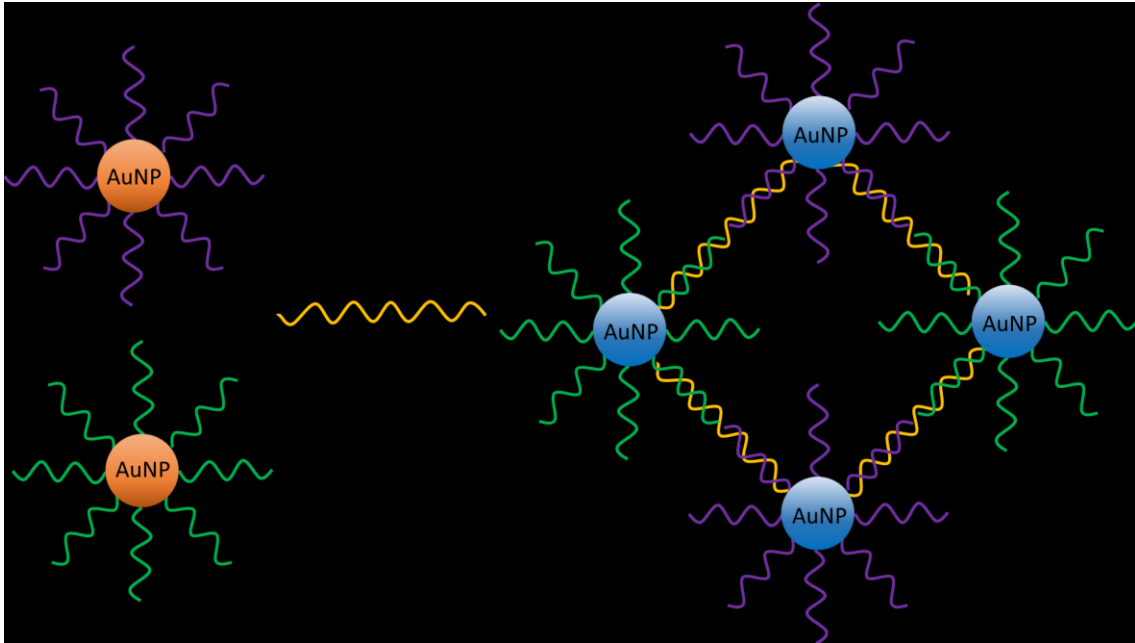
Normally, the colour of the colloidal AuNP with a particle size smaller than 40 nm is red due to the feature of the surface plasmon resonance; the blue portion of the spectrum is absorbed, and the red light is reflected³⁹⁻⁴⁰. When the AuNPs aggregate in the solution, because of the interparticle surface plasmon coupling and the shape change of the AuNPs, the AuNPs absorb red colour light and appear blue colour light, so the solution colour is switched gradually from red to blue.

Mirkin and coworkers reported the first colorimetric biosensor based on the DNA functionalized AuNPs (Figure 1-6A)⁴¹. They used two different thiol-group labeled DNA probes to conjugate on the surface of AuNPs; one DNA probe is complementary to the 5'-end of the target oligonucleotide, while the other DNA probe is complementary to the 3'-end. In the presence of target oligonucleotides, the DNA probes and target nucleic acids hybridized with each other and formed a cross-linked AuNPs aggregation. The shape and distance between the AuNPs changed, leading to the solution colour switching from red to blue. In addition, the temperature range for the dissociation of these cross-linked AuNPs is very narrow, and the DNA melting transitions were sharp enough for efficient discrimination of single-mismatched oligonucleotides. By understanding the unique features of AuNPs, a great effort was made for further improvement of colorimetric assays based on oligonucleotides functionalized AuNPs⁴².

Yang's group proposed a detection system that combined the cyclic enzymatic signal amplification (CESA) method with the colorimetric assay for highly sensitive detection of biomolecules⁴³. The CESA method utilizes enzymatic reactions or other signal amplification mechanisms to transduce target binding events to measurable signals. The advantages of this method are its simplicity, high sensitivity, low cost, and the ability to transform non-amplifiable proteins into amplifiable oligonucleotide signals. However, specific recognition sites often are required for the specific enzymes, which would limit the design of the oligonucleotides. Endonucleases and exonucleases are the most frequently used enzymes for CESA. Yang used a hairpin aptamer probe, a linker DNA, two sets of DNA-modified AuNPs, and a nicking endonuclease. As shown in Figure 1-6B, in the absence of a target, the hairpin aptamer probe and linker DNA can coexist stably in solution. Then, the linker

DNA can assemble two sets of DNA-modified AuNPs, inducing the aggregation of AuNPs. However, in the presence of a target, the complex is formed, and it can hybridize to the linker DNA. The nicking enzyme recognizes a specific nucleotide sequence and cleaves the linker DNA into two fragments. After nicking, the aptamer-target complex is released, and the cycle of binding and cleaving the linker DNA starts anew. The cleaved fragments of linker DNA are not able to assemble two sets of DNA-modified AuNPs, thus the red color of the separated AuNPs can be observed. With the naked eye, human thrombin can be detected with a detection limit of 50 pM and adenosine triphosphate (ATP) with a detection limit of 100 nM.

(A)



(B)

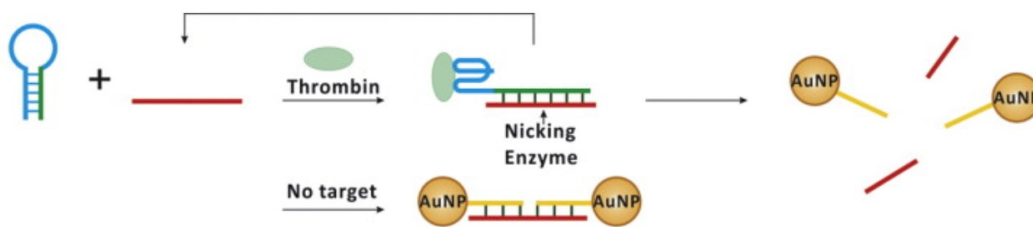


Figure 1-7. (A) Schematic illustration of a colorimetric oligonucleotide detection. DNA functionalized AuNPs aggregated after hybridization with complementary target oligonucleotides. The colloid colour changed from red to blue. The AuNPs and oligonucleotides are not drawn to scale. (B) Strategy for protein detection assay based on cyclic enzymatic signal amplification (CESA). AuNPs aggregation or dispersion by nicking endonuclease.

1.4.2 Fluorescence-based assays

Fluorescence assays have been developed for detection of proteins, nucleic acids, and small molecules. Different interaction mechanisms contribute to the diversity of fluorescence-based assays; one of the categories is using fluorescent-dye label on the DNA probe. In such methods, a quencher also exists, and the formation or dissociation of the quencher-fluorescent complex is used to control the turn-off or turn-on signal effect. Various quenchers were applied, including chemical quenchers and nanoparticles like AuNPs.

To generate the detection signal, conformational changes are necessary for the functional DNA probes. Wang *et al.* presented an assay using AuNPs as the fluorescence quencher to design the AuNPs thrombin aptamer beacon⁴⁴ (Figure 1-7A–C). Following the addition of thrombin, the aptamer switches structure due to its binding to thrombin, and the fluorophore labeled probe is no longer near the surface of AuNPs, restoring the fluorescence signal.

Quantum dots (QDs) also are used as a fluorescent indicator for functional DNA probes. Levy *et al.* labeled an aptamer with QDs and a short piece of competitor DNA with a quencher to construct a duplex beacon (Figure 1-7D)⁴⁵. When the target protein interacted with the duplex beacon, the conformational change disrupted the duplex structure (structure switching) and restored the fluorescence from QDs.

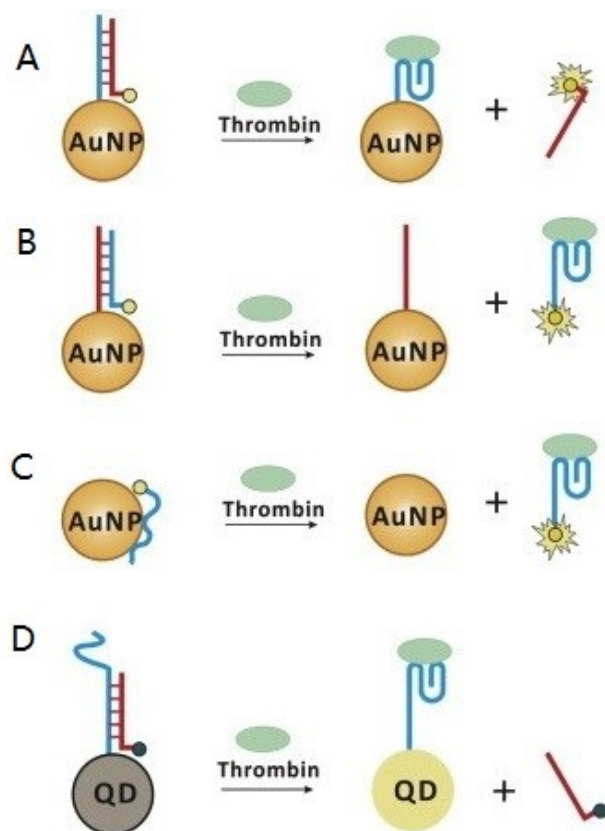


Figure 1-8. Strategies for fluorescence-based assays. (A–C) AuNPs thrombin aptamer beacon. (D) QDs and chemical quencher duplex beacon for thrombin detection.

MicroRNAs (miRNAs) are small, non-coding RNA molecules with a length of ~22 nucleotides. They exist widely in plant and animals and cause the breakdown of mRNAs⁴⁶⁻⁴⁸. MiRNAs also are recognized as regulators of gene expression during development and cell differentiation⁴⁷. Due to their surprisingly high stability in plasma, miRNAs are protected from nuclease degradation, they hold a great promise as a new class of cancer biomarkers for disease diagnostics and can be extracted for downstream analyses of humans. Because miRNAs are too short and often at very low concentrations in serum and precious tissue samples, it precludes the use of conventional diagnostic tools with low sensitivity. Mirkin and coworkers developed a rapid and sensitive miRNA detection method by using monolayer, single-stranded oligonucleotides functionalized AuNPs, called NanoFlare⁴⁹⁻⁵¹. Fluorescent labeled DNA probes with a complementary sequence were hybridized to the oligonucleotides on AuNPs, and because the fluorophores were close to the surface of the AuNP, the fluorescence was quenched. Target miRNAs would displace the fluorescent labeled DNA probes and release them in solution to turn on the fluorescence signal. As shown in Figure 1-8, a multiplexed NanoFlare was achieved by using two different fluorophores modified DNA probes that pre-hybridize with the oligonucleotides on AuNPs. After the uptake of AuNPs, two distinct target miRNAs were detected in living cells. This assay was able to detect 1 fM concentrations of miRNA in serum. Adenosine triphosphate (ATP) in living systems also was able to turn on the NanoFlare fluorescent signal when the adenosine aptamer was used to conjugate on AuNPs⁵², and MDA-MB-231 cells from breast cancer cell line can be identified from the whole blood⁵³.

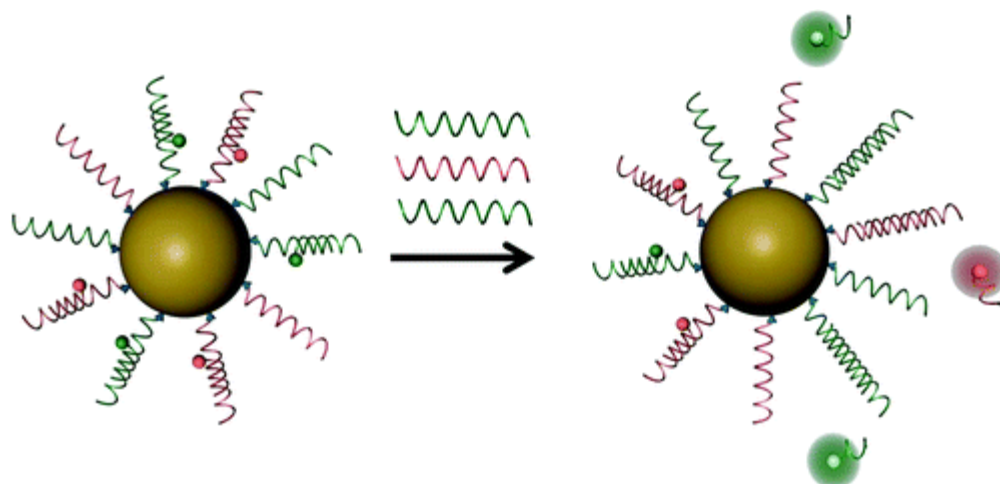


Figure 1-9. Schematic diagram showing the detection of two distinct target miRNAs by the multiplexed NanoFlare. Reprinted with permission⁵⁰. Copyright 2012 American Chemical Society.

1.4.3 Inductively coupled plasma mass spectrometry

Inductively coupled plasma mass spectrometry (ICP-MS) is a powerful analytical instrument used for the measurement of trace concentrations of metal and non-metal elements. Inductively heated argon gas energizes the inductively coupled plasma, which has a high temperature (maximum to $\sim 10,000$ K) and contains plenty of ions and electrons. The sample aerosol is atomized directly and ionized in this argon gas plasma. Then, the target metal ions are separated and detected by mass spectrometry via specific mass to charge ratio with high sensitivity, high selectivity, and wide dynamic range. Quadrupole mass spectrometry is used normally in ICP-MS, and multiple elements can be tested simultaneously. Single particle inductively coupled plasma-mass spectrometry (spICP-MS) was developed recently by Degueldre and coworkers to provide further information about nanoparticles on their size, size distribution, and concentration⁵⁴, eg. TiO_2 , ZrO_2 ⁵⁵, ThO_2 ⁵⁶,

and AuNP⁵⁷. Hassellöv explored the spICP-MS study for the case of AgNP⁵⁸ and demonstrated that it is a promising tool for bioassays and environmental analysis.

Our group studied the detection of biomolecules and cells using AuNP amplification and ICP-MS. The signal intensity at a mass-to-charge ratio of 197 corresponded to the AuNPs from the sample. Two thrombin binding aptamers were used to analyze the concentrations of human α -thrombin⁵⁹. One aptamer was conjugated on the AuNPs, and the other was functionalized on the magnetic beads (MBs). A sandwich structure was constructed in the presence of thrombin with both aptamers binding to the same target molecule. The nonreacted reagents were washed away, and the sandwich structure was dissociated at high temperature (~ 90 °C). After removing the MBs, the AuNPs were left in the solution and measured by ICP-MS. The size of the AuNP affects the signal amplification efficiency; larger AuNPs contribute to greater signal amplification and can improve the sensitivity.

Next, we applied the method on the detection of *Escherichia coli* O157:H7⁶⁰, which is one of the major bacteria that causes food-borne illness. We conjugated antibodies on the AuNPs and then used antibody coated AuNPs to label the *E. coli* O157:H7 cell. After centrifugation and separation of the nonreacted reagents, the AuNP labeled *E. coli* cells were digested with 1% nitric acid and analyzed by ICP-MS. A detection limit of 500 CFU/mL *E. coli* O157:H7 was achieved.

1.5 Affinity Separation

Affinity separation often is achieved through specific interactions between a pair of binding partners, such as antigen and antibody, enzyme and substrate, receptor and ligand, or aptamer and protein. Affinity interactions can be incorporated into traditional separation methods, such as chromatography, capillary electrophoresis, microfluidics, and magnetic beads.

1.5.1 Affinity separation using magnetic beads

Magnetic beads (MBs) serve both as a scaffold for aptamer immobilization and as a unique material for rapid magnetic separation of the captured target from the sample matrix. Many techniques take advantage of two affinity ligands binding to two separate sites of the same target protein, which allows for the formation of a sandwich complex. The thrombin and thrombin-binding-aptamer system is one of the most popular systems for protein detection. Li *et al.* immobilized the 15-mer aptamer (Apt15) on magnetic beads to capture and pre-concentrate thrombin, then separated it from the sample matrix⁶¹. They immobilized the 29-mer aptamer (Apt29) on AuNPs. Binding of thrombin to both aptamers resulted in the formation of the Apt15–thrombin–Apt29 sandwich complex (Figure 1-9A). Using a magnet, they separated the sandwich complex from the unbound AuNPs. The bound AuNPs on the sandwich complex catalyzed the reaction of methyl orange (MO), generating changes in colorimetric signals. By visualization with the naked eye, they were able to achieve a detection limit of 320 pM thrombin. This detection limit was decreased further to 30 pM with UV–vis absorption detection.

Similarly, Szymanski and coworkers used both aptamers to construct a sandwich assay

on magnetic beads⁶². But unlike Li, Szymanski conjugated Apt29 on magnetic beads and Apt15 on AgNPs. Despite the different binding affinities of the two aptamers for thrombin, both approaches worked. After magnetic separation of the Apt29–thrombin–Apt15 sandwich complex, they used ionic silver amplification and anodic stripping voltammetry to generate electrochemical detection signals. The detection limit for α -thrombin was 164 pM.

Wang and coworkers conjugated one aptamer (serving as the capture) on magnetic beads and the second aptamer (serving as the reporter) on quantum dots (QDs)⁶³. After capturing of the thrombin sandwich complex, fluorescence of the QDs was measured for quantitation; they achieved a detection limit of 50 pM. Similarly, Tennico *et al.* conjugated the two aptamers on magnetic beads and QDs respectively and performed assays on microfluidic chips⁶⁴. With fluorescence microscopy detection, they achieved a detection limit of 10 ng/mL (\sim 0.3 nM). With electrochemical detection, Centi *et al.* also reached a detection limit of 0.45 nM⁶⁵. With further modification and by incorporating aptamer-labeled silica nanocapsules (SiNCs) for electrochemical detection, Wang *et al.* improved the detection limit to 60 pM⁶⁶.

A second approach for the detection of protein, specifically thrombin, after capturing of thrombin on magnetic beads, is based on the catalytic activity of thrombin. Typically, thrombin catalyzes the conversion of a chromogenic/fluorogenic substrate to an optically measurable product (Figure 1-9B). Zhao and Wang used the aptamer-modified magnetic beads to capture and separate thrombin from the sample mixture⁶⁷. After 2 h of enzyme reaction, and with absorption detection, they were able to detect as low as 400 fM thrombin. Zhao further improved the detection limit to 2 fM thrombin and 100 fM human neutrophil

elastase by detecting fluorescent products generated from thrombin-catalyzed conversion of the fluorogenic substrate⁶⁸. With electrochemical detection of the enzymatic product of thrombin, Centi and coworkers reported a detection limit of 175 nM⁶⁹.

The third approach of using aptamers and magnetic beads has led to the development of a new signal transduction strategy (Figure 1-9C). Hecht developed a label-acquired magnetorotation (LAM) technique, which was able to detect thrombin at a concentration as low as 300 pM⁷⁰. They coated larger non-magnetic “mother” spheres (10 μm diameter) with one aptamer (Apt29), and they immobilized smaller magnetic “daughter” beads (1 μm diameter) with the second aptamer (Apt15); binding of thrombin to both aptamers formed a sandwich complex. In a rotating magnetic field, the rotational frequency of the sandwich complex was proportional to the number of attached magnetic beads, which depended on the concentration of thrombin in the sample solution. This principle gives rise to a new method of signal generation and can be applied to the detection of other target molecules.

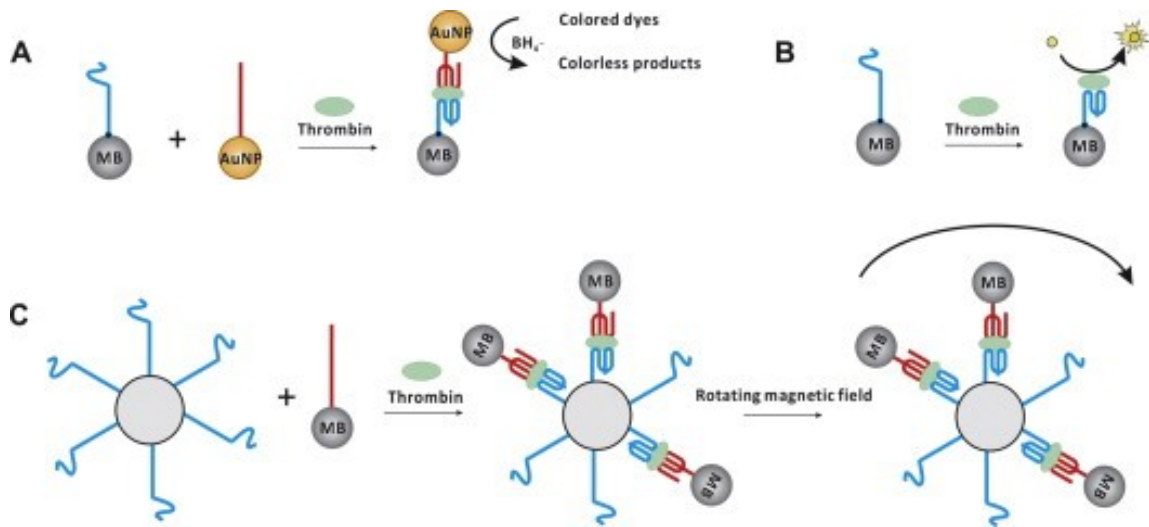


Figure 1-10. Magnetic beads (MBs) used in affinity separations that make use of specific interactions between aptamer and thrombin. (A) Apt15 is conjugated to the MBs and Apt29 is conjugated to AuNPs. MBs are used for separation and AuNPs are used for colorimetric detection. (B) The captured thrombin on MBs catalyzes the subsequent conversion of fluorogenic substrate to fluorescent products. (C) Apt29 is coated on the non-magnetic “mother” spheres (10 μm diameter), and Apt15 is coated on the magnetic “daughter” beads (1 μm diameter). Binding of thrombin to both aptamers forms a rotating sandwich complex. In a rotating magnetic field, the rotational frequency of the sandwich complex is proportional to the number of attached magnetic beads, which scales with the concentration of thrombin in the solution.

1.6 Rationale and Objective

DNA nanotechnology for detection of biomolecules is very popular and of much interest. This nanotechnology proves the capability of ultrasensitive detection for various targets, including proteins and nucleic acids, in a complicated environment. However, one of the difficulties is that a protein molecule itself cannot be amplified easily like nucleic acids. The binding-induced DNA nanostructure are promising to form a universal design for the detection of biomolecules, including target proteins, specific DNA, and miRNAs. Combined with the utility of nanomaterials, a potentially powerful DNA nanotechnology can be achieved.

The objective of this thesis is the study of binding-induced DNA nanotechnology for detection of biomolecules, including proteins and nucleic acids. My focus is on the study of binding-induced DNA TWJ and binding-induced molecular amplifier to construct the DNA structure. AuNP was the nanomaterial chosen for diverse roles, such as scaffold, quencher, and signal amplification label for ICP-MS. A general view of the dynamic DNA structures, nanomaterials, affinity separations, and assays for biomolecular detection was introduced here, and the outline of the thesis is designed as follows.

In **Chapter 2, Binding-Induced Formation of DNA Three-Way Junctions and Its Application to Protein Detection and DNA Strand Displacement**, the formation of binding-induced DNA TWJ triggered by proteins and the initiation of DNA strand displacement was investigated systematically. Real-time fluorescence monitoring of the binding-induced TWJ provides sensitive detection of the specific proteins, including PSA and human α -thrombin. The binding-induced DNA TWJ technique was compared to three other DNA strand-displacement strategies; this technique exhibited fast kinetics, extremely

low background, and high sensitivity. With no need for enzymes or thermal cycling, this new DNA TWJ approach expanded the scope of DNA nanostructure for many emerging applications.

In **Chapter 3, Protein and MicroRNA Detection Using a Binding-Induced DNA Three-Way Junction and AuNP Amplification by ICP-MS**, a binding-induced DNA TWJ was constructed to a molecular translator for the detection of proteins and miRNAs by ICP-MS using AuNPs as a signal amplifier. All the input target molecules are converted into the universal output DNA. To detect these output DNA, AuNPs were used as labels and MBs were used to separate them from nonreacted reagents. ICP-MS was used to measure the amount of corresponding Au in the solution. This strategy is able to respond to various targets, including human α -thrombin, miRNA 10b, and miRNA 128 at picomolar concentrations.

In **Chapter 4, Binding-Induced Molecular Amplifier as a Universal Detection Platform for Biomolecules and Biomolecular Interaction**, a universal detection platform for multiple classes of target biomolecules was designed. The novel binding-induced molecular amplifier (BIMA) was introduced not only to translate a broad range of biomolecules and interactions into a unified DNA barcode but also to enhance the translation efficiency by releasing multiple barcode molecules in response to a single binding event. The output DNA barcode is designed to trigger toehold-mediated strand displacement reactions. Using this strategy, the detection platform is able to respond to streptavidin, PSA, synthetic DNA target, PDGF-BB, and PDGF receptor β . As such, a simple strand displacement beacon that conventionally only detects single-stranded DNA target has been expanded for the detection of nucleic acids, proteins, and the protein–protein interaction.

In **Chapter 5, Universal Protein Detection Using DNA Assembly-Enhanced Binding-Induced Molecular Amplifier**, a DNA assembly-enhanced binding-induced molecular amplifier was established. By using the double-stranded DNA functionalized AuNP, the overall chemical stability of BIMA was enhanced compared to the single-stranded DNA functionalized AuNP; dsDNA was easier to control the modification on its probes, and a quencher and fluorescent labeled dsDNA decreased background signal substantially. The enhancement of local concentrations of dsDNA probes on AuNPs helped to accelerate reaction rates. Because the input target protein generated multiple output DNA molecules released from AuNPs, the signal amplified. The BIMA are able to detect streptavidin and human α -thrombin at picomolar concentrations.

In **Chapter 6, Conclusions and Future Work**, all contents of the thesis research projects are summarized and potential future directions for the research are discussed.

Chapter Two: Binding-Induced Formation of DNA Three-Way Junctions and Its Application to Protein Detection and DNA Strand Displacement

2.1 Introduction

DNA three-way junctions (DNA-TWJs) are important building blocks to construct DNA architectures and dynamic assemblies^{19, 71-78}. Target-responsive DNA TWJs also can be designed into DNA devices for molecular diagnostic, sensing, and imaging applications⁷⁹⁻⁸³. Successful TWJs have focused on DNA, but the benefits have not been extended to proteins because proteins do not possess the base-pairing properties of DNA. We hypothesize that the affinity bindings between target molecules and their ligands can serve as a trigger for the formation of DNA TWJs. This binding-induced TWJ would provide a new strategy to design protein-responsive DNA devices and assemblies.

The principle of our binding-induced TWJ technology is inspired by the previous observation that two separate DNA strands that are linked by a stable DNA duplex can facilitate toehold-mediated DNA strand displacements (associative DNA toehold)^{21, 84-85}. Although this TWJ strategy is highly successful for DNA, its application to proteins is challenging. To overcome this challenge, I have developed a binding-induced TWJ technique (Figure 2-1). Two DNA motifs, **TB** and **B*C** are each conjugated with an affinity ligand. Motif **TB** is designed to have a toehold domain **T** and a binding domain **B**, separated by a flexible linker of two thymidine bases. Motif **B*C** has a binding domain **B*** and a competing domain **C**. **TB** and **B*C** are designed to have only 6 complementary bases (domain **B** and **B***, green color in Figure 2-1), so that they cannot form a stable duplex at

room temperature in bulk solution. However, in the presence of the target molecule, the binding of two affinity ligands to the same target molecule brings **TB** and **B*C** to close proximity, greatly increasing their local effective concentrations⁹. Consequently, **TB** and **B*C** hybridize to each other to form a stable **TB:B*C** duplex. Once **TB:B*C** forms, the duplex triggers a subsequent toehold-mediated strand displacement reaction with **T*C*:C**, forming a binding induced TWJ (**TB:B*C:T*C***) and releasing the motif **C**.

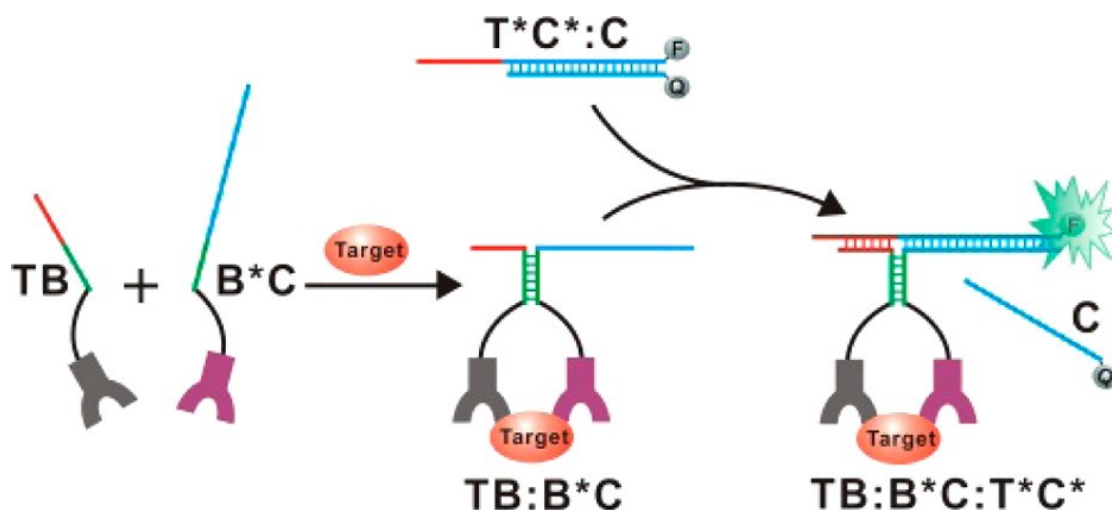


Figure 2-1. Schematic showing the principle of the binding-induced formation of DNA TWJ. Binding of the target molecule to the two specific affinity ligands brings two DNA motifs, **TB** and **B*C**, to close proximity, forming the **TB:B*C** duplex. The formation of **TB:B*C** triggers a subsequent strand displacement between **TB:B*C** and **C**, resulting in a stable binding-induced TWJ (**TB:B*C:T*C***) and the release of **C**. Symbols in this scheme do not reflect the actual sizes of the molecules.

2.2 Experimental

2.2.1 Materials and reagents

Streptavidin from *Streptomyces avidinii* (product number, S4762), biotin (product number, B4501), bovine serum albumin (BSA), prostate-specific antigen from human semen (PSA), sterile-filtered human serum, magnesium chloride hexahydrate ($\text{MgCl}_2 \cdot 6\text{H}_2\text{O}$), and $100\times$ Tris-EDTA (TE, pH 7.4) buffer were purchased from Sigma (Oakville, ON, Canada).

SYBR Gold and ROX Reference Dye (ROX) were purchased from Life Technologies (Carlsbad, CA). Biotinylated Human Kallikrein 3/PSA polyclonal antibody (goat IgG) was purchased from R&D Systems (Minneapolis, MN). Reagents for polyacrylamide gel electrophoresis (PAGE), including 40% acrylamide mix solution and ammonium persulfate, were purchased from BioRad Laboratories (Mississauga, ON, Canada). Tween 20 and 1,2-bis (dimethylamino)-ethane (TEMED) were purchased from Fisher Scientific (Nepean, ON, Canada).

NANOpure H_2O ($>18.0 \text{ M}$), purified using an Ultrapure Milli-Q water system, was used for all experiments. All DNA samples were purchased from Integrated DNA Technologies (Coralville, IA) and purified by high performance liquid chromatography (HPLC). The DNA sequences and modifications are listed in Table 2-1.

Table 2-1. (A) DNA sequences and modifications for constructing binding-induced DNA three-way junctions and (B) DNA sequences and modifications used in thrombin detection and (C) in the gel electrophoresis experiments

(A)

DNA name		Sequences and modifications
T*C*		5' - CTA GAG CAT CAC ACG GAC ACA TGG GAT ACA CGC TT - FAM - 3'
C		5' - Dabcyl-AA GCG TGT ATC CCA TGT GTC-3'
B*C		5' - AA GCG TGT ATC CCA TGT GTC - CCT CAC TGA GAC TCC-TTT TTT T - Biotin - 3'
TB	T₁₅B₆	5' - Biotin - TTT TTT TTTTTTTTT T - GTG AGG - TT - CGT GTG ATG CTC TAG - 3'
	T₉B₆	5' - Biotin - TTT TTT TTTTTTTTT T GTG AGG - TT - CGT GTG ATG - 3'
	T₈B₆	5' - Biotin - TTT TTT TTTTTTTTT T - GTG AGG - TT - CGT GTG AT - 3'
	T₇B₆	5' - Biotin - TTT TTT TTTTTTTTT T - GTG AGG - TT - CGT GTG A - 3'
	T₆B₆	5' - Biotin - TTT TTT TTTTTTTTT T - GTG AGG - TT - CGT GTG - 3'
T₉B₁₅		5' - GGA GTC TCA GTG AGG - TT - CGT GTG ATG - 3'
TC(T₈C₂₀)		5' - AA GCG TGT ATC CCA TGT GTCCGTGTGAT - 3'
Biotin-C*		5' - Biotin - TTT TTT TTTTTTTTTGAC ACA TGG GAT ACA CGC TT - FAM - 3'
C-Biotin		5' - AA GCG TGT ATC CCA TGT GTC TTT TTTTTTTTT TTT -Biotin - 3'

(B)

DNA name	Sequences and modifications
B*C	5' - AA GCG TGT ATC CCA TGT GTC - CCT CAC TGA G - TT TTTTTT TT - <u>GGT TGG TGT GGT TGG</u> - 3'
TB	5' - <u>AGT CCG TGG TAG GGC AGG TTG GGG TGA CT T TTT</u> TTTTTTTTTT T GTG AGG - TT - CGT GTG ATG - 3'

(C)

DNA name	Sequences and modifications
T*C*	5' - CTA GAG CAT CAC ACG GAC ACA TGG GAT ACA CGC TT - 3'
C	5' - FAM - AA GCG TGT ATC CCA TGT GTC - 3'

2.2.2 Probe preparation for the binding-induced DNA three-way junction

DNA probe (**T*C*:C**) for binding-induced TWJ was prepared at a final concentration of 5 μM by mixing 20 μL of 50 μM FAM-labeled **T*C*** with 20 μL of 100 μM dark quencher-labeled **C** in 160 μL of TE–Mg buffer (1 \times TE, 10 mM MgCl_2 , 0.05% Tween20). The mixture was heated to 90 $^\circ\text{C}$ for 5 min, and then the solution was allowed to cool down slowly to 25 $^\circ\text{C}$ over a period of 3 h.

Probe (**T*C*:C**) for gel electrophoresis also was prepared at a final concentration of 5 μM by mixing 20 μL of 50 μM unlabeled **T*C*** with 20 μL of 25 μM FAM-labeled **C** in 160 μL of TE–Mg buffer. Similarly, the solution was heated to 90 $^\circ\text{C}$ for 5 min and then cooled down to 25 $^\circ\text{C}$ slowly over a period of 3 h.

2.2.3 Real-time monitoring of the toehold-mediated DNA strand displacement

For a typical toehold-mediated DNA strand displacement reaction, the reaction mixture contained 20 nM probe **T*C*:C**, 50 nM ROX reference dye, 1 μ M polyT oligo, varying concentrations of the target DNA **TC (T₈C₂₀)**, and TE–Mg buffer. The reaction mixture was incubated at 25 °C for 45 min in a 96-well plate. Fluorescence was measured directly from the microplate using a multimode microplate reader (DX880, Beckman Coulter). The excitation/emission for the DNA probes were 485/515 nm, and the excitation/emission for the ROX reference dye were 535/595 nm. To monitor the kinetic process of a toehold-mediated DNA strand displacement reaction, we measured the fluorescence of the reaction mixture every 1.5 min for the first 30 min and then every 5 min for another 15 min.

2.2.4 Binding-induced TWJ probes for prostate specific antigen and human α -thrombin

To prepare DNA probes for the detection of PSA using binding-induced TWJ, we mixed 25 μ L of 2.5 μ M biotinylated probe **T₉B₆** or probe **B*C** with an equal volume of 2.5 μ M streptavidin (diluted in 20 mM Tris buffer, containing 0.01% BSA) and then incubated the solution at 37 °C for 30 min, followed by incubation at 25 °C for another 30 min. To this reaction mixture, 50 μ L of 1.25 μ M biotinylated PSA polyclonal antibodies (diluted in 20 mM Tris buffer saline, containing 0.01% BSA) were added. The solution was incubated at 25 °C for 30 min. Then, the prepared DNA probe was diluted to 250 nM with a solution containing 20 mM Tris buffer saline, 0.01% BSA, and 1 mM biotin.

Two distinct thrombin aptamer sequences (underlined in Table 2-1B) were added

respectively to the end of the **B*C** and **T₉B₆** sequences, forming DNA probes. They were used as the probes for the detection of thrombin.

2.2.5 Detection of PSA and thrombin using binding-induced TWJ

For the detection of PSA and thrombin in buffer or in diluted human serum, the reaction mixture contained 20 nM antibody-modified or aptamer-modified probe **TB**, 20 nM antibody-modified or aptamer-modified probe **B*C**, 50 nM ROX reference dye, 1 μ M polyT oligo, varying concentrations of the target proteins (PSA or thrombin), and TE–Mg buffer. The reaction mixture was incubated at 37 °C for 30 min and then transferred into a 96-well plate. Then, detection probe **T*C*:C** was added to the reaction mixture at a final concentration of 20 nM. Fluorescence was measured every 1.5 min for the first 30 min and then every 5 min for another 2 h. Fluorescence was measured directly from the microplate using a multimode microplate reader (DX880, Beckman Coulter). The excitation/emission for DNA strand displacement were 485/515 and excitation/emission for ROX reference dye were 535/595 nm. The measured fluorescent signal was normalized so that 1 normalized unit (n.u.) of fluorescence corresponded to the fluorescent signal generated by 1 nM **TC**. This normalization was achieved using a positive control containing 10 nM **TC**, 20 nM **T*C*:C**, 1 μ M polyT oligo, and 50 nM Rox in TE–Mg buffer, and a negative control containing identical reagents in positive control, except that there was no **TC** added.

The end-point detection of the target proteins (PSA and thrombin) was achieved by incubating the reaction mixture at 25 °C for 60 min in a PCR tube in the dark. Then, the reaction mixture was transferred to a 96-well microplate and fluorescence was measured using the multimode microplate reader as described above.

2.2.6 Monitoring the formation of binding-induced TWJ using gel electrophoresis

A reaction mixture contained 2 μM probe **B*C**, 2 μM probe **TB**, 1 μM **T*C*:C**, 1 μM **T*C***, 1 μM target protein, and TE–Mg buffer. The mixture was incubated at 25 °C for 30 min, and after incubation, the reaction mixture was assessed using 12% native polyacrylamide gel electrophoresis (PAGE). Before loading, DNA samples were mixed with DNA loading buffer on a volume ratio of 5:1. A potential of 12 V/cm was applied for gel electrophoresis separation.

After separation, PAGE gels were imaged using an ImageQuant 350 digital imaging system. Two approaches were used to measure the fluorescently labeled DNA and total DNA, separately. First, the PAGE gels were imaged without any staining procedure, therefore, only the fluorescently labeled (FAM-labeled) DNA bands were visualized. Then, same PAGE gels were stained with SYBR Gold, and images were taken again. All DNA bands were detected using the second approach (i.e., after the SYBR Gold staining).

2.2.7 Real-time detection of streptavidin using binding-induced TWJ

For real-time detection of streptavidin using binding-induced TWJ, the reaction mixture contained 20 nM FAM-labeled probe **T*C*:C**, 20 nM probe **TB**, 20 nM probe **B*C**, 50 nM ROX reference dye, 1 μM polyT oligo, varying concentrations of the target streptavidin, and TE–Mg buffer. The reaction mixture was incubated at 25 °C in a 96-well microplate. Fluorescence was measured directly from the microplate every 1.5 min for the first 30 min and then every 5 min for another 2 h. The measured fluorescent signal was normalized so that 1 normalized unit (n.u.) of fluorescence corresponded to the fluorescent signal generated

by 1 nM TC. This normalization was achieved using a positive control containing 10 nM TC, 20 nM T*C*:C, 1 μ M polyT oligo, and 50 nM ROX reference dye in a TE–Mg buffer, and a negative control containing identical reagents as in the positive control, with the exception that there was no TC added. The rate constant k_{obs} was determined from the following equation:

$$\frac{\ln(1 - [\text{output}]/[\text{input}])}{t} = k_{\text{obs}}$$

where, the [output] is the normalized fluorescence at each time point and the [input] is the total normalized fluorescence corresponding to the concentrations of target added.

A calibration was generated from the analyses of solutions containing varying concentrations of streptavidin from 0.16–10 nM. The reaction mixtures, as described above, were incubated in separate PCR tubes in the dark. Then, each mixture was transferred into a 96-well microplate and fluorescence was measured as described above.

2.2.8 Monitoring the kinetics of DNA strand displacement mediated by associative DNA toehold

For monitoring the kinetics of DNA strand displacement mediated by associative DNA toehold, the reaction mixture contained 20 nM FAM-labeled probe T*C*:C, 10 nM probe T $\text{\textcircled{9}}$ B $\text{\textcircled{15}}$, 10 nM probe B*C, 50 nM ROX reference dye, 1 μ M polyT oligo, and TE–Mg buffer. The reaction mixture was incubated at 25 °C in a 96-well plate. The subsequent fluorescence detection and signal normalization were the same as described above.

2.2.9 Monitoring the kinetics of binding-induced DNA strand displacement

For monitoring the kinetics of binding-induced DNA strand displacement, the reaction mixture contained 20 nM probe **Biotin-C*:C**, 20 nM probe **C-Biotin**, 10 nM target streptavidin, 50 nM ROX reference dye, 1 μ M polyT oligo, and TE–Mg buffer. The reaction mixture was incubated at 25 °C in a 96-well plate. Fluorescence was measured every 1.5 min for the first 30 min and then every 5 min for another 2 h. The measured fluorescent signal was normalized so that 1 n.u. of fluorescence corresponded to the fluorescent signal generated by 1 nM **TC**. This normalization was achieved using a positive control containing 10 nM **T₈C₁₅**, 20 nM **T*C*:C**, 1 μ M polyT oligo, and 50 nM ROX in the TE–Mg buffer, and a negative control containing identical reagents as in the positive control, with the exception that there was no **T₈C₁₅** added.

2.3 Results and Discussion

2.3.1 Assay for prostate specific antigen and streptavidin

We first constructed a binding-induced TWJ as a sensor for PSA in human serum. We conjugated polyclonal anti-PSA antibodies to DNA motifs **TB** and **B*C** through streptavidin–biotin interactions (Figure 2-2A). We also modified DNA motifs by labeling **T*C*** with a fluorescent dye FAM and labeling **C** with a quencher. Because the FAM-labeled **T*C*** initially was hybridized with the quencher-labeled **C**, the fluorescence was quenched. However, in the presence of the target PSA, the binding of PSA to two antibodies brings **TB** and **B*C** together, resulting in the formation of the FAM-labeled binding-induced TWJ (**TB:B*C:T*C***) and the simultaneous release of the quencher-labeled **C** (Figure 2-2A), then the fluorescence was restored. By monitoring this fluorescence increase, we are able to quantify the amount of the target PSA in real-time.

Figure 2-2B shows the increases in fluorescence signal from the determination of PSA (0–285 ng/mL) using the binding-induced TWJ. The measured fluorescence increases over a period of 150 min are proportional to the concentrations of PSA ranging from 4.5 to 285 ng/mL (Figure 2-2B). A calibration between the fluorescence intensity and the concentration of PSA is linear within the range of concentrations tested (Figure 2-2C, red line) with a detection limit of 2.8 ng/mL. Having constructed a binding-induced TWJ sensor for PSA, we further explored its ability to detect the target proteins in a complicated sample matrix (e.g., human serum samples). We spiked PSA to a 10× diluted human serum and then quantified the PSA concentrations using the binding-induced TWJ sensor. As shown in Figure 2-2C, we have achieved similar detection sensitivity for PSA in human serum samples (blue line) as in buffer solutions (red line), suggesting that our binding-induced TWJ

sensor can be applied to real-world sample analysis with no need for any separation.

A slight background increase was observed when comparing the two calibration curves generated from PSA in buffer and PSA spiked in serum. This small increase is due mainly to the background fluorescence from the serum samples. The slopes from the two calibration curves are comparable, suggesting that there is minimum matrix effect. Such ability to quantify minute amounts of PSA (ng/mL level) present in human serum samples, without need for any separation, suggests that our sensor is very specific to the target protein. Two characteristics of the binding-induced TWJ technique contribute to the high specificity: (i) the use of two affinity ligands to bind with the same target molecule; (ii) the assembly and formation of DNA TWJ is triggered by simultaneous binding of both affinity ligands to the single target molecule.

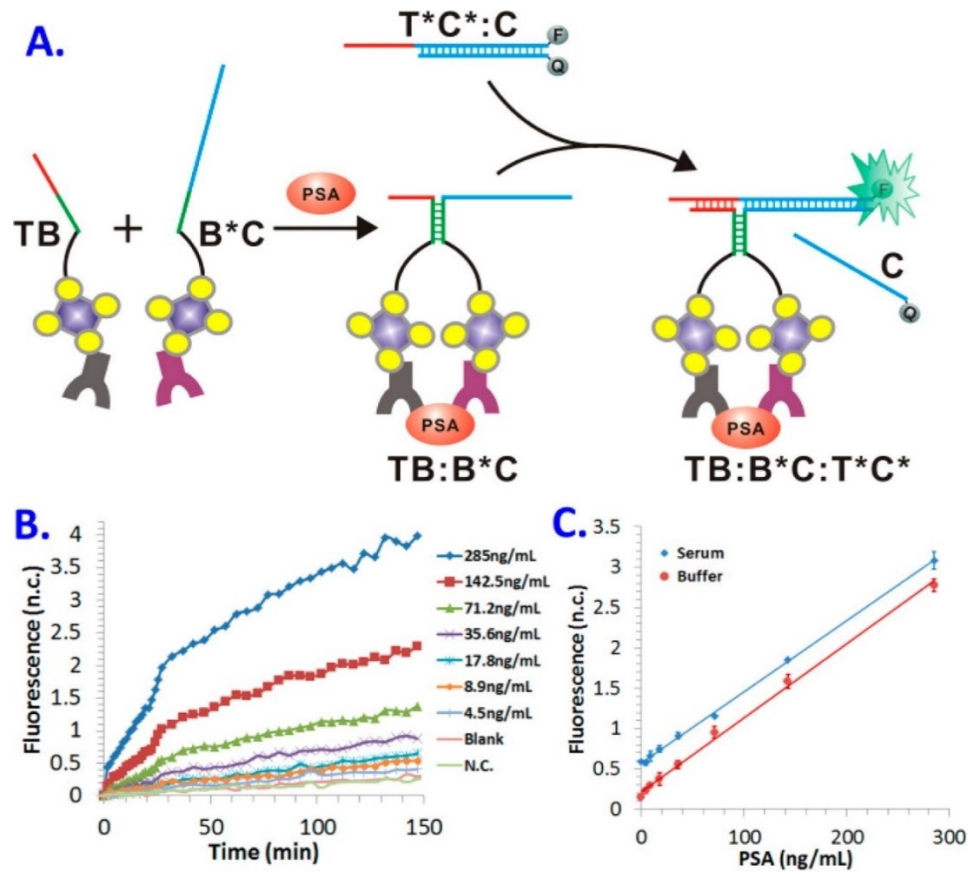


Figure 2-2. Detection of PSA using binding-induced TWJ. (A) Schematic showing the design of PSA-responsive TWJ. (B) Real-time monitoring of the fluorescence increases over time from the determination of varying concentrations (0–285 ng/mL) of PSA. The negative control (N.C.) contained only 20 nM T*C*:C in TE–Mg buffer. (C) Increases in fluorescence signals as a function of the concentration of PSA in buffer (red line) and in 10× diluted human serum (blue line). Fluorescence measurements were taken at 60 min.

On the basis of the same principle and design as for the detection of PSA, we have used biotin–streptavidin binding to achieve the detection of streptavidin (Figure 2-3), a second example of protein detection. A linear calibration was achieved between 50 pM and 10 nM.

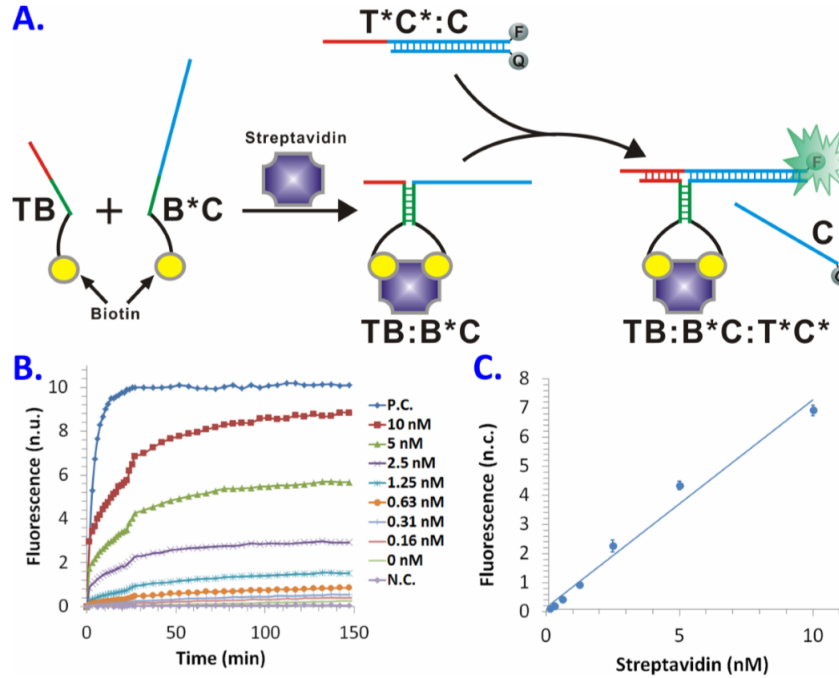


Figure 2-3. (A) schematic showing the binding of streptavidin to the two biotin-conjugated DNA probes resulted in the formation of TWJ and the displacement of the fluorescence quencher C. (B) Real-time monitoring of the fluorescence increase due to the binding-induced TWJ. The positive control (P.C.) contained 10 nM probe T_8C_{20} and 20 nM $T^*C^*:C$ in TE–Mg buffer. The negative control (N.C.) contained only 20 nM $T^*C^*:C$ in TE–Mg buffer. The tested concentration range of the target streptavidin was from 0.16 nM to 10 nM. (C) Increases in fluorescence signals as a function of the concentration of streptavidin. Fluorescence was measured after the reaction mixture was incubated at 25 °C for 60 min.

2.3.2 Assay for human α -thrombin

To explore the versatility of our approach further, we constructed another binding-induced TWJ sensor for the detection of human α -thrombin (Figure 2-4). We chose two DNA aptamers that can bind specifically to two distinct binding epitopes on the same thrombin molecule. We directly extended the sequences of the two aptamers (underlined in Table 2-1) by including the sequences of DNA motifs **TB** and **B*C**, respectively. Similar to the detection of PSA, we used the DNA motif **T*C*:C** that was labeled with fluorescent FAM on the **T*C*** strand and a quencher on the complementary **C** strand. Initially, the fluorescence of the DNA motif **T*C*:C** was quenched. However, the binding of the target thrombin to the two aptamers brings **TB** and **B*C** to the same molecule, forming the FAM-labeled binding-induced TWJ (**TB:B*C:T*C***) and simultaneously releasing the quencher-labeled **C** (Figure 2-4A).

Release of the quencher-labeled **C** leaves the binding-induced TWJ fluorescent. The fluorescence increase, measured in real-time, reflects the amount of the target thrombin in the sample. As shown in Figure 2-4B, a calibration between the fluorescence intensity (background subtracted) and the concentration of thrombin is linear within the range of concentrations tested (50 pM to 30 nM, $r^2 = 0.9848$).

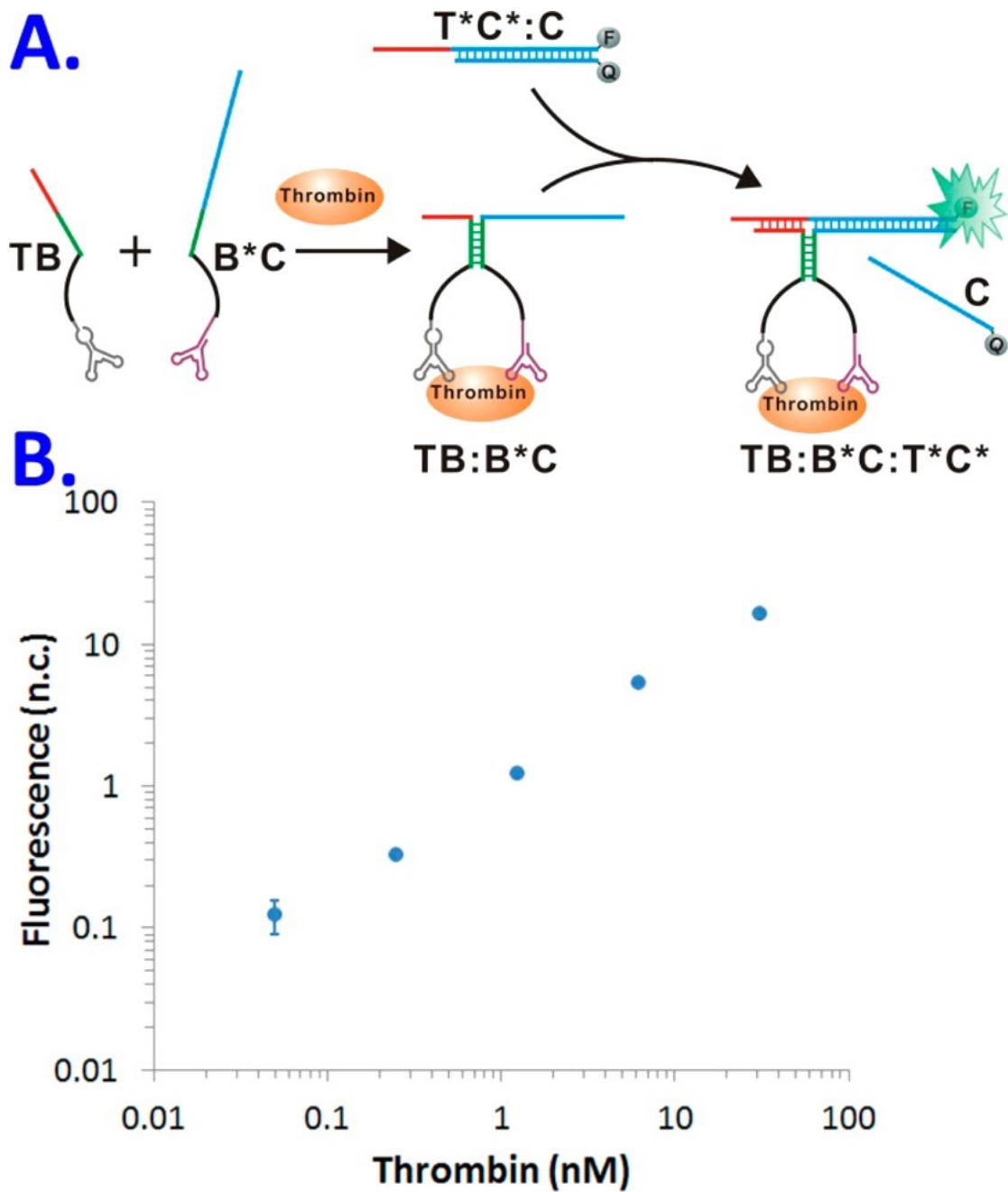


Figure 2-4. Detection of human α -thrombin using binding-induced TWJ. (A) Schematic showing the design of thrombin-responsive TWJ. (B) Increases in fluorescence signals as a function of concentration of thrombin in a buffer solution. Fluorescence measurements were taken at 60 min.

2.3.3. Key design parameters influencing the kinetics

The key to our success in constructing the real-time sensor for PSA is to achieve a fast DNA strand displacement between **TB:B*C** and **T*C*:C** upon the target binding while minimizing target-independent strand displacement. To fully understand the kinetics of the DNA strand displacement involved in the formation of binding-induced TWJ, we used streptavidin as a target and biotin as the affinity ligand to optimize the key reaction parameters.

By monitoring the released quencher-labeled **C** from **T*C*:C**, we confirmed the strand displacement between **TC** and **T*C*:C** (Figure 2-5). Using gel electrophoresis, we further characterized the oligonucleotides and their associated products that were involved in the formation of the binding-induced TWJ and the process of strand displacement. Figure 2-6 (Panels B and C) show the characterization of relevant oligonucleotides using polyacrylamide gel electrophoresis (PAGE). First, the same gels were imaged directly (Figure 2-6C), showing fluorescently labeled DNA, and then imaged again after staining with SYBR Gold (Figure 2-6B), showing all DNA. In the absence of the target streptavidin (Lane 4), the incubation of **TB**, **B*C**, **T*C*:C**, and an excess amount of **T*C*** for 30 min led to the formation of **TB:B*C:T*C*** (Figure 2-6B, Lane 4). There is no observable band corresponding to **C** from either the direct fluorescence imaging (Figure 2-6C, line 4) or imaging after staining (Figure 2-6B, lane 4), confirming no release of **C**. However, in the presence of the target streptavidin (Figure 2-6B, Lane 5), there is a strong band of the target-induced TWJ at the top of the lane and a clear band of **C**, indicating the formation of binding-induced TWJ and the strand displacement between **TB:B*C** and **T*C*:C**. In this set of experiments, fluorescence detection of the gels revealed only the fluorescent **C** and its

associated products, $T^*C^*:C$. Again, only in the presence of the target streptavidin, can the band of the released C be observed in the gel (Figure 2C, Lane 5). These results confirm the strand displacement between $TB:B^*C$ and $T^*C^*:C$ in response to the target binding. The use of an excess amount of T^*C^* in the experiments was to hybridize it to any free C in the absence of the target, thereby reducing the potential background.

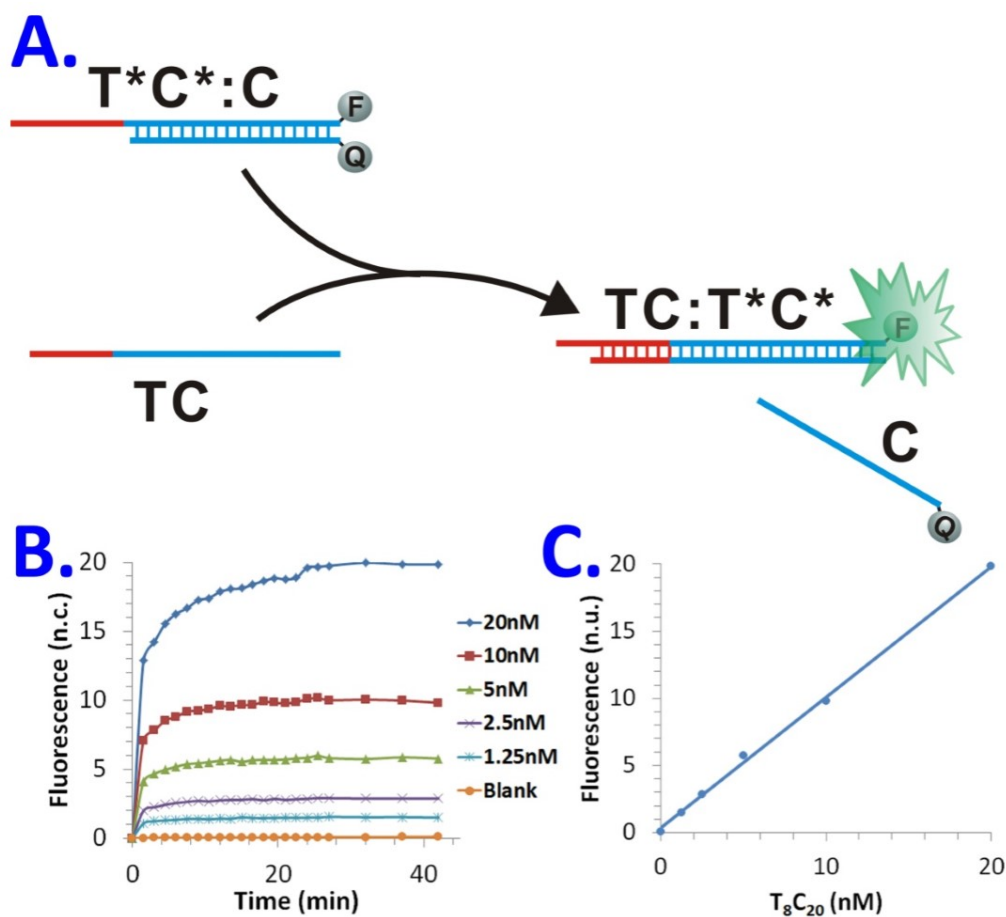


Figure 2-5. Monitoring the toehold-mediated DNA strand displacement. (A) Schematic showing the principle of toehold-mediated DNA strand displacement; (B) Kinetic profiles of toehold mediated DNA strand displacement obtained from the use of six different target concentrations; (C) Increase of fluorescence intensity as a function of the concentrations of the target DNA TC (T_8C_{20}). The reaction mixture contained 20 nM DNA probe $T^*C^*:C$ and varying concentrations of the target DNA TC .

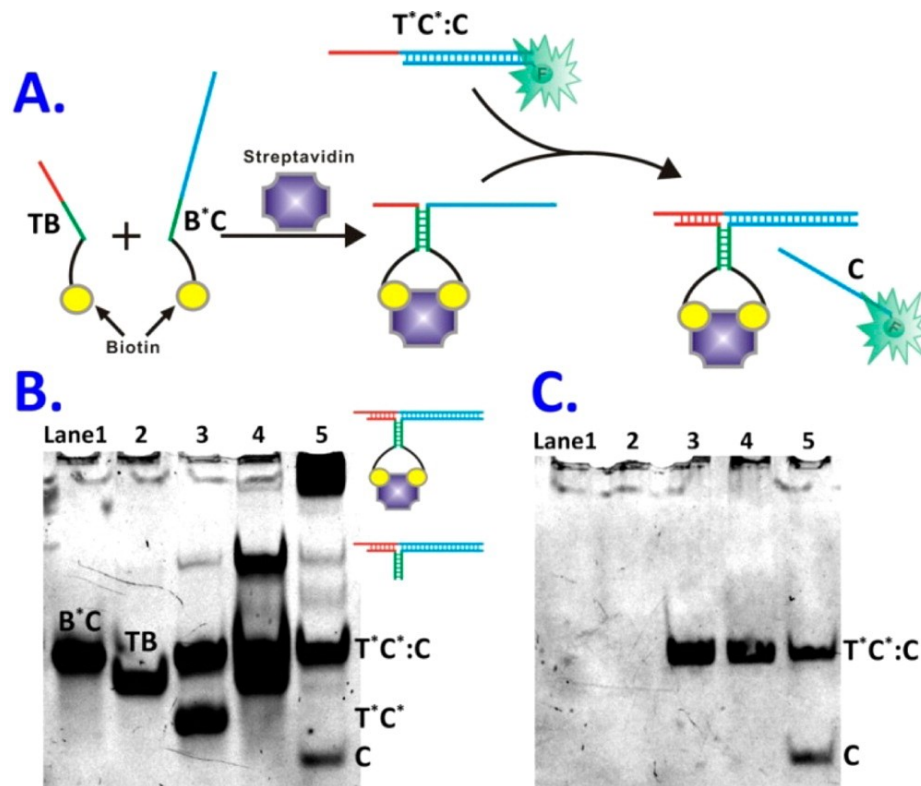


Figure 2-6. Characterization of the oligonucleotides involved in the formation of binding-induced TWJ and strand displacement. (A) Schematic showing that binding of the two probes to streptavidin triggers the formation of TWJ and the release of fluorescent oligo C. (B) Images of native PAGE gels after SYBR Gold staining. (C) Fluorescence images of native PAGE gels without staining. In this case, the bands correspond to FAM-labeled DNA. All native gel electrophoresis separations were performed at a potential of 12 V/cm. Lane 1 contained 2 μM B*C. Lane 2 contained 2 μM TB. Lane 3 contained 1 μM T*C*:C and 1 μM T*C*. Lane 4 was from the analysis of a mixture containing 2 μM B*C, 2 μM TB, 1 μM T*C*:C, and 1 μM T*C*. Lane 5 was from the analysis of a mixture containing 2 μM B*C, 2 μM TB, 1 μM T*C*:C, 1 μM T*C*, and 1 μM streptavidin. The addition of T*C* was to hybridize it to any free C, thereby reducing potential background.

In an effort to optimize the kinetics involved in the binding-induced TWJ processes, we designed the toehold domain **T** to have varying lengths from 6 nucleotides (nt) to 9 nt. As shown in Figure 2-7B, with the increase in the toehold length, the rate of fluorescence increase is accelerated 27×. This substantial enhancement is probably due to the increased kinetics for binding-induced strand displacement between **TB:B*C** and **T*C*:C¹²**. Increasing the length of the toehold further from 9 to 15 nt does not lead to a further increase in the reaction rate. Importantly, there is no noticeable background fluorescence signal increase for any of these designs, even after incubation for 150 min (Figure 2-7C), suggesting that our strategy is able to maintain an extremely low level of target-independent formation of TWJ.

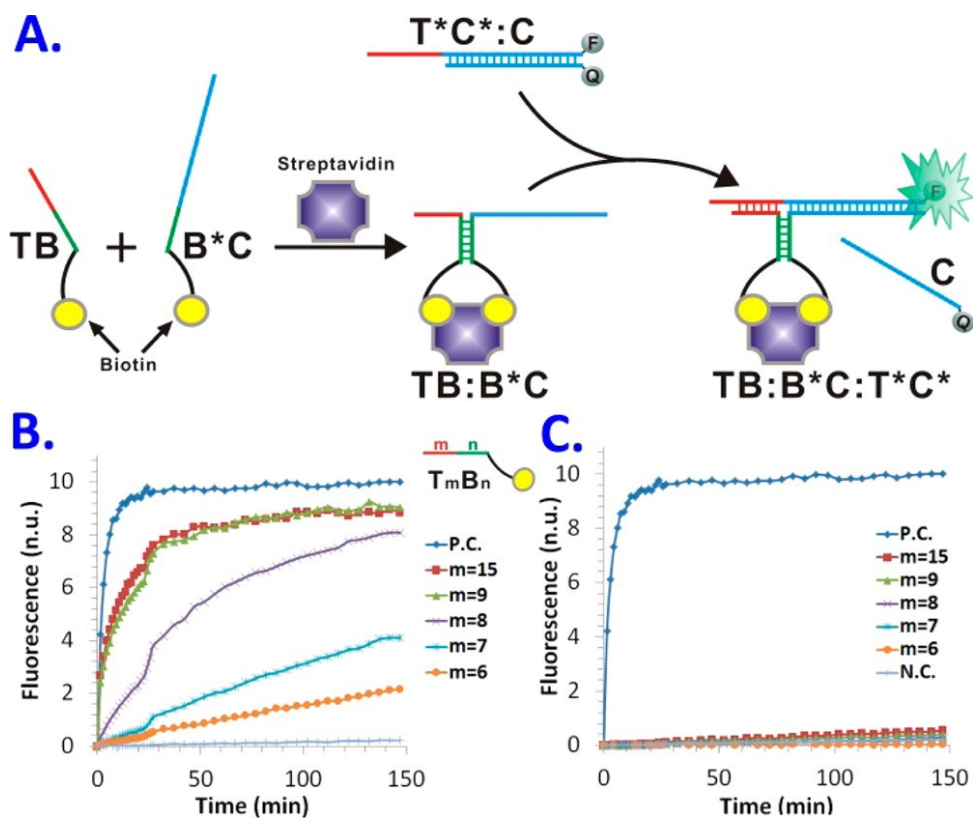


Figure 2-7. (A) Schematic showing the design for real-time monitoring of the formation of binding-induced TWJ. DNA motif **T*C*** was labeled with a fluorophore and motif **C** was labeled with a quencher. The fluorescently labeled **T*C*** was hybridized initially with **C**, thus its fluorescence was quenched by the quencher. Binding of the two biotinylated DNA motifs **TB** and **B*C** to the same target streptavidin triggered the formation of **TB:B*C:T*C*** TWJ and the simultaneous release of the quencher-labeled **C**, turning on the fluorescence. (B and C) Optimizing the kinetics of binding-induced TWJ (B) by using different designs of motif **TB** in the presence of 10 nM streptavidin and (C) in the absence of streptavidin. The length of the toehold domain **T** (m) was varied from 6 to 15 nt, and the length of domain **B** (n) was fixed at 6 nt. The positive control (P.C.) contained 10 nM probe **T₈C₂₀** and 20 nM **T*C*:C** in TE–Mg buffer. The negative control (N.C.) contained only 20 nM **T*C*:C** in TE–Mg buffer.

To maximize the speed of the binding-induced TWJ further, we increased the reaction temperature from 25 to 37 °C. As shown in Figure 2-8, the increase in the reaction temperature accelerated the formation of binding-induced TWJ ($k_{\text{obs}} = 1.58 \times 10^{-3} \text{ s}^{-1}$ at 37 °C and $k_{\text{obs}} = 0.60 \times 10^{-3} \text{ s}^{-1}$ at 25 °C). Over 90% fluorescence signal was generated within 10 min. Although target-independent strand displacement between **B*C** and **T*C*:C** may be expected to increase with the increase in reaction temperature, our results show no noticeable background fluorescence increase until after 60 min, providing a long enough time frame for its potential applications (e.g., biomolecular sensing or imaging).

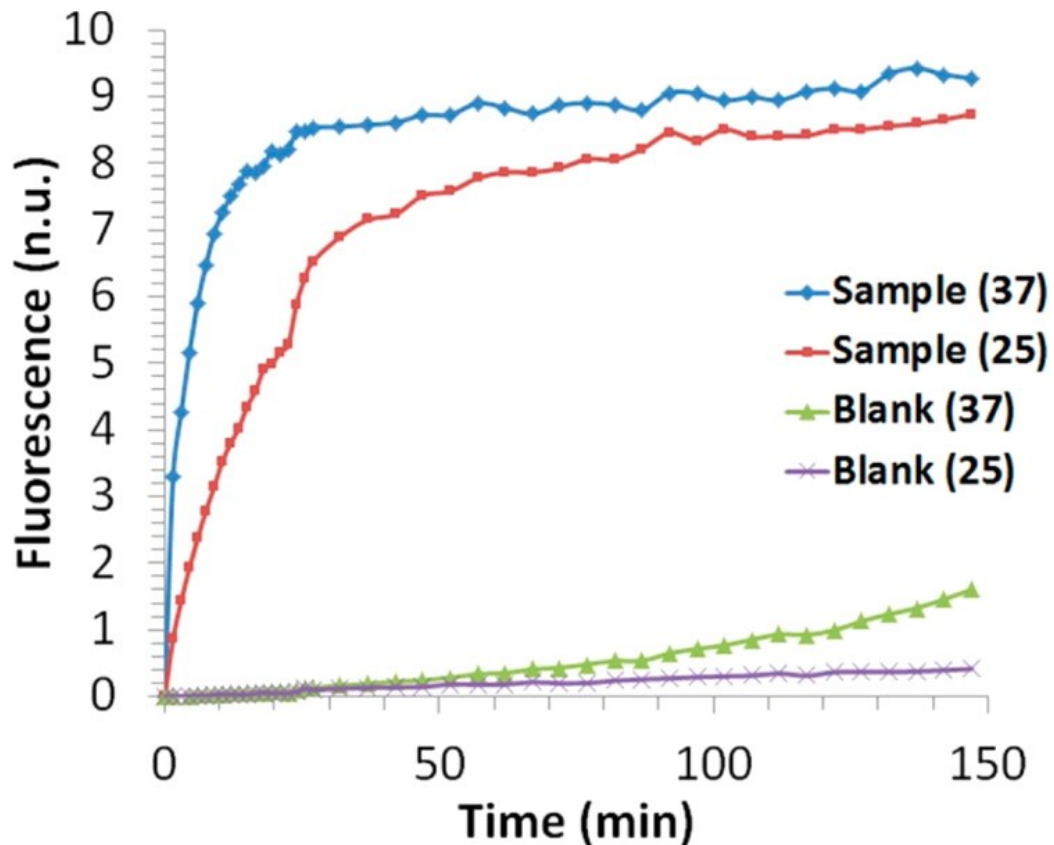


Figure 2-8. Effect of incubation temperature (37 and 25 °C) on the formation kinetics of binding-induced TWJ. The reaction mixture for the streptavidin sample contained 20 nM probe T*C*:C, 20 nM probe TB, 20 nM probe B*C, 10 nM target streptavidin, 50 nM ROX, 1 μ M polyT oligo, and TE-Mg buffer. In the blank, all reagents were the same as in the sample solution, except that there was no streptavidin added.

2.3.4. Comparison with DNA strand-displacement strategies

Our success in constructing protein-responsive TWJs suggests that this strategy potentially could be adapted to existing dynamic DNA assemblies, including DNA logic gates^{13, 86}, molecular translators^{16, 38, 87}, stepped DNA walkers⁸⁸⁻⁹⁰, and autonomous DNA machines⁹¹. To explore this potential, we compared our technique (b) with three other widely used DNA strand displacement strategies (Figure 2-9), a toehold-mediated DNA strand displacement (a)¹², an associative DNA toehold (also known as combinatorial toehold)-mediated strand displacement (c)^{21, 84-85}, and binding-induced DNA strand displacement (d)⁸³. For a meaningful comparison, we used the identical duplex sequences (blue color) for all four techniques. In addition, (a–c) have the same DNA toehold sequences (red color); (b and d) have the same linker length (black color). Results in Figure 2-9B show the kinetic profiles of four DNA strand-displacement techniques in the presence of a 10 nM target DNA or protein. In comparison to other techniques, our strategy (b) exhibited fast reaction kinetics (ranked as the second fastest displacement reaction in Figure 2-9B) and an extremely low background from the target-independent displacement (Figure 2-9C). The toehold-mediated DNA strand displacement (a) and the associative (combinative) toehold-mediated DNA strand displacement (c) have been used successfully in dynamic DNA assemblies. With a kinetic profile positioned between those two successful techniques (Figure 2-9B), our binding-induced TWJ technique (b) can also have great potential to be applied in dynamic DNA assemblies. Importantly, the binding-induced TWJ broadens the scope of dynamic DNA assemblies beyond DNA and to assemblies triggered by protein binding.

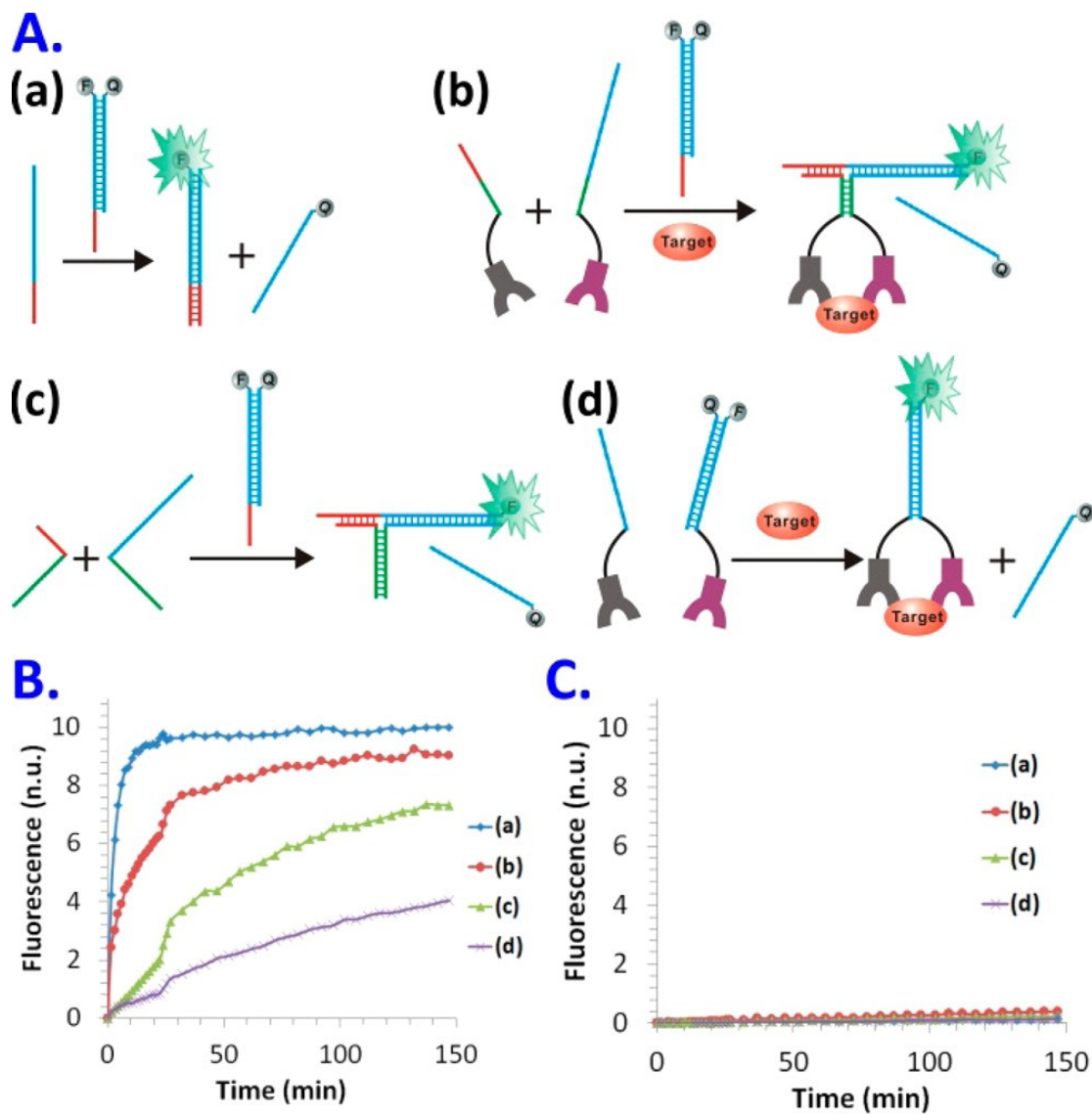


Figure 2-9. Comparison of four different DNA strand-displacement strategies and their kinetic profiles. (A) The four available strand-displacement strategies: (a) toehold-mediated DNA strand displacement, (b) binding-induced TWJ, (c) DNA strand displacement mediated by associative DNA toehold, and (d) binding-induced DNA strand displacement. (B) Kinetic profiles from the determination of 10 nM target using the four strand-displacement strategies. (C) Background fluorescence observed from comparing the four strand-displacement strategies. The observed rate constant k_{obs} was (a) 3.31×10^{-3} , (b) 0.61×10^{-3} , (c) 0.16×10^{-3} , and (d) $0.06 \times 10^{-3} \text{ s}^{-1}$.

2.4 Conclusions

We have developed a successful strategy to trigger the formation of DNA TWJs with specific proteins. The binding of two affinity ligands to the specific protein target triggers the assembly of DNA motifs and initiates the subsequent DNA strand displacement. Real-time fluorescence monitoring of the binding-induced TWJ provides sensitive detection of the specific proteins. A detection limit of 2.8 ng/mL was achieved for prostate-specific antigen, and 50 pM human α -thrombin was detectable. The ability to generate detection signals with high sensitivity and fast kinetics in homogeneous solutions with no need for enzymes or thermal cycling makes this technique ideal for many emerging applications, such as point-of-care disease diagnostics and molecular imaging in live cells. The new approach to accelerate DNA strand-displacement reactions through affinity binding to specific proteins opens up opportunities to expand the state-of-art DNA nanotechnology to proteins for diverse applications further.

Chapter Three: Protein and MicroRNA Detection Using a Binding-Induced DNA Three-Way Junction and Gold Nanoparticle Amplification by ICP-MS

3.1 Introduction

Binding-induced DNA TWJs have been studied and used to convert protein bindings to the formation of TWJs^{23, 92}. Proteins are not the only important biomarkers, miRNAs also play a significant role⁹³⁻⁹⁸. The aim of this chapter is to construct a binding-induced TWJ molecular translator and apply this technique to both protein and microRNA (miRNA) detection by using gold nanoparticle (AuNP) labeling inductively coupled plasma mass spectrometry (ICP-MS)^{59-60, 99-103}. The TWJ molecular translator is aimed at converting various input target molecules into a universal output DNA. After this, the quantitative information on each target can be obtained readily by measuring the amount of output DNA produced from the specific strand displacement reactions. AuNPs were chosen to label the output DNA. As a 20 nm size AuNP contains $\sim 2.4 \times 10^5$ gold atoms^{59, 104-105}, ICP-MS detection amplifies the gold signal, and the sensitivity is increased by using large AuNPs. In addition, ICP-MS can atomize the AuNPs directly¹⁰⁶⁻¹⁰⁸, and matrix interference can be avoided, reducing the background signal and improving the specificity.

MiRNAs play a significant role as important biomarkers. They are small, non-coding RNAs, and their lengths are normally 19–24 nucleotides¹⁰⁹⁻¹¹¹. MiRNAs widely exist in plants and animals¹¹²⁻¹¹⁵, some of them cause the breakdown of message RNA, and some are related to post transcriptional gene expression RNA silencing, recognized as regulators of gene expression during development and cell differentiation¹¹⁶⁻¹¹⁷. Furthermore, specific

miRNAs have been identified as being associated with various diseases¹¹⁸⁻¹²⁰. Due to their surprisingly high stability in plasma, miRNAs hold great promise as a new class of biomarkers of disease and downstream analyses. In this Chapter, the principle of this strategy is shown in Figure 3-1, and modified DNA probes was used to capture the target. In the presence of a target, two affinity ligand modified DNA probes can trigger a binding-induced TWJ. The formation of TWJs results in a DNA displacement from the double-strand output beacon, and a universal output DNA strand was released. The complementary sequence of output DNA strand was split from the middle into two probes, one binding on a MB and the other functionalized on an AuNP. In this case, the output DNA strand can link to both MB and AuNP by simultaneously hybridizing to these two individual complementary probes. After separating the MB-output DNA-AuNP reacted sandwich structures by washing away unreacted reactants, excess complementary DNA was added into the solution. It displaced the output DNA from the MB-output DNA-AuNP structures, and then AuNPs could be separated from MBs, diluted, and detected by ICP-MS^{59, 121}.

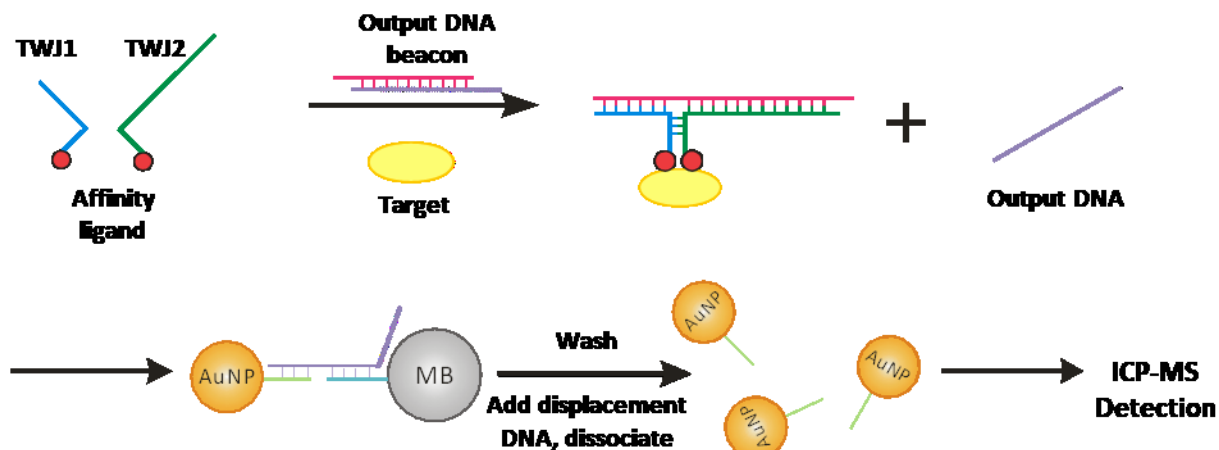


Figure 3-1. Schematic diagram showing the design for target protein detection using a DNA TWJ and AuNP amplification by ICP-MS. The TWJ1 probe and TWJ2 probe are labeled with affinity ligands to form a binding-induced TWJ structure that resulted in the displacement of the output DNA. The universal output DNA released in solution linked with both MB and AuNP by simultaneously hybridizing to these two individual complementary probes. After separating the MB-output DNA-AuNP reacted sandwich structures by washing away unreacted reactants, excess displacement probe, which had complementary output DNA sequence, was added into the solution. It displaced the output DNA from the MB-output DNA-AuNP structure, and then AuNPs could be separated from MBs, diluted, and detected by ICP-MS.

3.2 Experimental

3.2.1 Materials and reagents

Streptavidin from *Streptomyces avidinii* (product number: 189730), biotin (product number: B4501), bovine serum albumin (BSA, pH 7, $\geq 98\%$, product number: A7906), nitric acid (ACS reagent, $\geq 90.0\%$), magnesium chloride solution (1.00 ± 0.01 M, product number M1028), sodium chloride solution (5M, 0.2 μm filtered, product number: S5150), Trizma® hydrochloride ($\geq 99.0\%$, product number: T5941) buffer, phosphate buffered saline (PBS, pH 7.4, 10 x concentrate, product number: P5493), and 100 μL blunt tip CTC LC syringes (Hamilton®, needle size 22s ga, produce number: 2964-U) were purchased from Sigma-Aldrich.

Solutions of AuNPs (20 nm in diameter, product number: 15705) were purchased from Ted Pella, Inc. Streptavidin C1 MBs were purchased from Thermo Fisher Scientific, Inc. Ultrapure Milli-Q water system purified Nano pure H₂O (> 18.0 M Ω) was used for all dilutions and experiments.

All DNA and RNA samples were purchased from Integrated DNA Technologies, Inc. with HPLC purification. The DNA and RNA sequences and modifications are listed in Table 3-1.

Table 3-1. DNA sequences and modifications for constructing the binding-induced TWJ molecular translator for (A) streptavidin detection and (B) DNA sequences and modifications for human α -thrombin detection. (C) DNA and RNA sequences and modifications for miRNA 10b and miRNA 128 detection

(A)

Probe name		Sequences and modifications
TWJ1	TWJ1-9	5'- Biotin - TTT TTT TTT TTT TTT TTT TT - ACG AGT C - TT - GGT CTT CTG -3'
	TWJ1-11	5'- Biotin - TTT TTT TTT TTT TTT TTT TT - ACG AGT C - TT - GGT CTT CTG TA -3'
TWJ2		5'- CTT GTA GAC TAG CAT GAA CTA TCG - G ACT CGT -TTT TTT TTT TTT TTT TTT TT - Biotin -3'
Output		5' - TGT ACG ACT CTG ACT - CTT GTA GAC TAG CAT GAA CTA TCG -3'
Output beacon 1*		5' - CTA CAG AAG ACC - CGA TAG TTC ATG CTA GTC TAC AAG - 3'
MB-linker		5' - Biotin - TTT TTT TTT TTT TTT - ATG CTA GTC TAC AAG - 3'
AuNP-linker		5' - AGT CAG AGT CGT ACA - TTT TTT TTT TTT TTT - Thiol - 3'
F(AM)		5' - C ATG CTA - GTC TAC AAG - AGT CAG AGT CGT ACA - FAM - 3'
Q(uencher)		5' - Quencher - TGT ACG ACT CTG ACT - CTT GTA GAC - 3'
Output*		5' - CGA TAG TTC ATG CTA GTC TAC AAG - AGT CAG AGT CGT ACA -3'

(B)

Probe name	Sequences and modifications
TWJ1-TBA15	5' - <u>GGT TGG TGT GGT TGG</u> - TTT TTT TTT TTT TTT TTT TT - ACG AGT C - TT - GGT CTT CTG - 3'
TWJ2-TBA29	5' - CTT GTA GAC TAG CAT GAA CTA TCG - G ACT CGT -TTT TTT TTT TTT TTT TTT TT - <u>AGT CCG TGG TAG GGC AGG TTG GGG</u> <u>TGA CT</u> - 3'
TWJ1-TBA29	5' - <u>AGT CCG TGG TAG GGC AGG TTG GGG TGA CT</u> - TTT TTT TTT TTT TTT TTT TT - ACG AGT C - TT - GGT CTT CTG - 3'
TWJ2-TBA15	5' - CTT GTA GAC TAG CAT GAA CTA TCG - G ACT CGT -TTT TTT TTT TTT TTT TTT TT - <u>GGT TGG TGT GGT TGG</u> - 3'

(C)

Probe name	Sequences and modifications
MicroRNA 10b	5' - UA CCC UGU AGA AC - C GAA UUU GUG - 3'
DNA target 10b	5' - TA CCC TGT AGA AC - C - GAA TTT GTG - 3'
TWJ2-10b	5' - CTT GTA GAC TAG CAT GAA CTA TCG - TT - GT TCT ACA GGG TA - 3'
Output beacon 2*	5' - CAC AAA TTC - G - CGA TAG TTC ATG CTA GTC TAC AAG - 3'
MicroRNA 128	5' - U CAC AGU GAA CC - G - GUC UCU UUU - 3'
DNA target 128	5' - T CAC AGT GAA CC - G - GTC TCT TTT - 3'
TWJ2-128	5' - CTT GTA GAC TAG CAT GAA CTA TCG - TT - GG TTC ACT GTG A - 3'
Output beacon 3*	5' - AAA AGA GAC - C - CGA TAG TTC ATG CTA GTC TAC AAG - 3'

3.2.2 Preparation of DNA linker functionalized AuNPs

The thiolated AuNP-linker probe was received in a disulfide form. To activate this probe, it was diluted to 50 μM with 5mM TCEP and 100 mM Tris-HCl buffer for 1 h at room temperature. Then, 20 μL activated **AuNP-linker** probes were added to a 1 mL AuNPs solution (the ratio of **AuNP-linker** : AuNP is 1000 : 1) and incubated for 5 min. A 20 μL of Tween-20 solution were mixed with this solution, followed by 1 min sonication. This mixture was placed at room temperature for 1 h, and 350 μL of 5 M NaCl were added slowly and sonicated for 1 min. This solution was incubated at room temperature for 1 h, and a 1 min sonication was repeated three times at 20 min intervals. These steps can maximize the probe loading amounts and prevent the AuNPs aggregation at high levels of salt concentration. Centrifuge conditions and timing were adjusted accordingly, based on the supernatant colour. First, the solution was centrifuged at 10,000 rpm for 5 min, and if there was still a faint red colour in the solution, it was centrifuged for an extra 1 min to separate the AuNPs from nonreacted reagents. The supernatant was removed, and 1 mL of 10 mM Tris-HCl (pH 7.4) containing 0.05% Tween-20 was added as washing buffer. It was sonicated until all particles were dispersed well in the solution. This process was repeated two more times with the centrifuge conditions changed to 13,000 rpm for 15 min, then the AuNPs were resuspended in 200 μL of washing buffer. The **AuNP-linker** DNA-AuNPs solution was stored at 4 $^{\circ}\text{C}$ when it was not in use. It was found to be stable for at least two weeks.

3.2.3 Preparation of DNA linker functionalized MBs

The **MB-linker** probe was biotinylated by IDT Inc. To immobilize biotinylated MB-linker

probes on the streptavidin coated MBs, 200 μL of 10 mg/mL MBs were washed with 200 μL buffer A (50 mM Tris-HCl, pH 7.4, 2 M NaCl, 0.1% Tween-20) and resuspended in 100 μL buffer A. The maximum binding of the MBs are 500 nM single-strand oligonucleotides, so 10 μL of 50 μM **MB-linker** probe were diluted to 100 μL , followed by mixing with 100 μL washed MBs. This solution was incubated at room temperature using gentle rotation for 2 h. Then, the tube was placed in a magnet for 2–3 min, the biotinylated **MB-linker** probe coated MBs were separated, and the supernatant containing unreacted reagents was discarded. The functionalized MBs were washed three times with buffer B (20 mM Tris-HCl, pH 7.4, 140 mM NaCl, 5 mM KCl, 1 mM MgCl_2 , 1 mM CaCl_2) and resuspended in 200 μL of buffer B. The final concentration of **MB-linker** DNA-MBs solution was 10 mg/mL; the solution was stored at 4 $^\circ\text{C}$ when it was not in use.

3.2.4 Preparation of probes and beacons for binding-induced three-way junctions

To prepare the output beacon for TWJs formation and target detection, a final concentration of 5 μM solution was prepared by mixing 20 μL of 50 μM output DNA with a 50 μM output beacon* probe. In the solution, the amount of output beacon* probe was always equal to or higher than the amount of output DNA, and the different ratios between the output probe and output beacon* probe were achieved by adding various amounts of output beacon* probe. For example, a 1:1 ratio output beacon contained 20 μL of 50 μM output beacon* probe and 20 μL of 50 μM output DNA in 160 μL PBS (1xPBS, 10 mM MgCl_2 , 0.1% Tween-20) buffer. The solution was heated at 90 $^\circ\text{C}$ for 5 min and allowed to anneal slowly down to 25 $^\circ\text{C}$ over a period of 1.5 h. For a 1:1.1 ratio output beacon, 22 μL of 50 μM output beacon* probes were added to 158 μL of PBS buffer with 20 μL of 50 μM output DNA; for

a 1:1.2 ratio output beacon, 24 μL of 50 μM output beacon* probes were added to 156 μL of PBS buffer with 20 μL of 50 μM output DNA. Other ratio output beacons were prepared in a similar way.

FQ beacon, an indicator for testing the existence of displaced output DNA from the formation of TWJs, was also prepared at a final concentration of 5 μM by adding 20 μL of 50 μM of FAM-labeled DNA (**F**) and 20 μL of 100 μM quencher-labeled DNA (**Q**) to 160 μL of PBS buffer. The mixture was heated to 90 $^{\circ}\text{C}$ for 5 min and cooled down slowly to 25 $^{\circ}\text{C}$ over a period of 1.5 h. The ratio between **F** and **Q** was kept at 1:2 to fully quench the fluorescent labeled probe and minimize the background fluorescence.

3.2.5 Monitoring the salt effects on TWJ formation and output DNA displacement using fluorescence

To study the salt effects on TWJs formation and output DNA displacement, different concentrations of magnesium and sodium were added to the reaction buffer (1 x PBS buffer with 0.05% Tween 20); the concentration of Mg^{2+} was 5–40 mM, and Na^{+} was 100–300 nM. All test conditions responded to 1 nM target protein streptavidin. A 10 μL of 20 nM TWJ1 probe and an equal amount of TWJ2 probe were mixed together with 10 μL of 200 nM output beacon and then diluted in a microplate using different salt concentrations of reaction buffer to a final volume of 100 μL . A 10 μL of 200 nM FQ beacon were added finally as the fluorescent signal indicator. All probes were diluted using their reaction buffer with a specific salt concentration. Fluorescence was measured directly from the microplate using a multimode microplate reader (FilterMax 5, Molecular Devices, LLC.). The excitation/emission for the FAM-labeled DNA probes was 485/535 nm. To monitor the

kinetic process of output DNA displacement reaction, we measured the fluorescence of the reaction mixture every three min for 90 min.

3.2.6 Detection of output DNA using AuNP amplification by ICP-MS

An Agilent 7500cs octupole reaction system ICP-MS was used for AuNPs detection. It was operated in helium mode. Manual injection of 50 μL samples each time were done with a Rheodyne six-port injector (Model 7725i, Rheodyne, CA, USA).

For output DNA detection using AuNP amplification by ICP-MS, the MB-linker probe functionalized MBs were diluted to 2 mg/mL in buffer B (20 mM Tris-HCl, pH 7.4, 140 mM NaCl, 5 mM KCl, 1 mM MgCl_2 , 1 mM CaCl_2). Varying concentrations of the output DNA were mixed with 10 μL of 2 mg/mL MB-linker MBs to a final volume of 100 μL solution in the PCR tubes and gently rotated at room temperature over 30 min. The tube was placed in a magnet shelf for 2–3 min, the MBs were separated, and the supernatant containing unreacted substrates was discarded. Washing buffer (1 x PBS, 10 mM MgCl_2 , 0.1% Tween 20) was used to wash the output DNA captured MBs three times. The solution was resuspended in 90 μL of washing buffer, and 10 μL of 5 nM AuNP-linker probe functionalized AuNPs were added, with gentle rotation over 30 min. A magnet shelf was used to separate the MBs, the supernatant with unreacted probes and AuNPs was discarded, and the MBs were washed five times with washing buffer. Then, 100 μL of 50 nM output* probes were added to displace the output DNA that binds on both AuNPs and MBs, releasing the AuNPs. The mixture was rotated over 45 min. The output* probe was diluted using a dilution buffer (50 mM Tris-HCl, 10 mM MgCl_2 , 0.1% Tween 20). The tube was placed on a magnet shelf for 2–3 min, the MBs were separated and discarded, and the supernatant was

moved to another tube that contained 100 μ L dilution buffer. These solutions were the samples for ICP-MS, and for each sample, triplicate incubations were conducted.

An Agilent 7500cs ICP-MS octupole reaction system was used for the elemental analysis of AuNPs. The operating parameters of ICP-MS are summarized in Table 3-2. Prior to the ICP-MS analysis, the positions of the torch, the nebulizer gas flow, and the lens were optimized using the tuning solution (1 μ g/L each of Li, Mg, Y, Ce, Tl, Co in 2% nitric acid, obtained from Agilent). A 50 μ L sample was injected each time using a Rheodyne six-port injector (Model 7725i, Rheodyne, Rohnert Park) to a 1% HNO₃, 0.5% bovine serum albumin (BSA) carrier stream. Triplicate injections were analyzed for one sample incubation. A peristaltic pump (Mandel Scientific, Ontario, Canada) operating at a flow rate of 1.5 mL/min was used to deliver the carrier and the sample solution. A Teflon tubing (0.3 mm i.d., Supelco) was used to connect the sample injector to the ICP-MS system.

Table 3-2. Operating parameters of ICP-MS

Parameter	Value
RF power	1500 W
RF Matching	1.55 V
Argon carrier gas	0.95 L/min
Argon makeup gas	0.1 L/min
Helium gas	4 mL/min
m/z	197
Integration time per point	0.1 s

3.2.7 Detection of human α -thrombin and streptavidin using the TWJ and AuNP amplification by ICP-MS

For a typical detection of thrombin using TWJ and AuNP amplification, we mixed a 100 μ L reaction mixture that contained a 2 nM 15-nucleotide thrombin-binding-aptamer (TBA) modified **TWJ1** and an equal amount of 29-nucleotide TBA modified **TWJ2**, 10 nM **output** DNA and **output beacon 1*** probe prehybridized output beacon, varying concentrations of the target thrombin proteins, and reaction buffer (1 x PBS, 10 mM MgCl₂, 0.05% Tween 20). The mixture was incubated at room temperature over 60 min. Then, 10 μ L of 2 mg/mL MB-linker functionalized MBs were added to the solution, with gentle rotation for 30 min. A magnetic shelf was used to separate and remove unreacted reagents from MBs, the solution was washed three times using washing buffer, resuspended to 100 μ L using washing buffer, and 10 μ L of 5 nM AuNP-linker AuNPs were added. The reaction mixture was rotated over 30 min, placed on a magnetic shelf again for 2–3 min, washed five times to remove the unreacted probes and AuNPs, and resuspended in 100 μ L dilution buffer containing 50 nM displacement **output*** probe, with gentle rotation over 30 min. The MBs were discarded using a magnetic shelf, and the supernatant was removed to another tube that contained 100 μ L dilution buffer. These solutions were the samples for ICP-MS, and for each sample, triplicate incubations were conducted.

A 50 μ L sample of the mixture was injected to ICP-MS each time. The Au element concentration in the solution was measured using the carrier and ICP-MS operating parameters, as described above.

A streptavidin detection using a 100 μ L reaction mixture contained 2 nM biotin labeled TWJ1 and TWJ2 probes instead of TBA modifications. All the other beacon probes and

buffer remained the same. Varying concentrations of streptavidin were tested.

3.2.8 Detection of miRNA using the TWJ and AuNP amplification by ICP-MS

For a typical miRNA 10b detection, a 100 μ L reaction mixture contained 20 nM TWJ2-10b and 10 nM output beacon (prehybridized output DNA with output beacon 2* probe), varying concentrations of miRNA 10b, and reaction buffer (1 x PBS, 10 mM MgCl₂, 0.05% Tween 20). The mixture was incubated at room temperature for 12 h. Then, 10 μ L of 2 mg/mL MB-linker functionalized MBs were added to the solution, with gentle rotation over 30 min. A magnetic shelf was used to separate and remove unreacted reagents from MBs, the solution was washed three times using washing buffer, resuspended to 100 μ L, and 10 μ L of 5 nM AuNP-linker AuNPs were added. It was rotated over 30 min, placed on a magnetic shelf again for 2–3 min, and washed five times to remove unreacted probes and AuNPs. It was resuspended in a 100 μ L dilution buffer containing 50 nM displacement output* probe, with gentle rotation over 30 min. The MBs were separated and discarded using a magnetic shelf, and the supernatant was removed to another tube that contained a 100 μ L dilution buffer. These solutions were the samples for ICP-MS, and for each sample, triplicate incubations were conducted. A 50 μ L of the mixture were injected to ICP-MS each time. The Au element concentration in the solution was measured using the carrier and ICP-MS operating parameters, as described above.

For detection of miRNA 128, a 20 nM TWJ2-128 probe and a 10 nM output beacon (prehybridized output DNA with output beacon 3* probe) were reacted with target miRNA 128 in a 100 μ L reaction mixture. All the other beacon probes and buffer remained the same. Varying concentrations of miRNA 128 were tested.

3.3 Results and Discussion

3.3.1 Key design parameters influencing TWJs formation and displacement

We first designed a streptavidin target protein detection system to test the feasibility and study the key parameters influencing the binding-induced TWJs formation and reaction. By using two biotinylated TWJ probes, the binding of streptavidin to two biotin molecules brings the **TWJ1** and **TWJ2** probes together. This complex reacted with the output beacon and formed the binding-induced TWJ (**TWJ1:TWJ2:output beacon 1***), acting as a molecular translator and displaced the output DNA. In the presence of output DNA, a displacement happened to the **FQ** beacon. Initially, the FAM-labeled probe was hybridized with the quencher-labeled probe, and the fluorescence was quenched. After displacement, the quencher-labeled probe was released, the FAM-labeled probe hybridized with the output DNA and became fluorescent again (Figure 3-2). By monitoring the fluorescent signal in solution, the amount of the released **output** DNA was quantified in real-time.

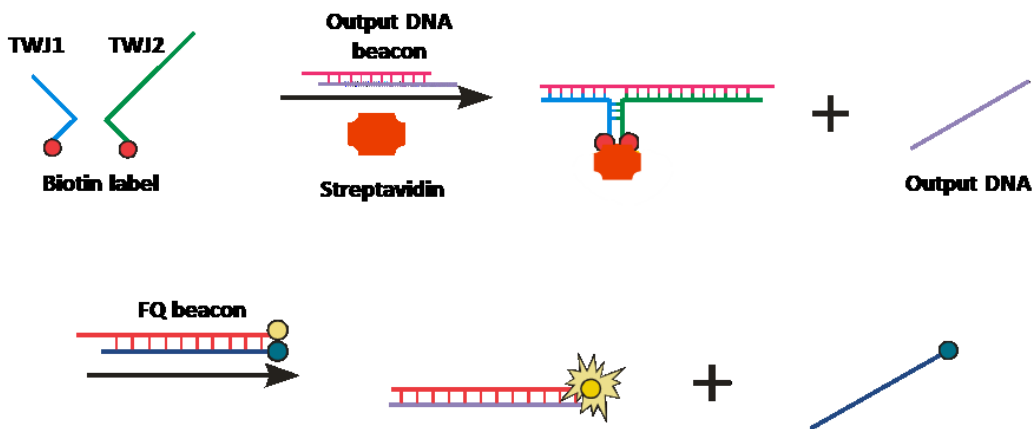


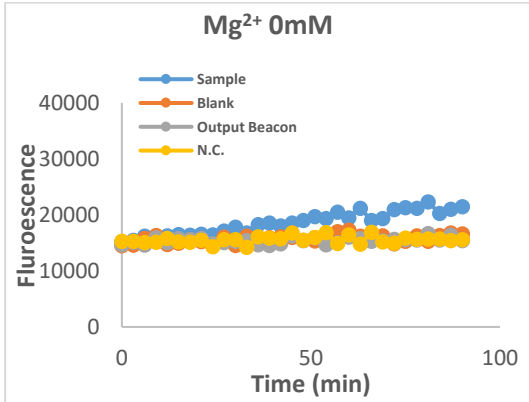
Figure 3-2. Schematic illustration of the streptavidin-biotin responsive binding-induced TWJ displaced output DNA detection. TWJ1 and TWJ2 probes were biotinylated, binding with streptavidin, and formed the binding-induced TWJ (TWJ1:TWJ2: output beacon 1*). The output DNA was displaced from the output beacon and released in solution. The presence of the output DNA triggered displacement of the quencher-labeled probe from the FQ beacon. As a result, the FAM-labeled probe was no longer quenched, and a fluorescent signal was generated.

Various metal ions affect oligonucleotide duplexes and protein-DNA binding stability. To compare the influence from both divalent cation and monovalent cation, we chose the most commonly applied ions, magnesium and sodium. We used identical reaction conditions and concentrations of substrates, except for the reaction buffer, for comparison. A 1 nM streptavidin was incubated with 2 nM TWJ1 and 2nM TWJ2 probes in a PCR tube, then a 20 nM **output** beacon and a 20 nM **FQ** beacon were added. The reaction mixture was transferred into a 96-well microplate, and fluorescence was measured every three min over 90 min using the multimode microplate reader. By monitoring the increased fluorescent

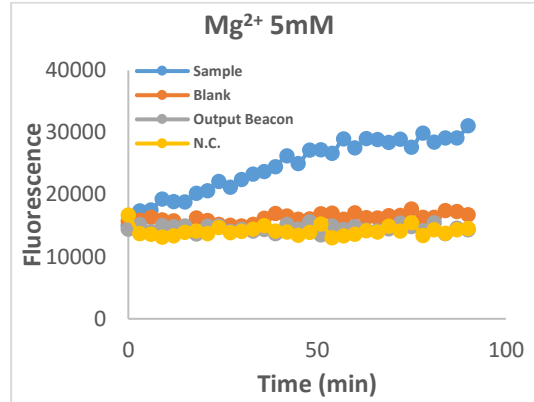
signal from the FAM-labeled probes that displaced from the **FQ** beacon, we confirmed that the strand displacement happened in the output beacon and output DNA were present in the solution. The output beacon signal containing 20 nM **output** beacon, and 20 nM **FQ** beacon worked as a background control. In the absence of target proteins and TWJ probes, the output beacon had little influence to generate the fluorescent signal. The negative control contained only a 20 nM **FQ** beacon in the reaction buffer, with different concentrations of salt ions.

Both Na^+ and Mg^{2+} helped the formation and stability of the oligonucleotides complex. When Na^+ and Mg^{2+} are added to a solution, the stability of complex TWJ structures increases until a maximum is reached. The peaks of maximum stability are wide and sequence dependent, especially related to the percentage of G-C base pairs. Higher concentrations of Na^+ increased the oligonucleotides hybrid stability nonlinearly. However, higher Mg^{2+} concentrations destabilized the hybridized oligonucleotides slightly (Figure 3-3A–E). Therefore, we tested different concentrations of Na^+ and Mg^{2+} reaction buffer. Compared to ~10 times higher concentrations of Na^+ , a Mg^{2+} reaction buffer generated a higher fluorescent sample signal (Figure 3-3F and G). Also, the higher the concentration of Mg^{2+} , the faster the reaction rate. A 10 mM or higher concentration of Mg^{2+} reaction buffer reached a plateau at 60 min. All the blank signals remained at the negative control background level, but they increased slightly when higher concentrations of Mg^{2+} were in the buffer, indicating that high concentrations of Mg^{2+} also stabilized the target-independent oligonucleotide complex and generated a background signal.

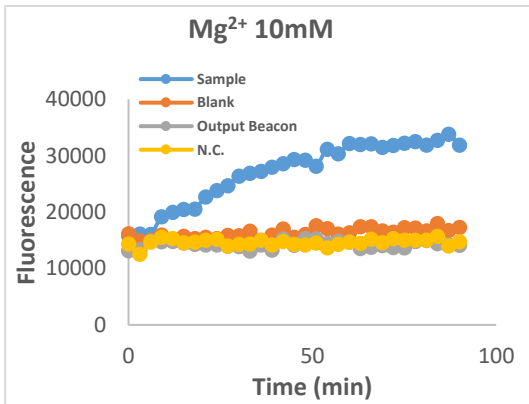
(A)



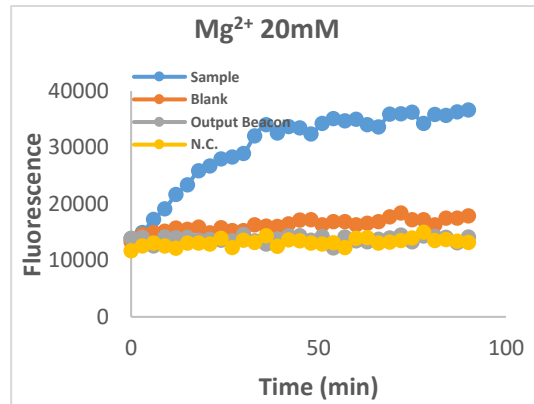
(B)



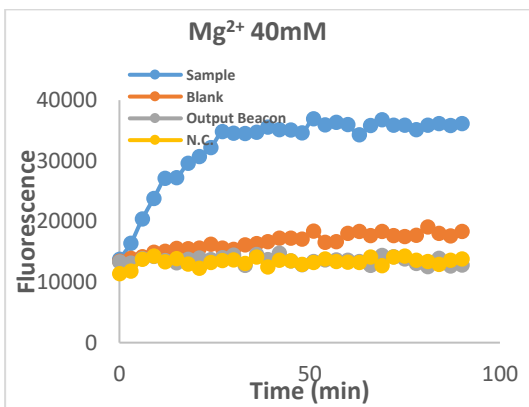
(C)



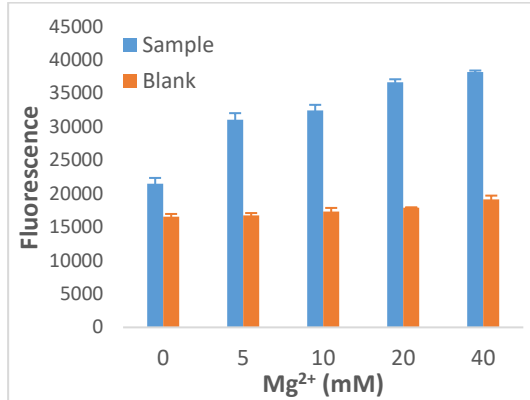
(D)



(E)



(F)



(G)

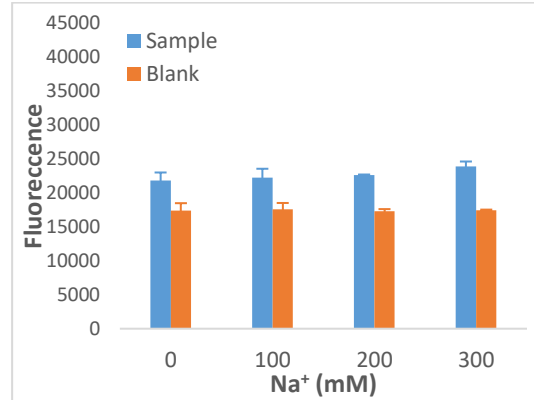


Figure 3-3. Salt effects of Mg^{2+} and Na^+ ions in the reaction buffer. The reaction signal responded to 1 nM streptavidin with 2 nM TWJ1 and TWJ2 probes, 20 nM output beacon (output DNA:output beacon1*), and 20 nM FQ beacon. (A-E) Kinetic studies of Mg^{2+} concentration effects on binding-induced TWJ formation and molecular translation. Varying concentrations of Mg^{2+} (0–40 nM) were added in the reaction buffer (1 x PBS, 0.05% Tween 20). Fluorescence was from the displaced FAM-labeled probe at room temperature. (F-G) Comparison of different concentrations of Mg^{2+} (0–40 nM) and Na^+ (0–300 nM) reaction buffer. Fluorescence measurements were taken at 90 min.

To optimize the binding-induced TWJ displacement efficiency, the toehold domain in **TWJ1** was designed to have different lengths; one is 9 nucleotides (nt), the other is 11 nt. As shown in Figure 3-4, the longer the toehold domain length, the faster the reaction rate of fluorescence and the higher the sample signal at the plateau. These results are likely due to the increased kinetics for binding-induced TWJ formation and the displacement of the output beacon. However, the background fluorescent signal also slightly increased when using a longer toehold **TWJ1-11** probe, suggesting that with higher T_m and a more stable DNA duplex formed at the toehold domain, target-independent displacement of the output beacon happened.

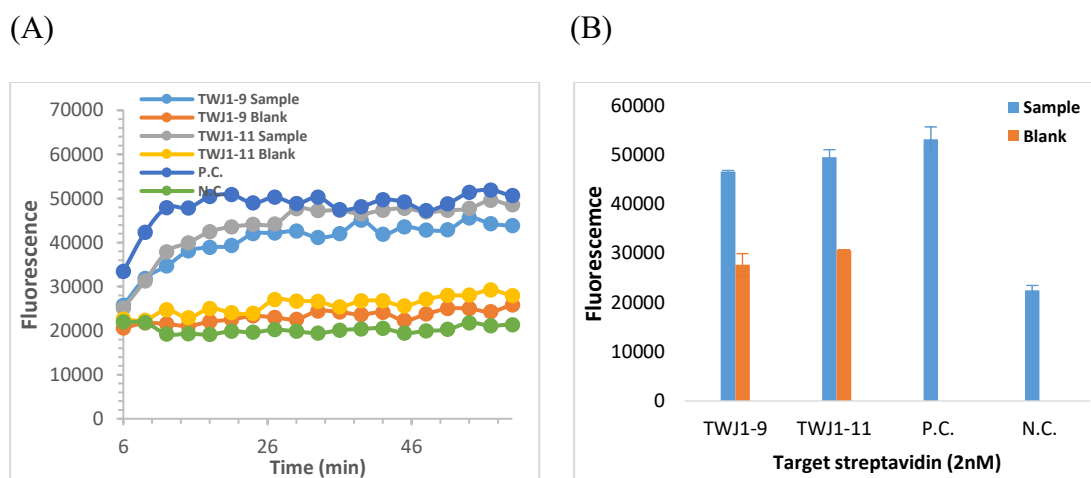


Figure 3-4. Optimization of the binding-induced TWJs by using different designs of TWJ1 probes in the presence of 2 nM streptavidin. The length of the TWJ1 probe toehold domain to displace the output DNA from the output beacon was designed to 9 nucleotides and 11 nucleotides. (A) Kinetic studies of the output DNA displacement obtained from different lengths of TW1 probes, forming binding-induced TWJ. (B) Fluorescence measurements were taken at 60 min. After mixing and incubating the reagents for 6 min, the signals were started to collect.

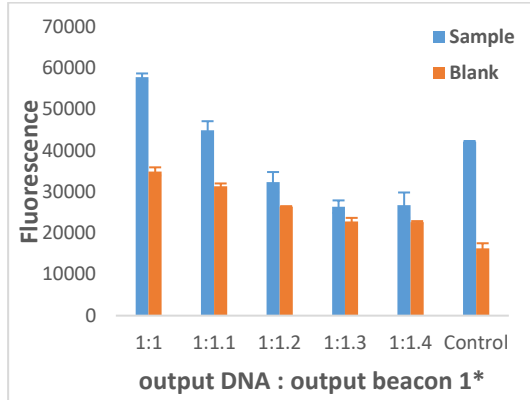
Different ratios of the two probes that form the output beacon were optimized. To prepare the output beacon, the amount of the output DNA remained unchanged, and the amount of the **output beacon 1*** was equal to or higher than that of the output DNA. We tested varying ratios of the **output DNA** and **output beacon 1*** (Figure 3-5A). The higher the concentration of **output beacon 1*** in solution, the lower the fluorescent signal generated, indicating that a lower amount of the output DNA was displaced. It is likely because the additional **output beacon 1*** probes were used to hybridize with any free output DNA, thereby potential background was reduced. However, over excessed **output beacon 1*** also can hybridize directly with the **TWJ1** and **TWJ2** probes, forming the **TWJ1:TWJ2:output beacon 1*** TWJ structure and competing with the displacement of the TWJ probes with the **output beacon 1*** from the output beacon. In this case, the binding-induced TWJ translation efficiency of the target protein information into the output DNA was suppressed.

A slight signal increase was observed when comparing the 1:1 ratio output beacon sample signal response to 1 nM streptavidin with the positive control response to 1 nM **output DNA** using the same concentration of 20 nM **FQ beacon** as the indicator. This small increase possibly is due to the free output DNA from the output beacon.

The ratio of the output beacon to the TWJ probes also was studied. We tested varying concentrations of the output beacon (1:1.1 ratio **output DNA** to **output beacon 1***, from 1–100 nM) reacted with 1 nM streptavidin, 10 nM **TWJ1** probes, and **TWJ2** probes with 20 nM **FQ beacon** added reaction buffer (1 x PBS, 10 mM Mg^{2+} , 0.05% Tween 20) at room temperature; the ratio between the output beacon to the TWJ probes ranged from 10:1 to 0.1:1. Fluorescent signals were measured at 60 min. The sample signal reached a maximum at 20 nM **output beacon**, which is 2:1 to the TWJ probes. For ratios from 0.1:1 to 2:1, the

sample signal was enhanced due to the increased kinetics for binding-induced TWJs formation and displacement. When the ratio increased from 2:1 to 10:1, the output beacon concentration also increased, and more free probes were in the reaction buffer. The existence of a large amount of free **output beacon 1*** probes affected the binding-induced TWJs molecular translate efficiency, which reduced the release of the **output DNA**.

(A)



(B)

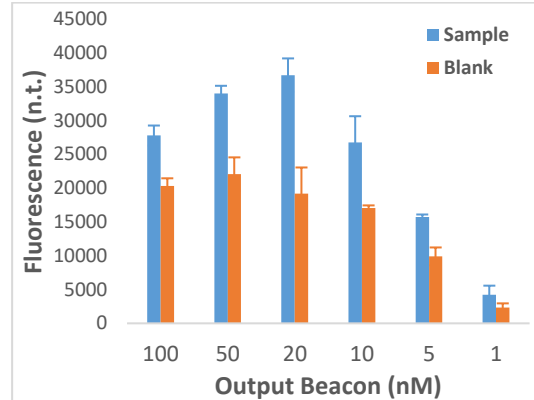


Figure 3-5. (A) Optimization of the two probe ratios for prehybridizing the output beacon (**output DNA:output beacon 1***). 50 nM different ratios of the output beacon reacted with 1 nM streptavidin, 10 nM **TWJ1** and 10 nM **TWJ2** probes, and a 20 nM **FQ** beacon. The positive control (control sample) contained 1nM **output DNA** with a 20 nM **FQ** beacon in the reaction buffer. The negative control (control blank) contained a 20 nM **FQ** beacon in the reaction buffer. Fluorescence measurements were taken at 60 min. (B) Optimization of the ratio between output beacon and the TWJ probes by using different concentrations of output beacon (from 1–100 nM).

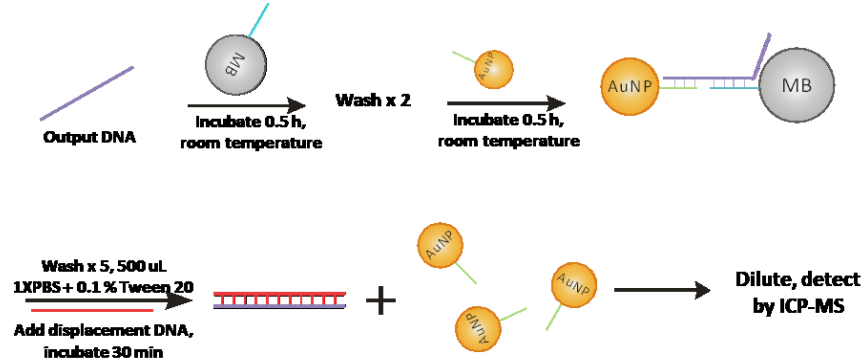
3.3.2 Output DNA detection using AuNPs amplification by ICP-MS

After successful formation of a binding-induced TWJ as a molecular translator to convert the target protein to the pre-designed output DNA, we estimated the detection of this output DNA further by using AuNPs amplification by ICP-MS (Figure 3-6A). First, the output DNA was incubated with MBs for 30 min and washed twice to discard unreacted reagents in solution. Because both the output DNA that was captured by MBs or was used to form output beacon can hybridize to the AuNP-linker, to reduce the competing binding, the functionalized AuNPs were added after the unreacted output beacon was removed from the mixture. The AuNPs were incubated with the reaction mixture for 30 min, then the output DNA was labeled by the AuNP-linker probes on its surface and washed five times to discard the unreacted reagents in solution. An excess amount of output* probe was added to displace the output DNA from the AuNP–output DNA–MB sandwich structure, leaving the AuNPs and the MBs separately in solution. After removing the MBs from the mixture using a magnetic shelf, the AuNPs remained in solution and were diluted to prepare the Au metal element sample for ICP-MS detection.

At the beginning, I chose the MB-linker MBs storage buffer (20 nM Tris-HCl with 10 mM Mg^{2+} and 0.1% Tween 20) as the washing buffer to remove unreacted reagents from solution. However, MBs aggregation was observed after the AuNPs were incubated and washed five times, probably because the salt concentration in the buffer was not high enough. After changing the washing buffer to 1 x PBS with 10 mM Mg^{2+} and 0.1% Tween 20, because the 1 x PBS buffer with 138 mM Na^+ and 2.7 mM K^+ increased the salt ions concentration, there was no longer MBs aggregation in the solution. Too high a concentration of salt ions affects the ICP-MS detection,

Two different carrier solutions were compared: (i) 1% HNO₃; (ii) 0.5% BSA added to 1% HNO₃. The (ii) carrier solution generated smoother and sharper peaks than the carrier (i) solution, and the peak tailing also was reduced. It was shown that the use of BSA lessens the adsorption of AuNPs on the surfaces of containers and tubing and thus improved the reproducibility of analysis. As shown in Figure 3-6B, a calibration between the Au metal element signal intensity and the concentration of the output DNA is linear within the range of concentration tests, from 100 fM to 1 nM, $r^2 = 0.9963$.

(A)



(B)

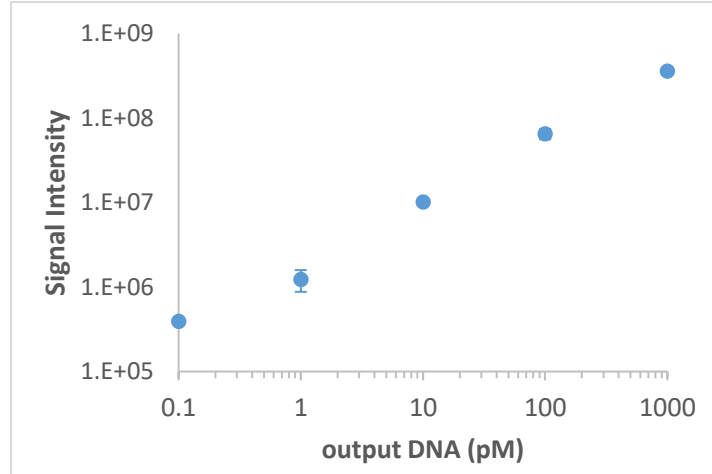


Figure 3-6. (A) Schematic showing the design of output DNA detection using AuNP amplification by ICP-MS. The output DNA was binding to a MB and an AuNP, forming a sandwich structure. The MBs were used to separate output DNA linked AuNPs from unreacted reagents. Only the captured AuNPs remained and were released in the final sample solution after the displacement of the output DNA and detected by ICP-MS. (B) Increases in Au metal signal intensity by ICP-MS as a function of concentration of output DNA.

3.3.3 Assay for human α -thrombin and streptavidin

To demonstrate the general applicability of the binding-induced TWJ and AuNP amplification by ICP-MS strategy, we chose human α -thrombin as the target protein. A thrombin molecule has two distinct binding epitopes, and two lengths of DNA aptamers can bind specifically to it. One thrombin-binding-aptamer (TBA) is 15 nt long, and its binding affinity is weaker than that of 29 nucleotides length of TBA. We designed two pairs of **TWJ1** and **TWJ2** probes to test the TBA binding affinity effects on the formation of TWJ. In the first pair, the 15-nucleotide TBA was modified on the **TWJ1** probe and the 29-nucleotide TBA was on the **TWJ2** probe. In the second pair, the 29-nucleotide TBA was modified on the **TWJ1** probe and the 15-nucleotide TBA was on the **TWJ2** probe. All the TBAs were extended directly on the sequences of the **TWJ1** and **TWJ2** probes (underlined in Table 3-1B). As shown in Figure 3-7, the **TWJ1-TBA29** and **TWJ2-TBA15** pair reaction rate was faster than that of the **TWJ1-TBA15** and **TWJ2-TBA29** pair. This substantial difference is likely due to the fact that the length of the **TWJ2** probe being much longer than that of the **TWJ1** probe. To bind with thrombin, the TBA needs to fold to a G-quadruplex form. The longer the sequence of a probe, the more possibilities exist for a complex secondary structure to be formed, suppressing the folding of G-quadruplex and reducing the speed of the thrombin-TBA binding reaction.

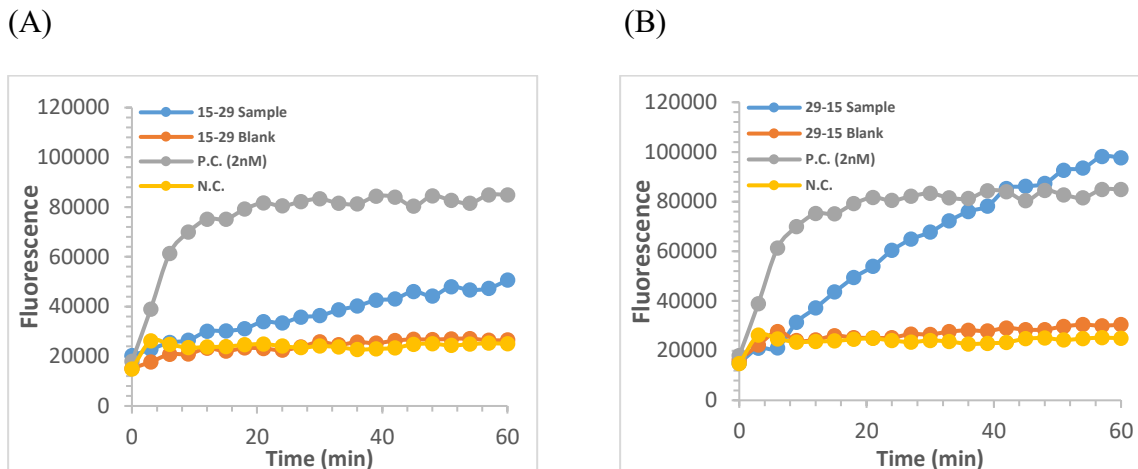
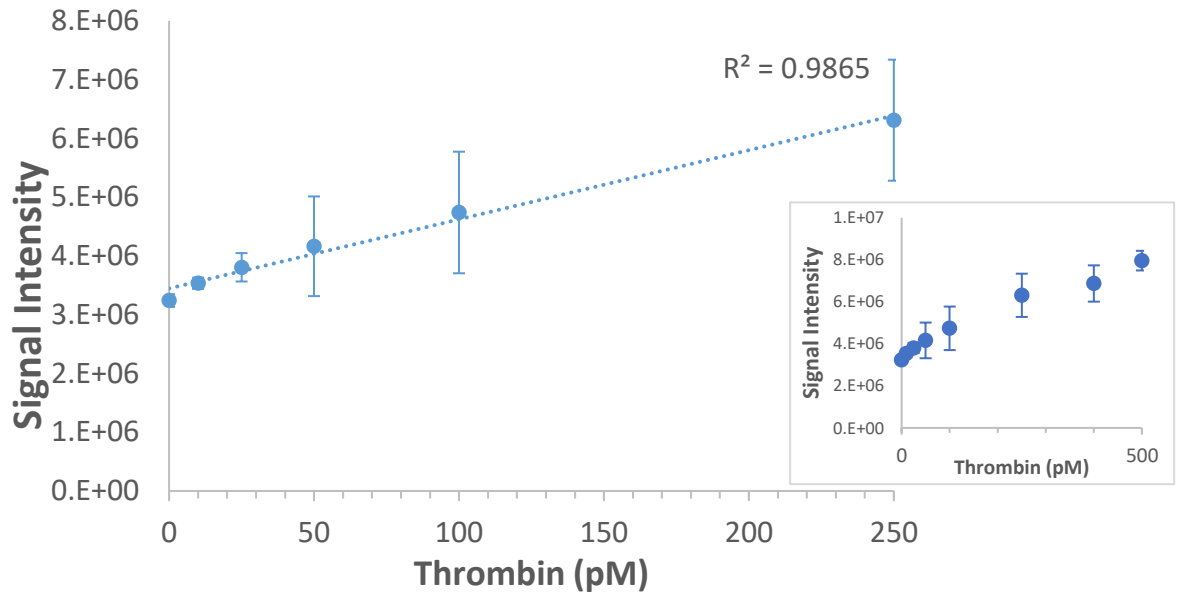


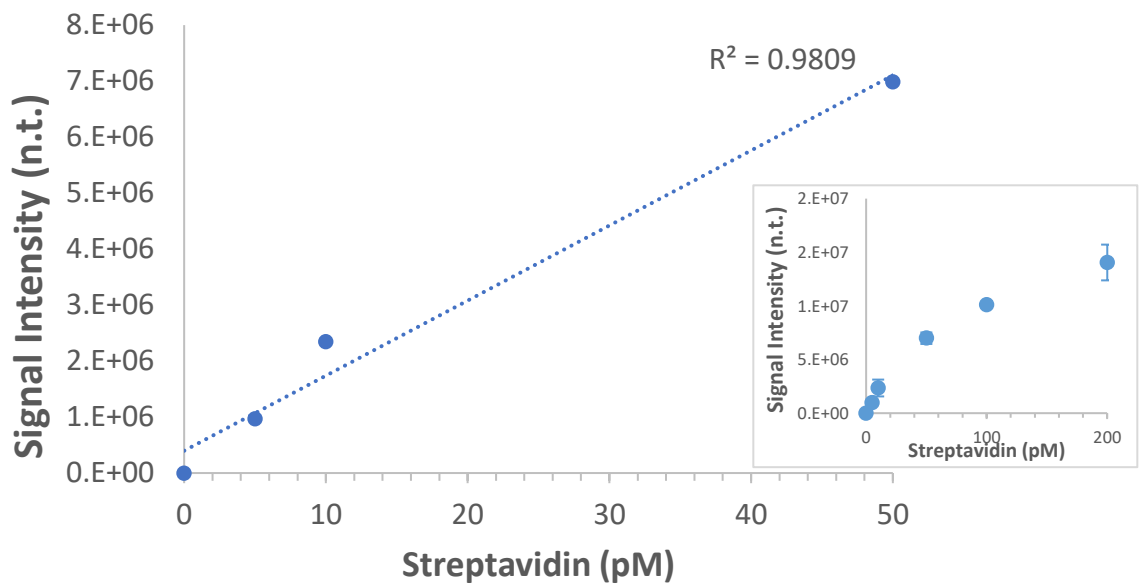
Figure 3-7. Comparison of different TBA modified TWJ1 and TWJ2 pairs. The fluorescent signal generated from the reaction of 5 nM thrombin, 5 nM of the TWJ1 and TWJ2 probes, 20 nM output beacon (**output DNA:output beacon 2***), and a 20 nM FQ beacon. (A) The kinetics of the **TWJ1-TBA15** and **TWJ2-TBA29** probes forming TWJ. (B) The kinetics of the **TWJ1-TBA29** and **TWJ2-TBA15** probes forming TWJ. Fluorescence of both reaction mixtures were measured every 3 min over 60 min.

The **TWJ1-TBA29** and **TWJ2-TBA15** pair probes reacted with varying concentrations of target thrombin (10–500 pM), with results shown in Figure 3-8A, and the detection limit was 10 pM.

To demonstrate the versatility of our approach, the detection of streptavidin was achieved (Figure 3-8B) as a second example of protein detection. Varying concentrations of streptavidin (5–200 pM) were tested using the binding-induced TWJ and AuNP amplification by ICP-MS, the detection limit was 5 pM.



(A)



(B)

Figure 3-8. Detection of proteins using binding-induced TWJ and AuNP amplification by ICP-MS. (A) Increases in Au metal signal intensity as a function of concentration of thrombin; (B) Increases in Au metal signal intensity as a function of concentration of streptavidin.

3.3.4 Assay for miRNA 10b and miRNA 128

To explore the versatility of our approach further, we constructed the TWJ molecular transformer and AuNP amplification for miRNA detection using ICP-MS (Figure 3-9).

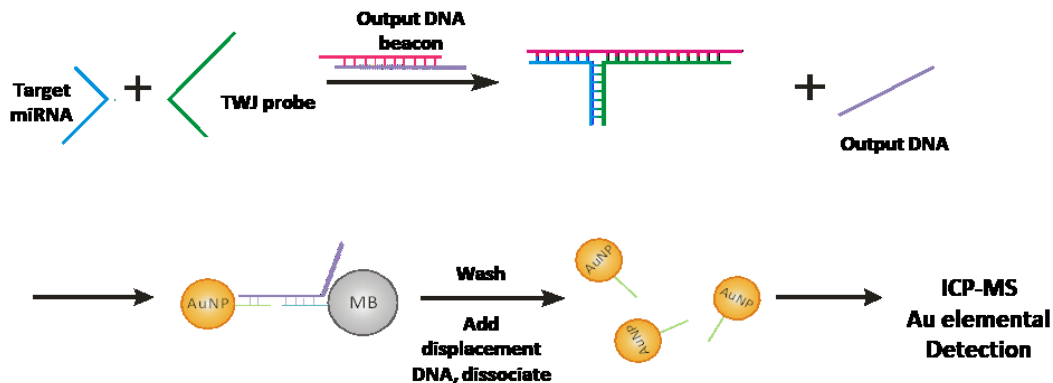


Figure 3-9. Schematic showing the design of miRNA detection using the TWJ and AuNP amplification by ICP-MS. The TWJ probe was designed to have a complementary sequence region with the target miRNA and to hybridize directly with it to form a target miRNA:TWJ:output beacon* TWJ structure. The output DNA was released after the TWJ formation and used as a linker to bind with the AuNP-linker probe that functionalized on the AuNP and the MB-linker probe that functionalized on the MB. After washing away the unreacted reagents, an excess amount of output* probe was added in solution to displace the output DNA from the sandwich structure. The MBs and AuNPs were able to separate, and the solution that contained the AuNPs was diluted; the Au element in the diluted sample was detected by ICP-MS.

Two miRNAs (miRNA 10b and miRNA 128) were detected as target miRNAs to show the universality of the TWJ molecular translator. By changing the target miRNA, the TWJ2 probe and the output beacon* probe were redesigned to react with the target miRNA specifically. The design of these **TWJ2** probes and output beacon probes is simple because their sequences are predefined by the target miRNA and the output DNA. The output DNA was prehybridized with the output beacon* probe, contained a toehold domain that was complementary to part of the miRNA. The **TWJ2** probe contained one fraction that was the same sequence as the output DNA hybridization part in the output beacon, and the other fraction was complementary to the non-toehold domain part of the miRNA target. In the presence of miRNA, the melting temperature (T_m) of the **TWJ2** probe and miRNA sequence complementary region was higher than room temperature (miRNA 10b designed system T_m was 48.1 °C, miRNA 128 designed system T_m was 49 °C), therefore, the hybridization is favorable at room temperature. Then, the miRNA and **TWJ2** binding complex displaced the output DNA from the output beacon and formed the TWJ structure. For miRNA 10b, the TWJ structure was **miRNA 10b:TWJ2-10b:output beacon 2***. For **miRNA 128b**, the TWJ structure was **miRNA 128:TWJ2-128:output beacon 3***. To detect trace concentrations of miRNA, a higher amount of the **TWJ2** probes was added to the reaction mixture compared to the amount that was added to the protein detection. The FAM-labeled probe and quencher-labeled probe hybridized FQ beacon was used as an indicator for the feasibility test of the miRNA formed TWJ molecular translator and the release of output DNA. These results are shown in Figure 3-10, where 1 nM of miRNA 10b and 500 pM of miRNA 128 are in the linear range of the calibration curve.

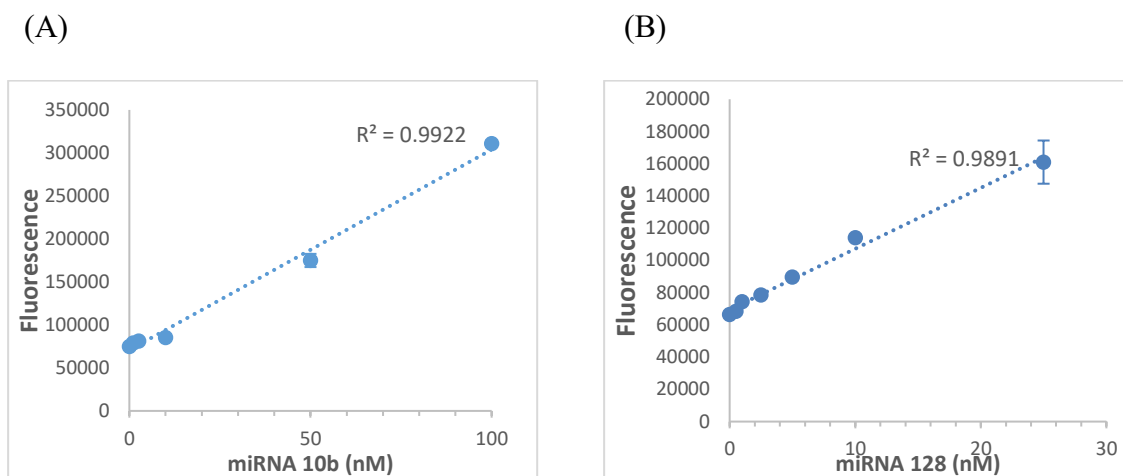


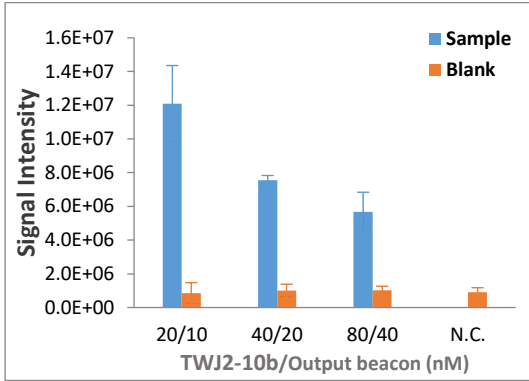
Figure 3-10. Detection of miRNA 10b and miRNA 128 using the TWJ and FQ beacon. Increases in fluorescent signals as a function of concentration of miRNA in a reaction buffer. Fluorescent signals were measured at 12 h.

AuNPs were used to amplify the signal and enhance the detection sensitivity. The ratio of TWJ2 probes and output beacon was optimized to obtain the best reaction conditions (Figure 3-11A and 3-11B). A DNA target was used as a template for condition optimization because DNA nucleotides are more robust in complex conditions than RNA nucleotides. The blank reaction contained identical reagents in the sample reaction, except the DNA target. The blank signal increased when higher concentrations of reaction probes were added because it contained more free output DNA. However, contrary to what I expected, higher concentrations of reagents reduced the sample signal. This is likely due to the fact that the TWJ2 probes had the same fraction of output DNA and a competing binding reaction happened between the TWJ2 probe and the output DNA to the MB-linker probes on MBs.

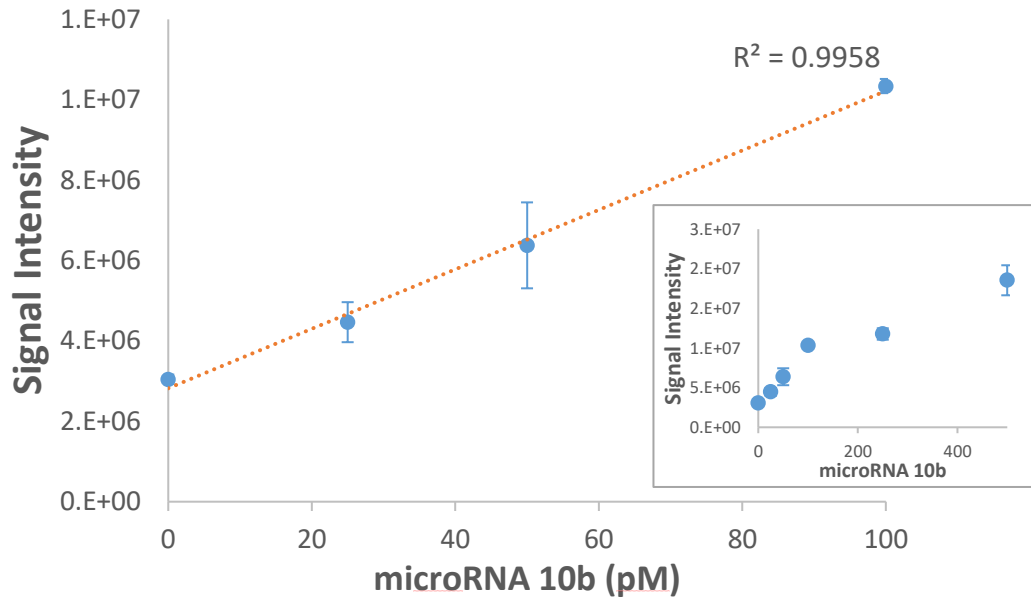
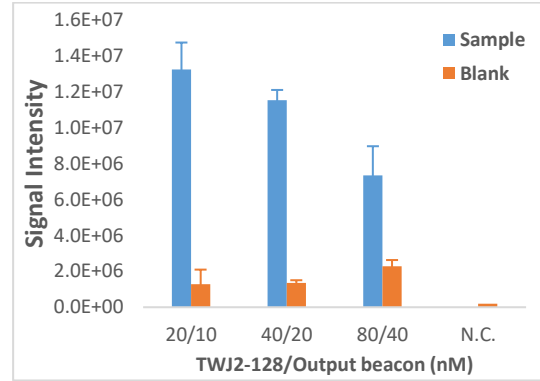
MiRNA results were measured by ICP-MS after all the optimizations. As shown in

Figure 3-11C and 3-11D, compared to the fluorescent signal tested by the FQ beacon, the limit of miRNA 10b improved ~40 times. The limit of miRNA 128 improved ~50 times, indicating the enhancement of using AuNP amplification.

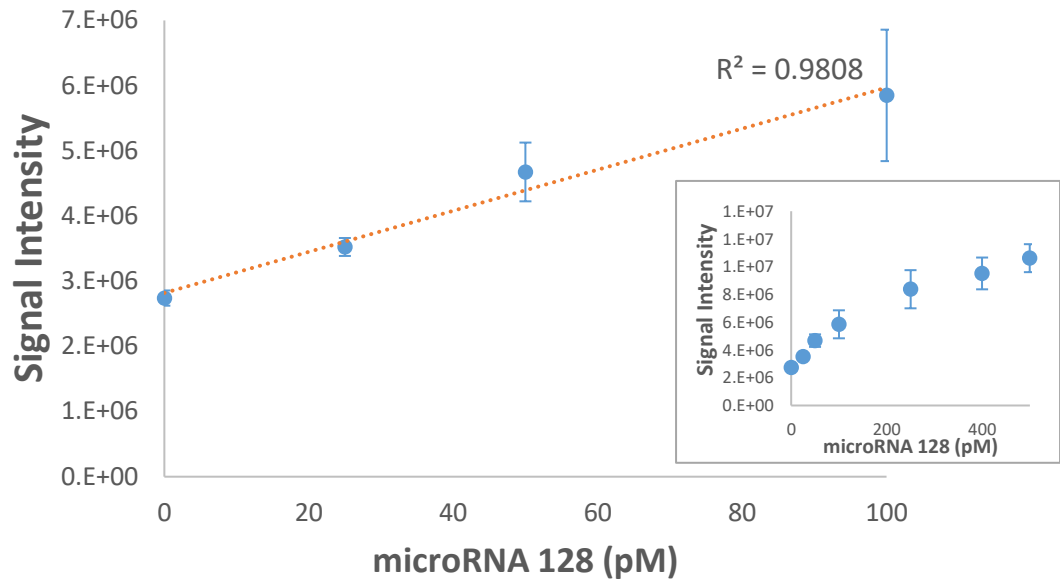
(A)



(B)



(C)



(D)

Figure 3-11. Detection of miRNA 10b and miRNA 128 dynamic ranges using the TWJ and AuNP amplification by ICP-MS. (A-B) Optimization of the TWJ2-10b probe and TWJ2-128 probe to the output beacon ratio. The negative control contained 100 μ L reaction buffer, incubated with MBs and AuNPs. (C-D) Detection of mi10b and mi128. Varying concentrations of miRNA 10b (from 500 to 25 pM) and miRNA 128 (from 500 to 10 pM) were measured. The detection limit of miRNA 10b was 25 pM and of miRNA 128 was 10 pM.

3.4 Conclusion

I have constructed a binding-induced TWJ and AuNP amplification strategy for the detection of proteins and miRNAs successfully. The TWJ worked as a molecular translator, and it is able to convert the input target information to the readily designed output DNA. For protein detection, the affinity binding of the specific protein target and two ligand modified TWJ probes triggers the formation of TWJs and released the output DNA from the prehybridized output beacon. For miRNA detection, the TWJ probe has a complementary region that can hybridize partially with target miRNA, and the binding of the duplex oligonucleotides leads to the formation of TWJs. The universal output DNA was displaced and ready for detection. For various miRNA targets with output DNA sequence, the TWJ detection DNA probes are predefined simply and can be achieved easily. The AuNP amplification also proved to enhance the detection limit compared to the fluorescent signal in solution, and a detection limit of ~ 10 pM level of proteins and miRNAs was achieved. Thus, this strategy reported here developed a universal protein and miRNA detection method.

Chapter Four: Binding-Induced Molecular Amplifier as a Universal Detection Platform for Biomolecules and Biomolecular Interaction

4.1 Introduction

Techniques capable of detecting multiple classes of biomolecules, such as nucleic acids and proteins, and biomolecular interactions in biological or clinical samples are highly desirable for applications ranging from accurate disease diagnosis to deciphering complicated biological processes¹²²⁻¹²⁵. Using a universal detection platform offers a single simplified testing strategy that traditionally has required the use of multiple types of assays and instrumentation¹²²⁻¹²⁵. However, because of the large variations in target recognition, signal transduction, and instrumentation across varying classes of biomolecules, the development of universal detection platforms is very challenging. To address this challenge, a viable solution is to translate the recognition of multiple classes of analytical targets into unified surrogate molecules for detection and quantification¹²³⁻¹³¹. For example, through target-induced release of invertase from magnetic particles, Lu and co-workers have expanded the use of a personal glucose meter to measure multiple classes of analytes¹²⁵⁻¹²⁸. Similar strategies also have enabled the use of litmus tests¹²⁹, pregnancy test strips¹³⁰, and pressure sensors¹³¹ for the detection of alternate target analytes. Das *et al.* achieved the ultrasensitive detection of a panel of nucleic acids, proteins, and small molecules on a single nanostructured electrochemical platform by using a displaced peptide neutralizer as a unified barcode¹⁶. Leveraging recent advances in dynamic DNA nanotechnology, several DNA-mediated molecular translators also have been created, which allow the rapid conversion of

nucleic acid, proteins, and small molecule targets into a predesigned DNA barcode in homogeneous solutions^{9, 16, 23, 38, 132-134}. In particular, Picuri *et al.* introduced the first DNA-mediated molecular translator operated by toehold-mediated strand displacement for the universal detection of nucleic acids¹⁶. Recently, we have developed a series of binding-induced molecular translators capable of producing DNA outputs in response to specific target proteins through binding-induced DNA strand displacement reactions^{9, 23, 38, 132-135}. So far, most molecular translation strategies only allow the release of maximally one barcode molecule (e.g., invertase, neutralizer, or output DNA) in response to one molecular binding event; this limits the overall translation efficiency. Herein, we introduce a novel binding-induced molecular amplifier (BIMA) that not only translates a broad range of biomolecules and interactions into a unified DNA barcode but also enhances the translation efficiency by releasing multiple barcode molecules in response to a single binding event.

The principle of BIMA is illustrated in Figure 4-1. This design is inspired by our recent successes in constructing stochastic three-dimensional (3D) DNA nanomachines¹³⁶⁻¹³⁷, where an enzyme-powered DNA walker travels along a 3D track made of a spherical nucleic acid (SNA) and cleaves hundreds of track molecules. However, the current 3D DNA nanomachines only can release short fluorescence-labeled DNA fragments, thus, they are not capable of molecular translation. Also, this BIMA method has benefit of potential second amplification step comparing Figure 4-1 to Figure 1-5(C), although I did not have time to test. As such, BIMA that contains two designed motifs is introduced, including a DNA walker (DW) and a 3D SNA track (SNA). The DW is composed of a nicking recognition domain and a target recognition domain (e.g., complementary DNA probe, antibody, or aptamer). The two domains are connected through a flexible linker made of 40 thymine

nucleotides. The 3D track is a SNA constructed by co-conjugating an additional target recognition domain and hundreds of hairpin probes (HPs) on a single 20 nm AuNP. The two target recognition domains bind to the same input analyte but at different epitopes. HP contains a nicking cleavage domain and a caged DNA barcode. The complementary sequences between DW and HP are designed to be only 7-bp long so that no duplex forms at the operation temperature (e.g., 37 °C). As a result, no nicking cleavage occurs in the presence of nicking endonuclease. However, in the presence of a target molecule, the binding of the two recognition domains to the same target molecule assembles the DW onto the SNA. The close proximity between DW and HP greatly increases their local effective concentrations and thus triggers the formation of DNA duplex between DW and HP, resulting in subsequent cleavages by the nicking endonuclease. The DNA barcode is then released and activated for downstream reactions. Because of the walking mechanism enabled by DW on the 3D track, each input molecule can release and activate multiple DNA barcodes and thus amplify the molecular translation.

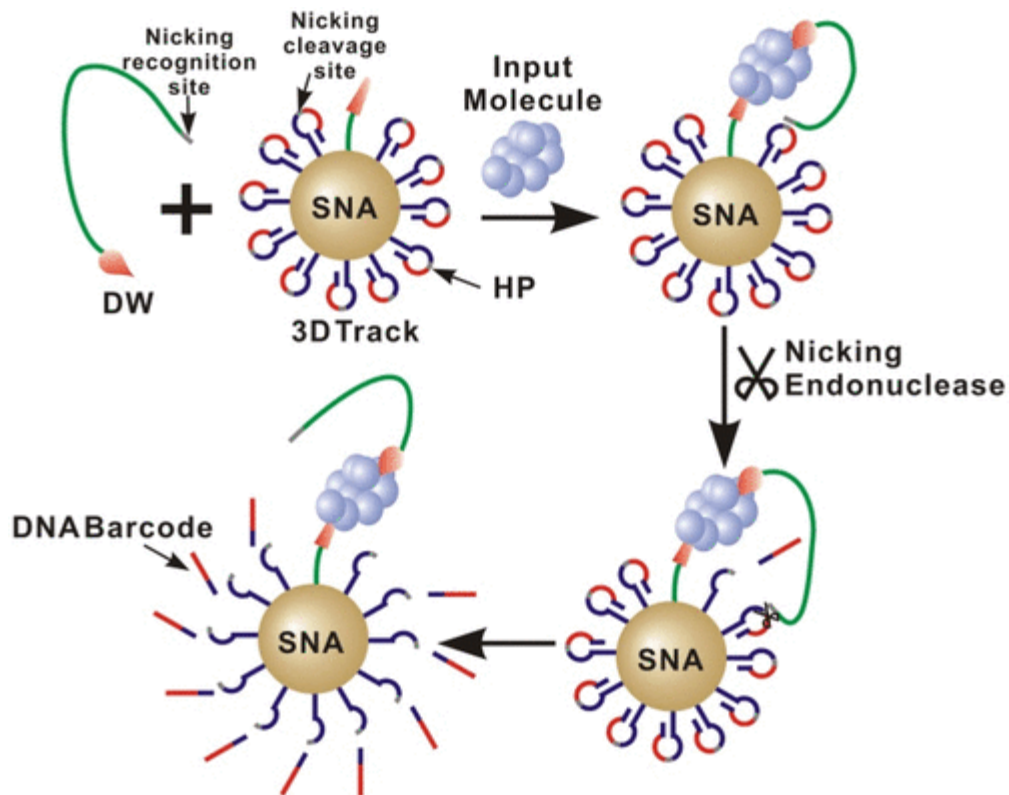


Figure 4-1. Principle of the Binding-Induced Molecular Amplifier (BIMA). BIMA is operated by simply mixing the sample with DW, SNA, and nicking endonuclease at 37 °C. The input molecule (target analyte) assembles DW onto SNA through a sandwiched binding that triggers a cascade of nicking cleavage reactions. As a result, multiple unified DNA barcode molecules are released and activated, which can be quantified using a single detection platform.

4.2 Experimental

4.2.1 Materials and reagents

All DNA oligonucleotides were purchased from Integrated DNA Technologies (Coralville, IA) and purified by HPLC. The DNA sequences and modifications are listed in Table 4-1. In DW and capture probes, compared to other sequences, PolyT was modified as a spacer because it has the lowest binding affinity to the AuNP surface. Nicking endonucleases, Nt.BbvCI, and 10× CutSmart buffer (500 mM potassium acetate, 200 mM Trisacetate, 100 mM magnesium acetate, and 1 mg/mL BSA, pH 7.9 at 37 °C) were purchased from New England BioLabs (Whitby, ON). Streptavidin from *Streptomyces avidinii*, biotin, prostate specific antigen (PSA), bovine serum albumin (BSA), and human serum were purchased from Sigma-Aldrich (Oakville, ON). Biotinylated polyclonal anti-PSA antibody, platelet derived growth factor BB (PDGF-BB), and PDGF receptor β were purchased from R&D Systems (Minneapolis, MN).

A solution of gold nanoparticles (AuNPs, 7.0×10^{11} particle/mL) with 20 nm diameter was purchased from Ted Pella, Inc. (Redding, CA). NANOpure water (>18.0 M Ω), purified using an Ultrapure Milli-Q water system, was used for all experiments.

Table 4-1. DNA sequences and modifications for BIMA

DNA name		Sequences and modifications
3D Track for BIMA	HP	5'-SH-TTTTTTTTTTTTTTTT CTC GTA GTTT GC*TG AGG TAC ACA TGA ATC TAC TGA CTT CTA CGA G-3'
	FAM-HP	5'-SH-TTTTTTTTTTTTTTTT CTC GTA GTTT GC*TG AGG TAC ACA TGA ATC TAC TGA CTT CTA CGA GT-FAM-3'
Strand Displacement Beacon	DNA barcode (P.C.)	5'-TGAGG TAC ACA TGA ATC TAC TGA CTT CTA CGA G-3''
	F	5'-FAM-TAC ACA TGA ATC TAC TGA CTT-3'
	Q	5'-CTCGTAG AAGTCAGTAG ATTCATGTGTA-Iowa black-3'
Fluorescence turn-on assay for screening the optimal stem length of HP	Target DNA	5'-TCTT TGTA C CTC AGC AAA TTCT-3'
	HP-stem 5	5'-CTCGT TT TTT GC*TG AGG TAC ACA TGA ATC TAC TGA CTT CT ACGAG-3'
	HP-stem 6	5'-CTCGTA T TTT GC*TG AGG TAC ACA TGA ATC TAC TGA CTT CT ACGAG-3'
	HP-stem 7	5'-CTCGTAG TTT GC*TG AGG TAC ACA TGA ATC TAC TGA CTT CTACGAG-3'
	HP-stem 8	5'-CTCGTAGA TTT GC*TG AGG TAC ACA TGA ATC TAC TGA CT TCTACGAG-3'
	HP-stem 9	5'-CTCGTAGAA TTT GC*TG AGG TAC ACA TGA ATC TAC TGA C TTCTACGAG-3'
HP-stem 10	5'-CTCGTAGAAGT TTTGC*TG AGG TAC ACA TGA	

		ATC TAC TG ACTTCTACGAG-3'
	HP-stem 11	5'-CTCGTAGAAGT TTTGC*TG AGG TAC ACA TGA ATC TAC TG ACTTCTACGAG-3'
	HP-stem 12	5'-CTCGTAGAAGTC TTTGC*TG AGG TAC ACA TGA ATC TAC T GACTTCTACGAG-3'
BIMA for Streptavidin & PSA	Capture probe on SNA	5'-SH-TTTTTTTTTTTTTTTT ATG TTC TTG TTA TTT TTC TTG TTC AT-Biotin-3'
	DW	5'-Biotin-TTTTTTTTTTTTTTTTCTTGTT ATC TTC CTC AGC-3'
BIMA for PDGF-BB	Capture probe on SNA	5'-SH-TTTTTTTTTTTTTTTT CAC AGG CTA CGG CAC GTA GAG CAT CAC CAT GAT CCT GTG-3'
	DW	5'-CAC AGG CTA CGG CAC GTA GAG CAT CAC CAT GAT CCT GTG TTTTTTTTTTTTTTTTCTTGTT ATC TTC CTC AGC-3'
BIMA for nucleic acid	Target	5'- CAT ACG ACG TAC TGC ACA TT ATG GTC AAG AAA CGT GAC TA-3'
	DW	5'- TGT GCA GTA CGT CGT ATG TTT TTT TTT TTT TTT CTT GTT ATC TTC CTC AGC -3'
	Capture probe on SNA	5'-SH-TTTTTTTTTTTTTTTT TAG TCA CGT TTC TTG ACC AT -3'

* Cleaving site of nicking endonuclease

4.2.2 Preparation of BIMA

To prepare the DNA functionalized AuNPs (SNA), the thiolated HPs and capturing DNA oligonucleotides (complementary DNA, biotinylated DNA, or anti-PDGF aptamer) were mixed at a ratio of 10 to 1. A 20 μL solution of this mixture containing 50 μM DNA HP and 5 μM capturing DNA oligonucleotides were mixed with 1 mL of 1 nM AuNPs. This mixture was placed at room temperature for 12 h and then slowly mixed with 20 μL of 3 M NaCl, followed by 10 s of sonication. Addition of NaCl and sonication was repeated for five times with 1 h intervals, to maximize the oligonucleotide loading amounts. Then, the solution was incubated at room temperature for 24 h. After incubation, the solution was centrifuged at 13500 rpm for 30 min to separate the SNA from unconjugated DNA probes. The SNAs were washed three times with 1 \times PBS buffer (pH 7.4) containing 0.01% Tween20 followed by dispersal in PBS buffer. The number of HP probes loaded on each AuNP was established by measuring the concentrations of FAM-labeled DNA hairpins in each sample, and this number could be used to reflect the density of unlabeled DNA hairpins under the same conjugation protocols. For their typical use in BIMA, the loading amount of HPs was measured to be ~ 150 probes per AuNP on average.

4.2.3 Molecular translation using BIMA

In a typical BIMA reaction, a mixture containing 2.5 nM **DW**, 0.5 nM SNA, 0.2 U/ μ L nicking endonuclease, 1 \times CutSmart buffer, and varying concentrations of the target molecules (target DNA, streptavidin, PSA, or PDGF-BB) were incubated at 37 °C for 2 h. Strand displacement beacon **FQ** was then added to this mixture at a final concentration of 20 nM. This reaction mixture was incubated at 25 °C in a 96-well microplate, and fluorescence was measured directly from the microplate using a multimode microplate reader (DX880, Beckman Coulter) with excitation at 485 nm and emission at 515 nm. Fluorescence increase was measured every 1.5 min for the first 30 min and then every 5 min for another 15 min. The measured fluorescence signals were normalized so that 1 n.u. of fluorescence corresponded to the fluorescence signal generated by 1 nM DNA barcode. This normalization was achieved using a positive control containing 10 nM DNA barcode as a standard and a 20 nM **FQ** beacon in 1 \times CutSmart buffer and a negative control containing identical reagents as in the positive control, except that there was no DNA barcode added.

4.2.4 BIMA for probing the interaction between PDGF-BB and PDGFR- β

In a typical reaction, 200 pM of PDGF-BB was incubated with varying concentrations of PDGFR- β in 1 \times CutSmart buffer at 37 °C for 30 min. BIMA components, including final concentrations of 2.5 nM **DW**, 0.5 nM SNA motif, and 0.2 U/ μ L nicking endonuclease, were added to the reaction mixture and incubated for another 2 h at 37 °C. The strand displacement beacon **FQ** was then added to this mixture at a final concentration of 20 nM. This reaction mixture was incubated at 25 °C in a 96-well microplate, and fluorescence was measured from the microplate using the same multimode microplate reader. The dissociation constant K_d between PDGF-BB and PDGFR- β was calculated by fitting the data in Figure 4-10C into a one-site binding equation:

$$y = \frac{[\text{PDGFR-}\beta]}{K_d + [\text{PDGFR-}\beta]}$$

where y stands for the relative fluorescence, which was calculated by normalize fluorescence at different concentrations of PDGFR- β against that was generated by 200 pM PDGF-BB in the absence of the PDGFR- β .

4.3 Results and Discussion

4.3.1 Designing and screening the hairpin probes for the SNA track

A critical feature of molecular translators is the ability to trigger downstream reactions in response to an upstream binding event. BIMA is designed to use target recognition to trigger toehold-mediated strand displacement reactions^{6, 138}. Specifically, BIMA uses a HP structure to initially cage a barcode DNA. Upon target binding, nicking endonucleases cleave the barcode DNA, which contains a toehold domain and a branch migration domain that are required for strand displacement reactions. The toehold domain is initially sequestered in the stem of HP such that no strand displacement will be triggered in the absence of the target analyte (Figure 4-2A). The loop of HP contains the branch migration domain and a nicking cleavage domain. After target binding and nicking cleavage, HP is split at the nicking cleavage site, resulting in the release of the barcode and the exposure of the toehold domain. The exposed toehold domain on the barcode allows subsequent strand displacement reactions.

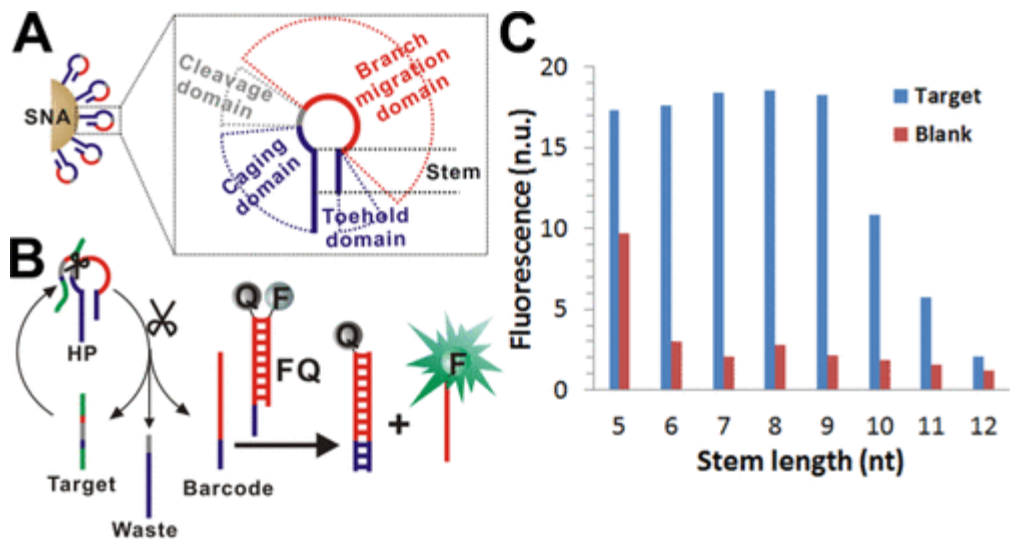


Figure 4-2. (A) Schematic illustration of the design of hairpin probes. (B) Schematic illustration of the fluorescence turn-on assay for determining the optimal HP design. (C) Fluorescence readout as a function of stem length varying from 5 to 12 bp. A reaction mixture containing 2.5 nM targets, 75 nM **HP**, 2 units of the nicking endonuclease, and 20 nM **FQ** were incubated at 37 °C for 1 h before the fluorescence measurement. Blanks contained the same reagents as for the sample, except that there was no target DNA added. The fluorescence intensity was normalized such that 1 normalized unit (n.u.) corresponds to 1 nM DNA barcode (P.C.).

To maximize the performance of BIMA, it is critical to optimize the stem length of **HP**. A short stem will not be sufficient to sequester the toehold domain (Figure 4-3), and a long stem may prevent the release of barcode from the SNA motif after the nicking cleavage. To maximize the target-specific release of the barcode and minimize the target-independent activation, we designed a series of **HPs** with stem lengths varying from 5 bp to 12 bp and systematically screened the optimal design using a fluorescence turn-on assay (Figure 4-2B). In the screening assay, an artificial DNA target was designed to hybridize to **HP** with an estimated melting temperature (T_m) of 53 °C to mimics the target-induced hybridization between **DW** and **HP** in BIMA. A molecular beacon (**FQ**) was designed to undergo toehold-mediated strand displacement with cleaved DNA barcodes and generate a fluorescence signal (Figure 4-2B). By comparing the target to blank signals in Figure 4-2C, the optimal stem length ranges from 6 to 9 bp. As we initially expected, when the stem length was shorter than 6 bp, high levels of FQ were activated in the absence of target, which is due to the insufficient sequestering of the toehold domain (Figure 4-3). On the other hand, HPs with stem lengths longer than 9 bp resulted in lower target triggered fluorescence signal because the DNA barcode did not completely release from the HP after cleavage. On the basis of this screening test, we chose a stem length of 7 bp HP for all BIMA designs.

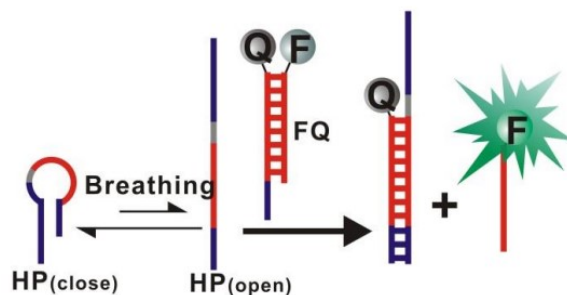


Figure 4-3. Schematic illustration of the possible source of the target-independent opening of the **HP** and the nonspecific activation of the strand displacement beacon. The breathing of **HP** becomes significant when the stem length is shorter than 6 bp.

4.3.2 Real-timing characterization of BIMA using fluorescently labeled HPs

Having optimized the HP design, we then constructed a BIMA for streptavidin as a model target (Figure 4-4A). As affinity ligands, biotin molecules were conjugated to both DW and SNA motifs. To monitor the performance of BIMA in real-time, we modified HP with a fluorescent dye, fluorescein amidite (FAM). Because of the close proximity, the fluorescence of FAM initially was quenched by the AuNP. Upon streptavidin-induced assembly, the DW moves along the 3D track, liberating the FAM-labeled DNA barcode, thus turning on the fluorescence (Figure 4-4A). Figure 4-4B shows a typical kinetic profile of the streptavidin-specific BIMA. Immediately after 2 nM streptavidin was added into a solution containing 5 nM DW, 500 pM SNA, and 0.2 U/ μ L nicking endonuclease, a steady fluorescence increase was observed that reached saturation within a period of 120 min, suggesting that BIMA can release DNA barcodes effectively in response to the target binding. We further confirmed that the response of BIMA to streptavidin was concentration-dependent, in the range of 30 pM–2 nM (Figure 4-5). A noticeable fluorescence increase also was observed in the blank

due to the spontaneous release of HP by the residue dithiothreitol (DTT) associated with the nicking endonuclease (Figure 4-4B).

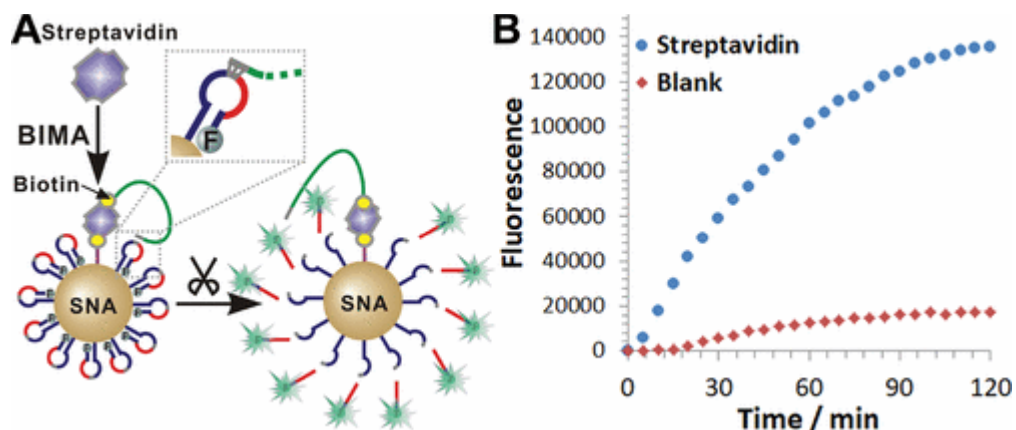


Figure 4-4. (A) Schematic illustration of a streptavidin-specific BIMA that releases FAM-labeled DNA barcodes in response to streptavidin. (B) Real-time monitoring fluorescence increases of BIMA in the presence and absence of 2 nM streptavidin. The reaction mixtures containing 2 nM streptavidin (or no streptavidin for the blank), 2.5 nM DW, 500 pM SNA, and 0.2 U/ μ L nicking endonuclease were incubated at 37 °C and monitored using a multimode microplate reader.

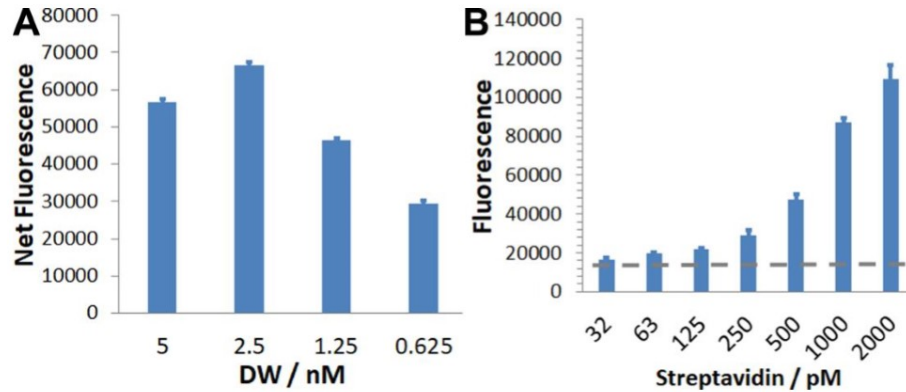


Figure 4-5. (A) Optimization of DW concentration for BIMA. The concentration of streptavidin was fixed at 1 nM, and the concentration of SNA with FAM-labeled HP was fixed at 0.5 nM. The reaction mixtures containing streptavidin, SNA, and varying concentrations of DW were incubated at 37 °C for 1 h before fluorescence reading. The net fluorescence is equal to the total fluorescence signal after subtracting that of the blank. (B) Concentration dependency of BIMA to the input streptavidin. The horizontal dashed line corresponds to the average fluorescence signal in the absence of streptavidin. Each error bar represents one standard deviation from triplicate analyses.

4.3.3 Characterizing BIMA using a strand displacement beacon

As the ultimate goal of BIMA is to translate and amplify various target molecules into a unified barcode for subsequent manipulations, it is essential that BIMA can trigger subsequent reactions in a target-specific manner. As BIMA is designed to trigger toehold-mediated strand displacement reactions, the characterization was performed using streptavidin as a model target and FQ as a unified readout (Figure 4-6A). In a typical experiment, we first mixed the streptavidin with BIMA for 1 h to allow the accumulation of barcode molecules and followed by adding FQ at a final concentration of 20 nM. By measuring the fluorescence increases from FQ in real-time, we observed a rapid fluorescence increase in the presence of streptavidin and BIMA, suggesting that target-activated DNA barcode molecules could trigger subsequent toehold strand displacement reactions effectively (Figure 4-6B). A noticeable fluorescence increase also was observed in the blank. By making comparisons to a control that contained only the 3D track, we confirmed that this target-independent strand displacement was a result of the breathing of HP probes (Figure 4-3) rather than the nonspecific release of DNA barcode molecules. Using FQ as a unified detector and external calibration (Figure 4-7), we also were able to measure the amount of released DNA barcode accurately and thus estimate the translation/amplification efficiency of BIMA. We found that a net of 8.2 nM DNA barcode molecules have been released by BIMA in response to 0.8 nM streptavidin, corresponding to an amplification efficiency (AE) of 10. To evaluate the maximum AE of BIMA, we systematically reduced the input concentrations of streptavidin, so that maximally only one DW assembled to each SNA (Figure 4-6C and Figure 4-8). By doing so, we were able to estimate the maximum AE to be ~ 75 for the streptavidin-specific BIMA.

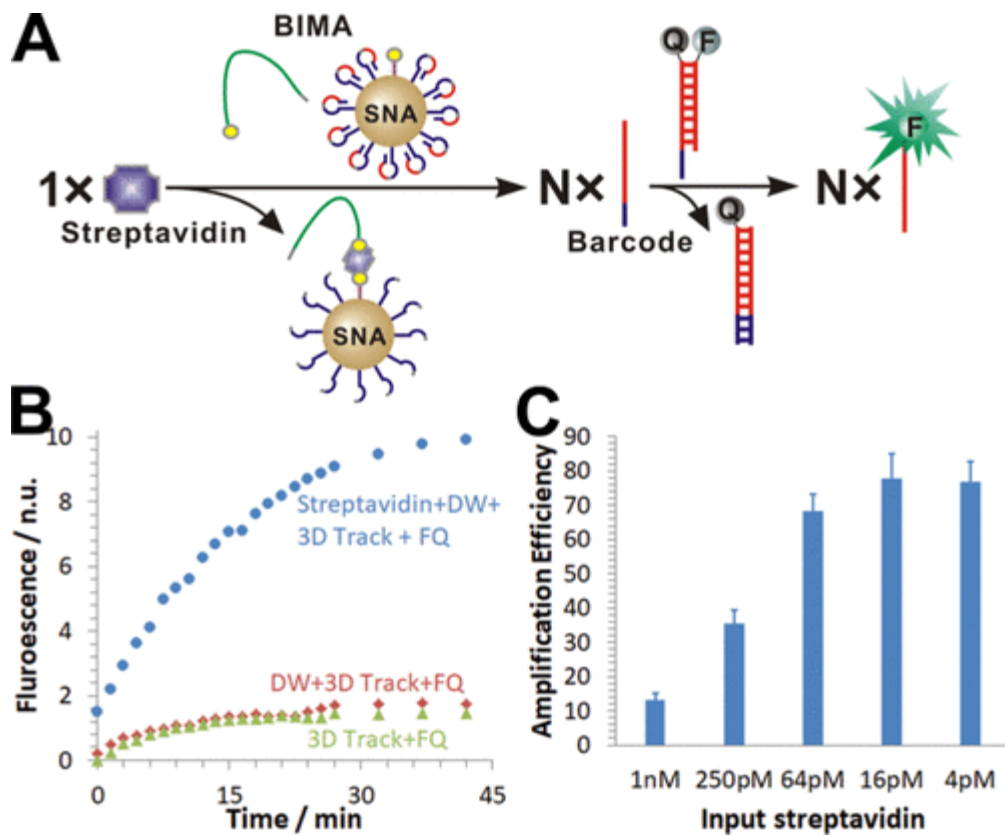


Figure 4-6. (A) Schematic illustration of a streptavidin-specific BIMA that releases multiple DNA barcode molecules in response to a single streptavidin, triggering the subsequent quantification using a unified beacon FQ. (B) Real-time monitoring fluorescence increases of BIMA in the presence and absence of 2 nM streptavidin. (C) Amplification efficiencies (AE) of BIMA as a function of concentrations of the input streptavidin, where $AE = \frac{F_{input} - F_{blank}}{[Input]}$. Each reaction mixture containing varying concentrations of streptavidin, 2.5 nM DW, 500 pM SNA, and 0.2 U/ μ L nicking endonuclease was incubated at 37 °C for 60 min and then mixed with FQ at a final concentration of 20 nM. Real-time monitoring of fluorescence was performed immediately after FQ was added. The fluorescence intensity was normalized such that 1 normalized unit (n.u.) corresponds to 1 nM DNA barcode as a positive control. Each error bar represents one standard deviation from triplicate analyses.

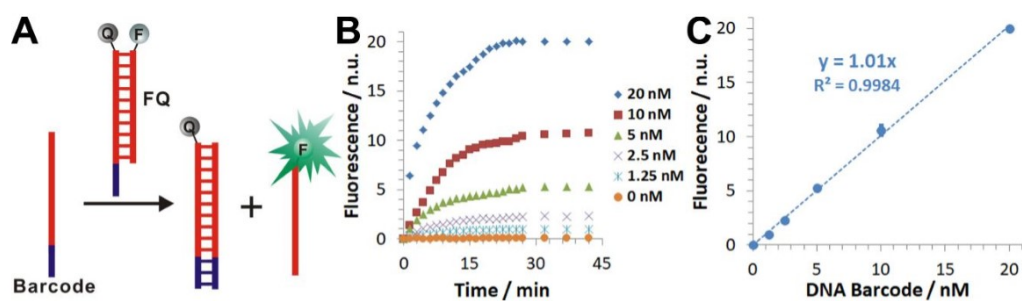


Figure 4-7. (A) Schematic illustration of the principle of toehold-mediated strand displacement beacon (FQ) that quantifies the DNA barcode generated from BIMA. (B) Real-time characterization of strand displacement beacon using 20 nM FQ and varying concentrations of the barcode. (C) Standard external calibration curve established by plotting normalized fluorescence (at 45 min) of FQ as a function of the concentration of the DNA barcode as a standard. Each error bar represents one standard deviation from triplicate analyses.

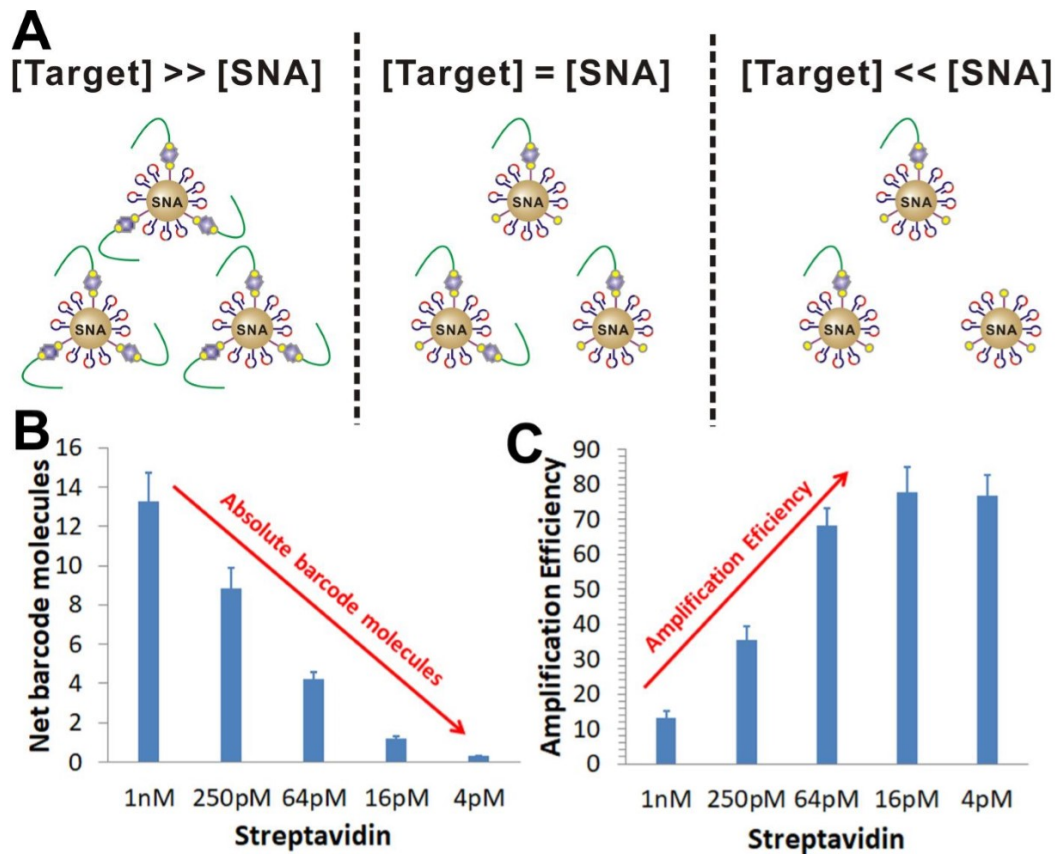


Figure 4-8. (A) Schematic illustration of the impact of target concentration on the amplification efficiency of BIMA. (B) Net DNA barcode molecules produced by BIMA in response to varying concentrations of the input streptavidin molecules. (C) Amplification efficiency of BIMA as a function of varying concentrations of input streptavidin. The concentration of SNA was fixed at 500 pM, so maximum amplification efficiency could be achieved when $[streptavidin] \ll 500$ pM. Each error bar represents one standard deviation from triplicate analyses.

4.3.4 BIMA as a versatile and amplifiable platform for translating a broad range of targets

After confirming the ability of BIMA for translating streptavidin, we attempted to demonstrate the versatility of BIMA for a broader range of targets. To do so, we integrated the BIMA with three most commonly used ligands for biomolecular detections, including antibodies, aptamers, and complementary DNA probes. All three BIMAs are designed to release the identical DNA barcode so that the same strand displacement beacon can be expanded to quantify all three classes of analytes.

Figure 4-9A is a schematic illustration of the BIMA assay for prostate-specific antigen (PSA), a widely used serum marker for prostate cancer diagnosis and screening. To be PSA specific, anti-PSA polyclonal antibodies that are conjugated to DW and SNA motifs serve as target recognition domains. The assay was carried out using the same protocol as described above for streptavidin. As observed for streptavidin, BIMA has translated PSA into the DNA barcode successfully, which was then quantified using the strand displacement beacon FQ. The signal changes for PSA (50 ng/mL) spiked in both buffer and human serum samples were over 2 times higher than those of the blanks (Figure 4-9B). The higher background fluorescence in buffer systems suggests the existence of nonspecific adsorption of DW to the SNA via the antibody domain. The target-independent translation of BIMA was reduced significantly in the serum samples, likely due to the competitive adsorption of the high abundant serum proteins to SNA (Figure 4-9B). Moreover, the BIMA assay could quantify as low as 0.8 ng/mL serum PSA, which was significantly lower than the clinical cutoff (4 ng/mL) used for the prostate cancer screening (Figure 4-9C)¹³⁹. The maximum *AE* for PSA-specific BIMA was estimated to be ~ 10 , which is significantly lower than that of

streptavidin (~75). The lower translation efficiency is likely due to the use of bulky antibodies and the streptavidin–biotin conjugation, which can be addressed potentially by using smaller affinity ligands, such as aptamers, as the target recognition domains.

To demonstrate the potential uses of aptamers in BIMA, we further engineered a BIMA specific to platelet-derived growth factor BB (PDGF-BB) by integrating anti-PDGF aptamers as target recognition domains with DW and SNA (Figure 4-9D)¹⁴⁰. PDGF-BB is one of the PDGF isomers that regulate cell growth and division¹⁴¹. To better understand the biological function and interactions of PDGF-BB, it is essential to quantify a minute amount of PDGF-BB and discriminate from its close related isomers, such as PDGF-AB¹⁴¹⁻¹⁴². As shown in Figure 4-9E, the use of aptamers significantly enhances the assay sensitivity, and the maximum *AE* was estimated to be ~60. As low as 8 pM PDGF-BB could be distinguished clearly from the blank. Moreover, our PDGF-BIMA system effectively discriminated PDGF-BB from the AB isomer (Figure 4-9F). This is because the anti-PDGF aptamer has a much stronger binding affinity ($K_d = 0.5$ nM) to the B-chain over the A-chain ($K_d > 100$ nM)¹⁴⁰, and two B chains are required to assemble DW to SNA.

Besides protein-based analytes, it also is possible to translate various nucleic acid sequences to a unified barcode using BIMA. We next investigated BIMA for nucleic acid translation and amplification with a 40-mer synthetic DNA target (Figure 4-9G). A pair of 20-nt complementary DNA sequences was integrated to BIMA for the specific hybridization with the target DNA. As shown in Figure 4-9H, BIMA effectively amplifies the target into the barcode DNA, triggering the subsequent quantification using FQ. The detection limit was determined to be 8 pM, and the maximum *AE* was estimated to be ~25. As the sequence selectivity of BIMA was determined by the sandwiched hybridization among the target DNA

and the two DNA probes, it is possible to expand BIMA to any nucleic acid targets by designing proper complementary DNA probes on the SNA and DW motifs. It also is possible to design BIMA that discriminates single nucleotide mismatches by fine-tuning the length and GC content of the complementary DNA probes.

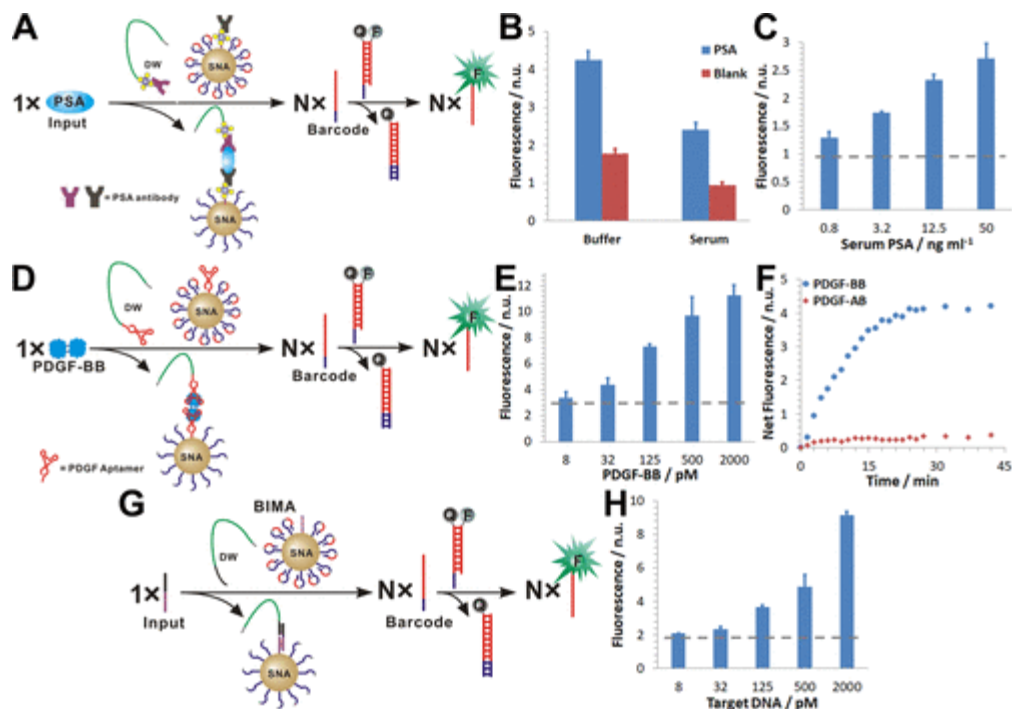


Figure 4-9. (A) Schematic illustration of the antibody-modified BIMA for amplifying prostate specific antigen (PSA). (B) Quantitative analysis of 50 ng/mL PSA in buffer and 10-time diluted human serum samples using BIMA and the unified beacon FQ. (C) Quantification of varying concentrations of PSA spiked in human serum samples using BIMA assay. (D) Schematic illustration of the aptamer-modified BIMA for amplifying platelet-derived growth factor BB (PDGF-BB). (E) Quantification of varying concentrations of PDGF-BB using BIMA translation and the beacon FQ. (F) Real-time monitoring the net fluorescence of BIMA for the quantification of 100 pM PDGF-BB vs 100 pM PDGF-AB. The net fluorescence = total normalized fluorescence – the normalized fluorescence of the blank. (G) Schematic illustration of BIMA for amplifying the 40-mer synthetic DNA target. (H) Quantification of varying concentrations of synthetic DNA targets using BIMA translation and the beacon FQ. In a typical BIMA assay, reaction mixtures containing varying concentrations of targets, 2.5 nM DW, 500 pM SNA, 0.2 U/ μ L nicking endonuclease,

and 20 nM FQ were incubated at 37 °C for 2 h and then subjected to fluorescence measurements. The fluorescence intensity was normalized such that 1 normalized unit (n.u.) corresponds to 1 nM DNA barcode. The horizontal dashed line corresponds to the average fluorescence signal in the absence of the target. Each error bar represents one standard deviation from triplicate analyses.

4.3.5 Application of BIMA to probing the protein-protein interaction

Having established BIMA for the translation and amplification of multiple classes of target molecules, we aimed to expand the BIMA further for studying molecular interactions. To achieve this goal, we tailored BIMA for probing the interactions between PDGF-BB and its receptor, PDGF receptor β (PDGFR- β). The assay principle is illustrated in Figure 4-10A. As has been demonstrated above, BIMA could amplify PDGF-BB effectively into large amounts of DNA barcode molecules for the subsequent quantification using FQ. Because PDGFR- β shares the same binding epitope with the anti-PDGF aptamer¹⁴⁰, the interaction between PDGF-BB and the receptor β could inhibit the BIMA amplification competitively by blocking the target recognition. Then, the attenuated fluorescence signals can be used to quantitatively probe the interaction between PDGF-BB and PDGFR- β . Figure 4-10B shows a near complete inhibition of BIMA by premixing 200 pM PDGF-BB with 200 nM PDGFR- β . Moreover, the inhibition is concentration dependent and a dose-response binding curve was established by varying concentrations of PDGFR- β from 0.2 to 200 nM (Figure 4-10C). By fitting the binding curve into a one site binding isotherm, we estimated the dissociation constant K_d between the two proteins to be 2.7 ± 0.2 nM, which is consistent with the value previously estimated using capillary electrophoresis.

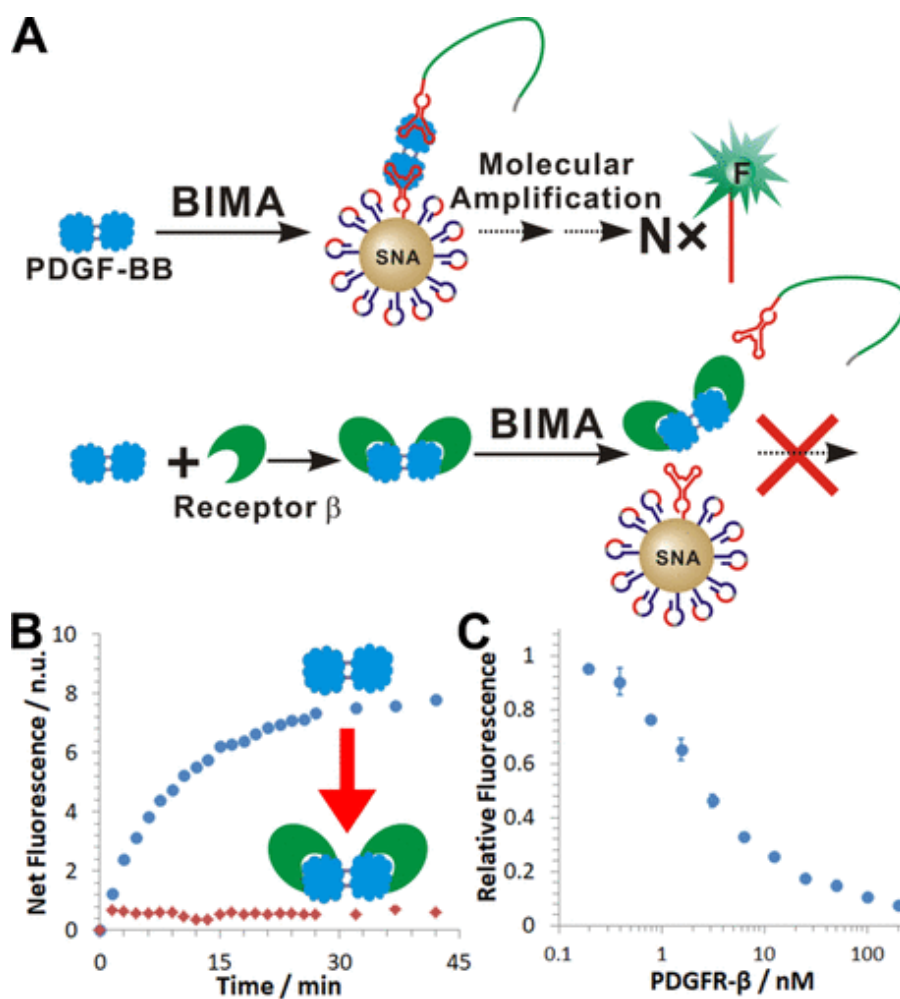


Figure 4-10. (A) Schematic illustration of the principle of using BIMA to probe the interaction between PDGF-BB and PDGF receptor β . PDGF receptor β blocks the aptamer binding sites on PDGF-BB and thus deactivates the PDGF-BB-specific BIMA. (B) Real-time monitoring BIMA using FQ in response to 200 pM PDGF-BB in the presence or absence of 200 nM PDGFR- β . (C) Relative fluorescence of the PDGF-BB-BIMA system as a function of varying concentrations of PDGFR- β from 200 pM to 200 nM.

4.4 Conclusions

Molecular translation is a powerful approach to enable the detection of diverse classes of molecular targets in a single detection platform. Here, we successfully have introduced the binding-induced molecular amplifier that not only translates multiple classes of biomolecules and biomolecular interactions into a unified DNA barcode but also amplifies the translation by allowing the production of up to 75 barcode molecules per input target. The target recognition is achieved on the basis of sandwiched binding events rather than structure-switching aptamers commonly used in other universal detection systems. Such a universal target recognition strategy will ensure the applicability of BIMA to most targets of interest. The output DNA barcode is designed to trigger toehold-mediated strand displacement reactions. As such, a simple strand displacement beacon that conventionally only detects single-stranded DNA target has been expanded for the detection of nucleic acids, proteins, and the protein–protein interaction. As the toehold-mediated strand displacement is a universal principle in most dynamic DNA circuit and device designs, it is possible to amplify detection signals further by integrating BIMA with catalytic DNA reactions, such as hybridization chain reactions¹⁴³, catalytic hairpin assemblies¹⁴⁴, noncovalent DNA catalysis¹⁴⁵, and entropy-driven catalytic DNA circuits¹⁴⁶. It also is possible to achieve sophisticated stimuli-responsive control of dynamic DNA systems via BIMA as a translation and cascading motif. In summary, we anticipate that our success in fabricating BIMA for one-step wash-free molecular translation and amplification will lead to a new concept and strategies in biosensing and dynamic DNA nanotechnology, which may spur the development of novel multianalyte detection platforms and dynamic DNA devices.

Chapter Five: DNA Assembly-Enhanced Binding-Induced Molecular Amplifier as Applied to the Detection of Thrombin

5.1 Introduction

Nanodevices and nanomachines have been developed successfully over the past 30 years and have seen increased usage in recent years due to their modularity and versatility^{91, 147-148}. DNA is a key component in constructing nanodevices and nanomachines because it has predictable structures, large diversity, is affordable, and is easily modified. Various types of DNA nanodevices have been developed, including DNA motors^{37, 149-154}, DNA walkers^{88, 155-158}, DNA switches^{81, 159-162} and others^{86, 163-165}. Most applications of DNA nanomachines use DNA self-assembly in response to nucleic acids. However, it is challenging to leverage the utility of DNA nanomachines in protein-activated systems¹⁶⁶⁻¹⁶⁷.

In this Chapter, a binding-induced molecular amplifier (BIMA) that uses DNA functionalized AuNP was developed to generate a target-induced cleavage of caged output DNA molecules. AuNPs are used because they act as scaffolds that are easily functionalized with DNA and can act as fluorescence quencher. Using AuNPs, we constructed a three-dimensional DNA nanomachine with high DNA probe density¹⁶⁸ to act as a molecular amplifier.

Figure 5-1 shows a general detection scheme in the presence of target proteins. A BIMA includes two main aspects: a binding-induced DNA assembly and signal amplification¹⁶⁹. We modified the output DNA with a fluorescent label (**Y1-F**) and conjugated an affinity ligand to the support DNA. Both probes contain a 5-nucleotide poly-thymine spacer and an 18-nucleotide complementary region. These two probes were pre-hybridized to form a

double-stranded DNA (dsDNA) before being conjugated to the AuNP surface via thiol–Au interaction. An additional affinity ligand used was conjugated to the swing arm of the probe DNA (**NB**). The tail of the **NB** had a 7-nucleotide (nt) complementary region with **Y1-F**. The melting temperature (T_m) of this short 7nt region is ~ 2 °C. When the target protein is absent, the hybridization between the **NB** and the output is unstable at room temperature. When the target proteins exist in the reaction solution, a single target protein can be bound by both **NB** and **Y1-F**. The binding of both probes to a single target protein greatly increases the hybridization between **NB** and **Y1-F** because the high local concentration of **Y1-F**. Both probes anchored to the same target protein also result in the hybridization between complementary regions being an intra-molecular interaction, as opposed to an inter-molecular interaction when probes are free in solution. A nicking site was designed on this double-stranded DNA, which can be recognized by a nicking endonuclease and cleaves only the **Y1-F** strand. The cleaved portion of **Y1-F** contains the fluorophore which is initially quenched by the AuNP but has increased fluorescence when it is released from the surface of the AuNP. The **NB** remains intact and dissociates to allow hybridization with another **Y1-F** strand. Therefore, a single target binding can result in the cleavage of many **Y1-F**.

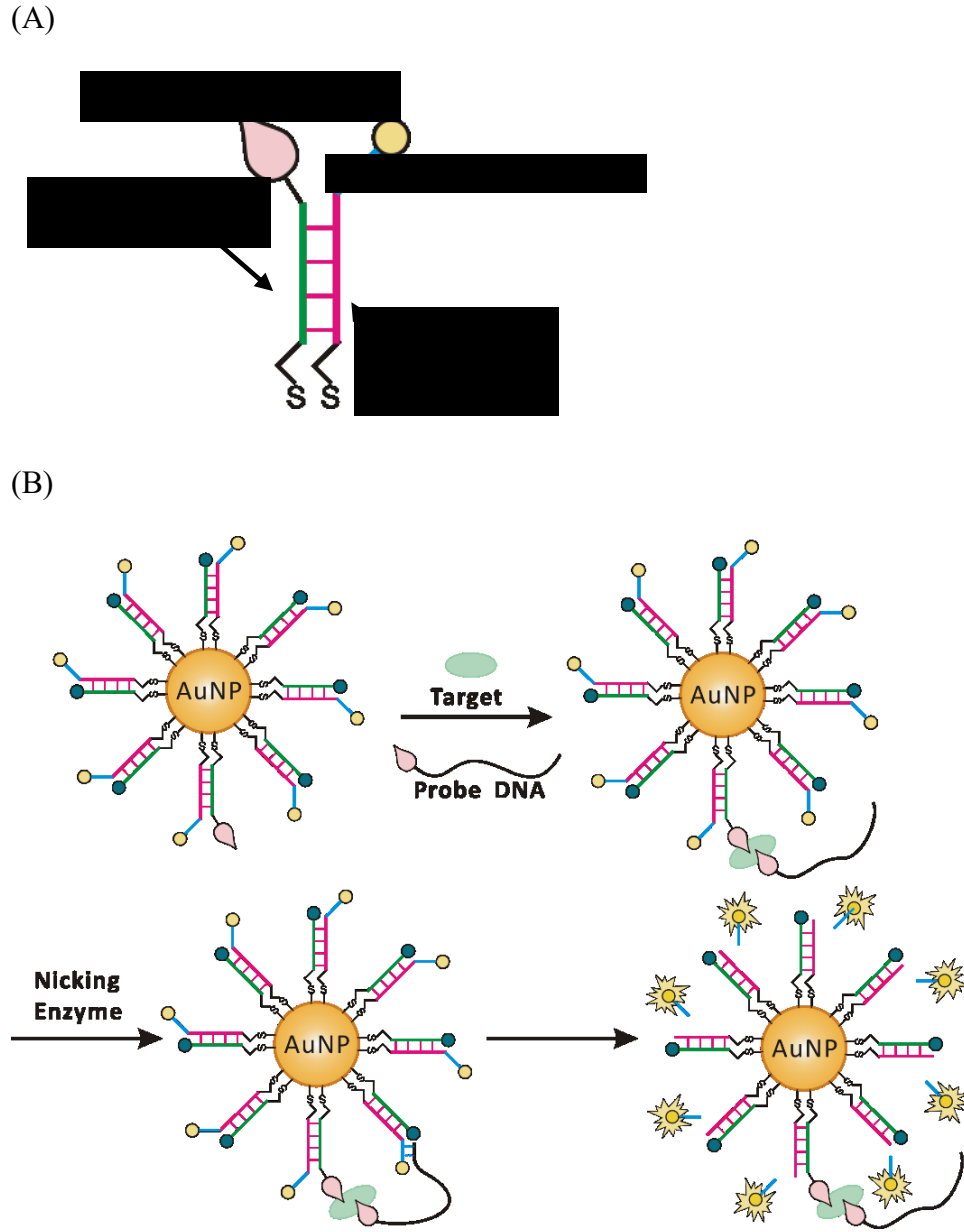


Figure 5-1. Schematic illustration of a protein triggered BIMA. (A) Structure of dsDNA probe. (B) Detection of a target protein using a nicking endonuclease to cleave the detection probes from AuNP. The dsDNA is functionalized on AuNPs with one output DNA fluorescently labeled and the other one labeled with an affinity ligand. Another affinity ligand is conjugated to the swing arm of the DNA probe. In the presence of the target molecule, the binding of the target-affinity ligands brings the DNA probe and the output

DNA together and forms a complementary double-stranded sequence, which can be recognized and cleaved by the nicking enzyme. The fluorescence of the cleaved output DNA is released, leaving the dissociated probe DNA to hybridize with another output DNA, resulting in multiple cleavage events and subsequent signal amplification.

5.2 Experimental

5.2.1 Materials and reagents

All solutions of gold nanoparticles (from 20 nm to 50 nm in diameter) were purchased from Ted Pella (Redding, CA). DNA oligonucleotides were obtained from Integrated DNA Technologies (Coralville, IA) with HPLC purification. Sequences and modifications are listed in Table 5-1. PolyT was modified as a spacer because it has the lowest binding affinity to the AuNP surface¹⁷⁰.

Streptavidin from bacterium *Streptomyces avidinii*, biotin, bovine serum albumin (BSA), human serum, sodium chloride (NaCl), magnesium chloride hexahydrate ($\text{MgCl}_2 \cdot 6\text{H}_2\text{O}$), potassium chloride (KCl), and Tris-HCl (TE, pH 7.4) buffer were purchased from Sigma-Aldrich (Oakville, ON). Phosphate buffered saline (PBS) 10X solution and Tween 20 were purchased from Fisher Scientific. Human α -Thrombin and human prothrombin were purchased from Haematology Technologies Inc. (Essex Junction, VT). Nicking endonuclease Nb.BbvCI was purchased from New England Biolabs Inc. (Whitby, ON).

NANOpure water ($> 18.0 \text{ M}\Omega$) was purified using an Ultrapure Milli-Q water system and autoclaved before applying to all experiments.

Double-strand DNA (dsDNA) annealing buffer contained 1 X PBS and 0.05% Tween 20. The washing buffer was made of 20 mM Tris-HCl and 0.1% Tween 20, pH 7.4. Nicking endonuclease reaction buffer contained 10 mM Tris-HCl, 50 mM NaCl, 10 mM MgCl_2 , 0.02% Tween 20, pH 7.9.

Table 5-1. DNA sequences and modifications for streptavidin-biotin system and thrombin-thrombin binding aptamer (TBA) system

Probe	Sequences and modifications
Y1-F	5'- Thiol - TTTTT - ACG AGT TGT CTA CTG TAG - TT - GC'TGAGG - T - FAM -3'
Y1-F31	5'- Thiol - TTTTT - ACG AGT TGT CTA CTG TAG - GC'TGAGG - T - FAM -3'
Y1-S	5'- T - CTA CAG TAG ACA ACT CGT - TTTTT - Thiol -3'
Y1-Q	5'- Quench - CTA CAG TAG ACA ACT CGT - TTTTT - Thiol -3'
Y1-B	5'- Biotin - TTTTT - CTA CAG TAG ACA ACT CGT - TTTTT - Thiol -3'
NB36	5'- Biotin - TTT TTT TTT TTT TTT TTT CTT GTT ATC TTC CTC AGC-3'
NB48	5'- Biotin - TTT CTT GTT ATC TTC CTC AGC-3'
NB60	5'- Biotin - TTT CTT GTT ATC TTC CTC AGC-3'
Y1-Block1	5'- GAG G - AA GA -3'
Y1-Block2	5'- GAG G - AA GAT -3'
Y1-Block3	5'- GAG G - AA GAT A -3'
Y1-Block4	5'- GAG G - AA GAT AA -3'
Y1-15A	5'- <u>GGT TGG TGT GGT TGG</u> - TTTTT - CTA CAG TAG ACA ACT CGT - TTTTT - Thiol -3'
Y1-29A	5'- <u>AGT CCG TGG TAG GGC AGG TTG GGG TGA CT</u> TTT TTT TTT TTT TTT TTT CTT GTT ATC TTC CTC AGC-3'

5.2.2 Preparation of DNA molecular amplifier on AuNPs

Thiolated DNA oligonucleotides were used to functionalize AuNPs and construct the DNA assembly-enhanced binding-induced amplifier. For single strand probes, the oligonucleotides were diluted to 5 μM in 200 μL using 1 \times PBS buffer. For double strand probes, the oligonucleotides with complementary region (**Y1-F** to **Y1-S**, **Y1-B** and **Y1-Q**) were mixed to a final concentration of 5 μM each in 200 μL . The mixture was heated to 95 $^{\circ}\text{C}$ for 5 min and cooled to 25 $^{\circ}\text{C}$ over a period of 1 h. Then, the prepared probes were added to 1 mL AuNP solution (the ratio between probes to AuNPs was 1000:1) and incubated at 4 $^{\circ}\text{C}$ for 24 h. Then, 50 μL 3 M NaCl was added slowly to the mixture followed by sonication for 10 s. This process was repeated seven times at 30 min intervals. The resulting solution was stored at 4 $^{\circ}\text{C}$ for 48 h to maximize the probe loading amount. After 48 h, the solution was centrifuged at 13000 rpm for 30 min to separate the DNA-AuNPs from unreacted reagents. The mixture was washed three times with washing buffer, redispersed in 200 μL , and stored at 4 $^{\circ}\text{C}$ in the dark when not in use.

5.2.3 Characterization of ssDNA-AuNP and dsDNA-AuNP molecular amplifier

Both ssDNA and dsDNA loading amount on AuNPs were measured using a fluorescence turn-on assay. A Beckman Coulter DTX 800 Multi-Mode Microplate Reader was used to quantify the fluorescence signal.

10 μL of DNA functionalized AuNPs (DNA-AuNPs) were incubated with 90 μL of 50mM 2-mercapto ethanol (ME) at room temperature overnight in the dark; this cleaved all DNA from the surface of AuNP. Then, the solution was transferred to a 96-well microplate, and the fluorescence performance was measured using the microplate reader with

excitation/emission wavelengths of 485/535 nm. A fluorescence calibration curve was constructed with various concentrations of FAM labeled Y1-F probe from 5 nM to 5 μ M as an external standard. All DNA-AuNP were prepared in triplicate and under the same conditions as those for measuring the calibration curve.

The loading amount was calculated from the concentration of cleaved DNA probe divided by the concentration of AuNPs and is listed in Table 2-2.

To compare the chemical stability of ssDNA-AuNP and dsDNA-AuNP, we conjugated both Y1-F as ssDNA and pre-hybridized Y1-F and Y1-S as dsDNA to AuNPs in separate batches. Both types of DNA-AuNPs were treated with 20 μ M DTT solution and incubated at 37 °C in the microplate reader (Table 5-2). The initial rate constant, k_i , for released DNA was determined from the following equation:

$$\ln(1-[\text{Released}]/[\text{Total}]) = k_i t, t = 5-40 \text{ min}$$

where the value of $[\text{Released}] / [\text{Total}]$ was defined as fluorescence signal at each time point over the final fluorescent signal.

Table 5-2. DNA loading amount on 20 nm size AuNPs. ssDNA was a fluorescence labeled single strand probe (Y1-F). dsDNA was a fluorescence labeled DNA hybridized with its complementary supporting DNA (Y1-F+Y1-S). The dsDNA loading amount per AuNP was slightly lower than that of ssDNA because of steric effects

	Avg (DNA per AuNP)	Std. Dev.
ssDNA-AuNP	209	5
dsDNA-AuNP (Y1-F+Y1-S)	160	6

5.2.4 Target detection using a DNA-AuNP molecular amplifier

Typical procedures for target protein detection using a DNA assembly-enhanced binding-induced molecular amplifier consisted of mixing 250 pM of DNA-AuNP, 2.5 nM probe DNA (NB36, NB48, or NB60), 1 × CutSmart buffer, and varying concentrations of target protein. All reacted with 2 units of nicking endonuclease (Nb.BbvCI), and its activity buffer were added to a final volume of 100 μL.

The reaction mixture was incubated at 37 °C in a 96-well plate, and the released fluorescence was measured directly in a microplate reader. To monitor the real-time reaction kinetics, the fluorescent signal was collected every 5 min for 2 h. A mixture of 250 pM DNA-AuNP and the same amount of nicking enzyme was used as a negative control to monitor any target independent cleavage of FAM labeled output DNA (Y1-F) and correct for the thermal stability of DNA-AuNP.

5.3 Results and Discussion

5.3.1 Biotin labeled DNA-AuNP binding-induced molecular amplifier for streptavidin

A streptavidin and biotin model system were used to test the feasibility of this binding-induced molecular amplification strategy (Figure 5-3). This model system was chosen because of the extremely strong binding affinity between streptavidin and biotin ($K_d = 10^{-14}$ M)¹⁷¹. This pair ensures minimal influence of the target binding process in optimization of the best reaction conditions. In a typical experiment, biotin worked as an affinity ligand labeled on the support DNA of dsDNA-AuNP (**Y1-B**) and DNA probe, and streptavidin was the target protein. To improve the stability of dsDNA and reduce thermal dissociation, the melting temperature of dsDNA (eg. **Y1-FS** or **Y1-FB**) was ≥ 58 °C, which is higher than nicking enzyme reaction temperature of 37 °C.

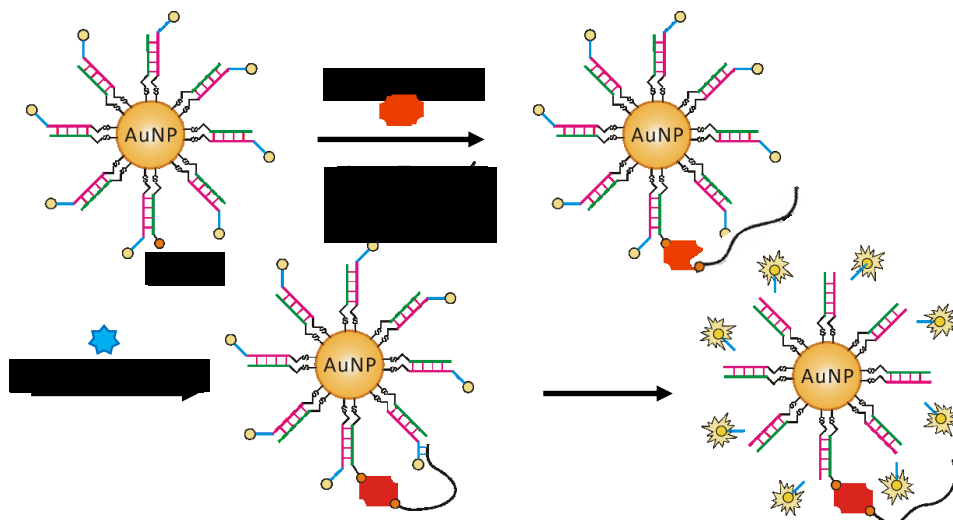


Figure 5-2. Schematic illustration of streptavidin–biotin dsDNA-AuNP molecular amplifier model system. FAM labeled output DNA (Y1-F) pre-hybridized with support DNA constructed dsDNA-AuNP. The ratio between non-labeled support DNA (Y1-S) and biotinylated support DNA (Y1-B) was 20:1. The NB probe also was biotinylated. Both NB and Y1-B binding with the same target streptavidin brought NB close to Y1-F, the local concentration of NB increased, and it formed a double-strand that can be recognized by a nicking enzyme. As a result, Y1-F was cleaved and released in solution, generated a fluorescent signal, and NB moved on to hybridize with next Y1-F on the same AuNP.

The chemical stability was tested between Y1-F functionalized ssDNA-AuNP and Y1-FS functionalized dsDNA-AuNP. The observed initial dissociation rate of ssDNA-AuNP ($k_i = 3.5 \times 10^{-3} \text{ min}^{-1}$) was faster than that of dsDNA-AuNP ($k_i = 7.1 \times 10^{-4} \text{ min}^{-1}$). These results suggested that, ssDNA-AuNPs react more readily with competing thiols compared to dsDNA-AuNPs that uses both DNA strands to anchor to the AuNP. This shows the chemical stability was enhanced using dsDNA compared to ssDNA.

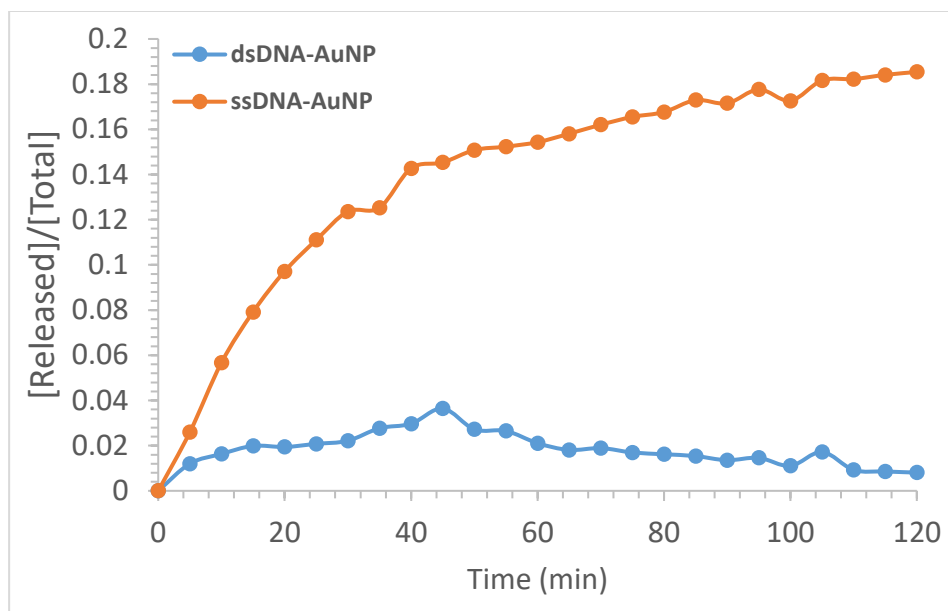


Figure 5-3. Kinetics of the chemical dissociation of ssDNA-AuNP and dsDNA-AuNP induced by 20 μ M DTT over a period of 2 h at 37 $^{\circ}$ C. The released signal was the fluorescence signal that was detected after reaction with DTT. The total signal was the total maximum fluorescence signal generated by functionalized AuNPs.

The length of the swing arm probes (**NB**) was investigated as it must be long enough to reach many **Y1-F** on the AuNP surface. A short swing arm would only be able to reach a low amount of **Y1-F** and would limit the amount of cleavage from each streptavidin–biotin binding event. Figure 5-4 shows the results of using different lengths of a swing arm NB probe DNA (36, 48, or 60 nucleotides in total length). The NB probe was biotinylated on the 5'-end and consisted of a poly-thymine spacer and a 7-nucleotide nicking enzyme recognized region. The reaction rate and signal plateau of different lengths of NB under the same conditions were very similar, which indicated that all three NB probes were sufficiently long enough to reach the Y1-F on the AuNP sphere.

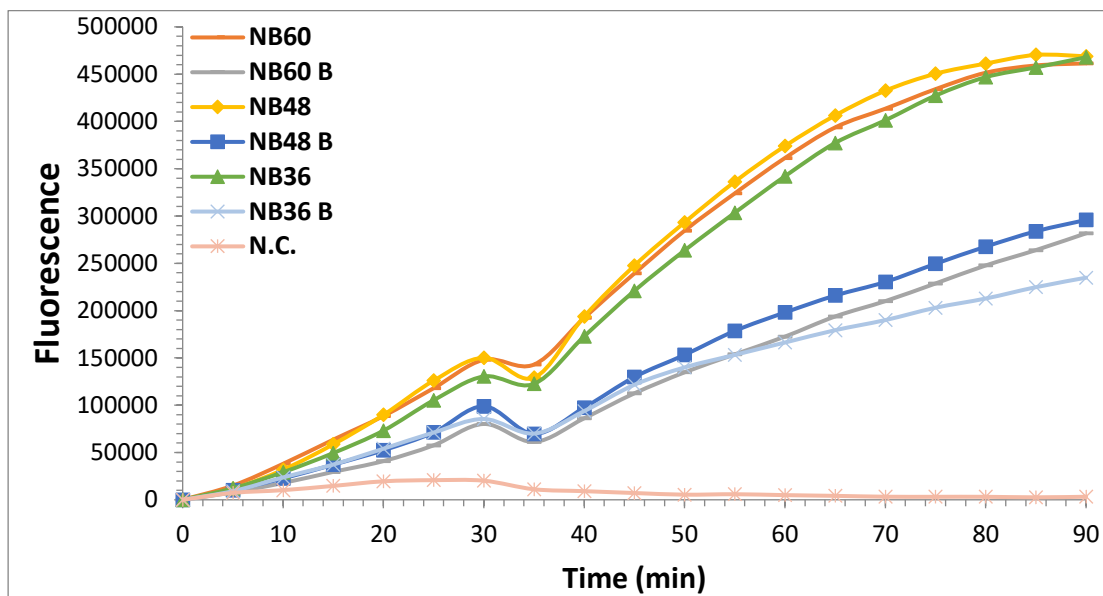
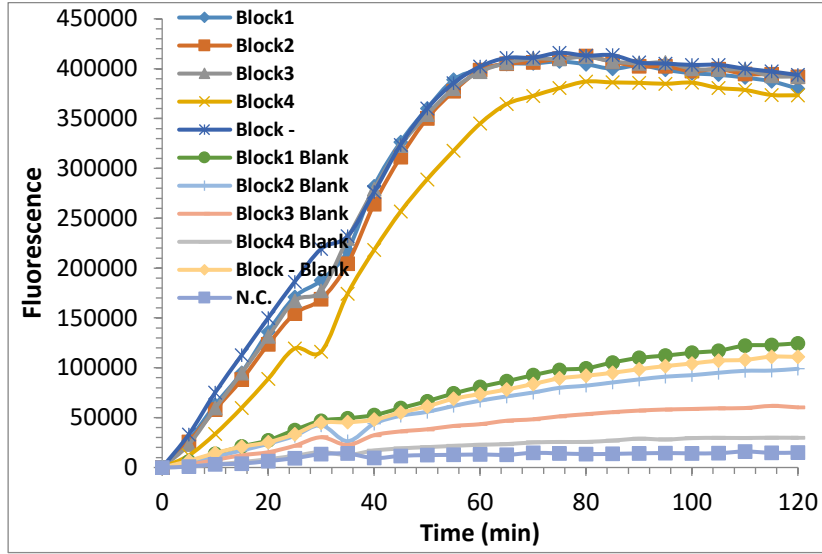


Figure 5-4. Characterization of using various lengths of NB probes. Fluorescence was from cleaved probes due to the reaction of 0.25 nM dsDNA-AuNP with 500 pM streptavidin and 6.25 nM NB probes at 37 °C. The blank reaction conditions contained every matrix substrate except for target streptavidin. Different lengths of NB probes finally reached a similar plateau, and NB36 had relatively low blank signal compared to others. The apparent decrease in fluorescence intensity for 30 min to 35 min might be due to an unknown instrumental issue (from plate reader).

5.3.2 Reduction of background signal for dsDNA-AuNP amplifier

We have successfully achieved detection of streptavidin by using a dsDNA assembly-enhanced binding-induced amplifier. However, comparing the blank to the N.C. signals in Figure 5-4, a high background signal is generated. One possibility for the high background signal is that target-independent cleavage took place. This could occur by biotinylated **NB** probes hybridizing with the AuNP anchored **Y1-F**. Hybridization between **NB** and **Y1-F** generates the nicking enzyme site, which can be cleaved by the nicking enzyme and generate background signal. There are only seven complementary nucleotides between **NB** and **Y1-F**, with an estimated T_m of 2 °C, so the hybrid should be unstable at the nicking enzyme reaction temperature. To reduce the background signal, a DNA blocker was designed to minimize target-independent hybridization by competing with the NB probe in hybridizing with **Y1-F**. **NB** probes were incubated first with blockers for 15 min before mixing with other substrates. Different lengths of blockers were tested, and the results are shown in Figure 5-5A. Longer blockers with higher melting temperatures were more effective at preventing nonspecific hybridization. The blank signal decreased the most in the presence of the longest blocker (**Blocker 4**). The blocker concentration also was tested (Figure 5-5B) from 0 to 100 nM. Higher concentrations of **Blocker 4** were more effective at competing with nonspecific hybridization, and 100 nM of **Blocker 4** showed the lowest background signal and the highest signal-to-noise ratio.

(A)



(B)

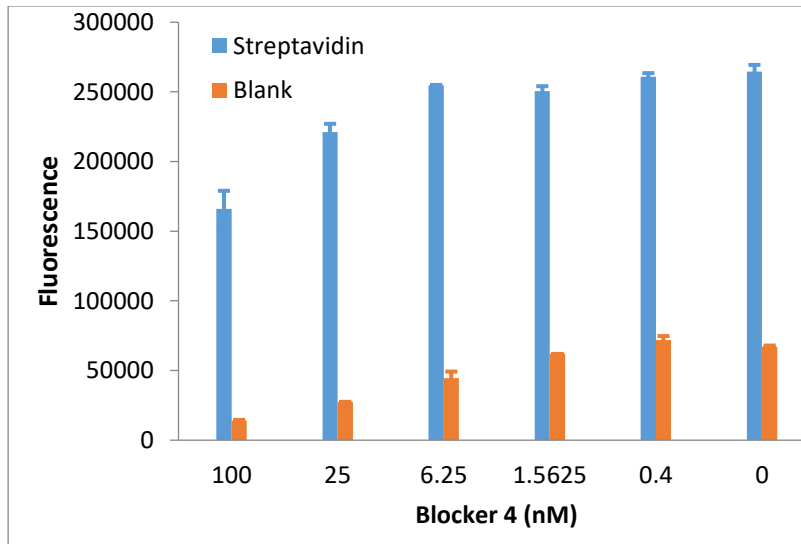


Figure 5-5. (A) Kinetic studies of different blockers on quencher-labeled dsDNA-AuNP. Fluorescence was from the cleaved probes due to the 0.25 nM Y1-FQB dsAuNP-AuNP reaction with 1 nM streptavidin and 2.5 nM NB36 probes in a 2 unit nicking enzyme at 37 °C. 100 nM of Blocker 1 to Blocker 4 were added, and the Blocker– sample and blank signal show the reaction signal without adding any blocker. Blocker 4, the longest blocker,

has the highest signal-to-noise ratio. (B) Optimization of Blocker 4 (from 400 pM to 100 nM). Fluorescence was measured at 120 min. Fluorescence cleaved from the 0.25 nM Y1-FQB dsDNA-AuNP reaction with 1 nM streptavidin and 2.5 nM NB36 in a 2 unit nicking enzyme at 37°C.

Another cause of high background may be due to incomplete quenching of **Y1-F** fluorescence. AuNP quenching is distance dependent and the conjugated dsDNA is orientated perpendicular to the AuNP, placing the fluorophore further from the AuNP; this is not the case with ssDNA which is more flexible and allows the fluorophore to be closer to the AuNP surface. Furthermore, the more dsDNA probes packed per AuNP, the more repulsion between individual dsDNA resulting in more dsDNA to be perpendicular to the surface. Therefore, we designed a quencher-modified support DNA (**Y1-Q**) to replace the use of **Y1-S**. When dsDNA was released from AuNP, a closer quencher label on one probe of dsDNA always helped absorb fluorescence from the other probe. We compared **Y1-Q** and **Y1-F** pre-hybridized dsDNA functionalized AuNP to **Y1-S** and **Y1-F** dsDNA-AuNP (Figure 5-6); as we suspected, the background signal decreased.

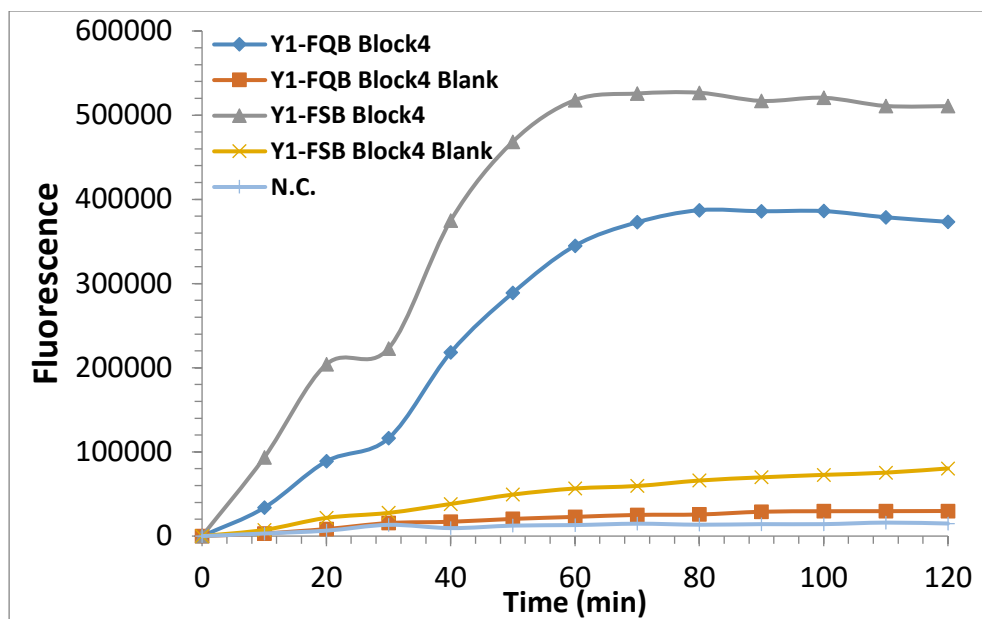


Figure 5-6. Kinetic studies comparing quencher labeled dsDNA-AuNP (Y1-FQB) to non-quencher labeled dsDNA-AuNP (Y1-FSB). A 0.25 nM AuNP were mixed with 1 nM streptavidin and 2.5 nM NB 36 probes that were pre-incubated with 100 nM Blocker 4 in a 2 unit nicking enzyme at 37 °C.

5.3.3 Effect of spacer on the generation of output DNA from dsDNA-AuNP

The **Y1-F** output DNA has a 2-T spacer structure between the dsDNA complementary region and the nicking enzyme recognition region at the fluorophore labeled 3'-end. The spacer was used to separate and increase the flexibility of **Y1-F**. To demonstrate the importance of this structure, **Y1-F31** was designed by removing the 2-T between the dsDNA support and nicking enzyme recognition. The loading amount of **Y1-F31SB** dsDNA-AuNP was 147 ± 6 per AuNP, which was similar to the loading amount of **Y1-FSB** dsDNA-AuNP (160 ± 6). Therefore, the maximum signals of each probe system should be similar. Each output DNA probes was tested with a non-quencher labeled dsDNA-AuNP (Figure 5-7A) and quencher

labeled dsDNA-AuNP (Figure 5-7B). The cleavage efficiency of the **Y1-F31** probe was lower under both conditions, most likely due to steric effects and because the output DNA without spacer was too stiff to hybridize quickly with NB probes.

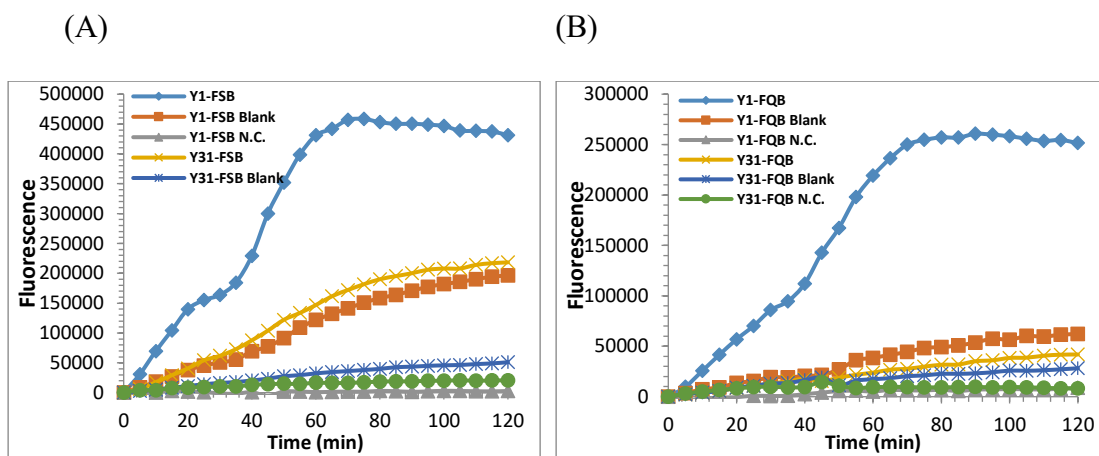


Figure 5-7. Comparison of different lengths of output DNA using (A) dsDNA-AuNP without quencher labels (B) dsDNA-AuNP with quencher labels. Fluorescence was from the cleaved probes due to the 0.25 nM AuNP reaction with 2.5 nM NB36 in a 2 unit nicking enzyme at 37 °C.

5.3.4 Effect of AuNP size on dsDNA assembly-enhanced binding-induced molecular amplifier

Signal amplification efficiency is dependent on the amount of dsDNA per AuNP. We have examined different sizes of AuNP functionalized with dsDNA. Since the surface area of AuNPs increased when using larger AuNP particles, the loading amount of dsDNA probe on the surface also increased with larger AuNPs (Table 5-3). For the target binding-induced NB probe, a higher output dsDNA density helped probe hybridization and nicking enzyme cleavage. However, it was difficult to have high concentrations of AuNP in solution because the larger particles aggregated easily. Therefore, the balance between AuNP size and concentrations was tested (Figure 5-8); a 30 nm size AuNP showed best signal to noise ratio.

Table 5-3. Loading amount of double strand DNA on different size AuNPs. Y1-F probe pre-hybridized with Y1-S to form fluorescence labeled dsDNA-AuNP

AuNP size (nm)	Avg (dsDNA per AuNP)	Std
20	160	6
30	216	5
50	363	32

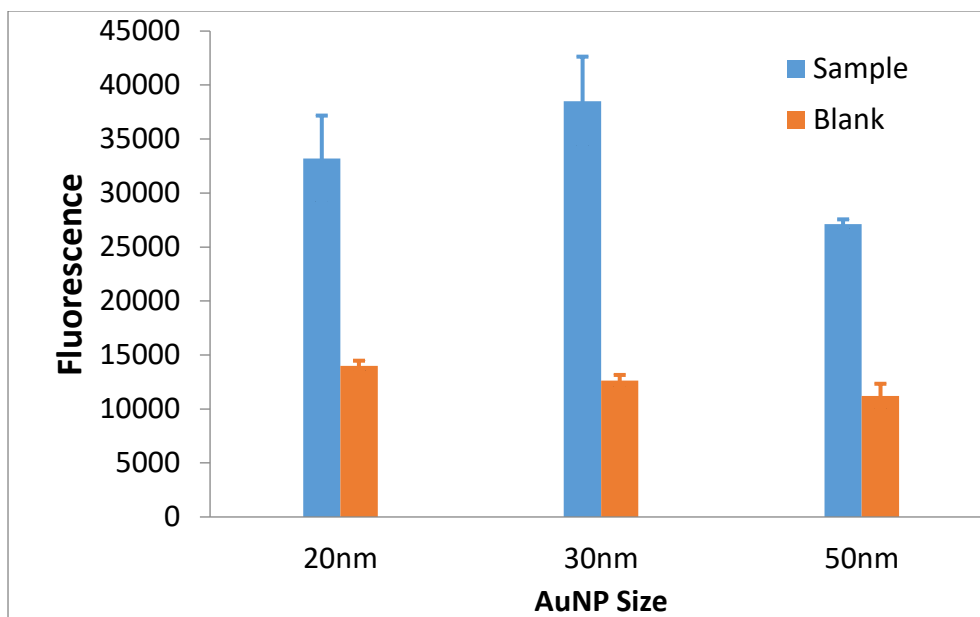
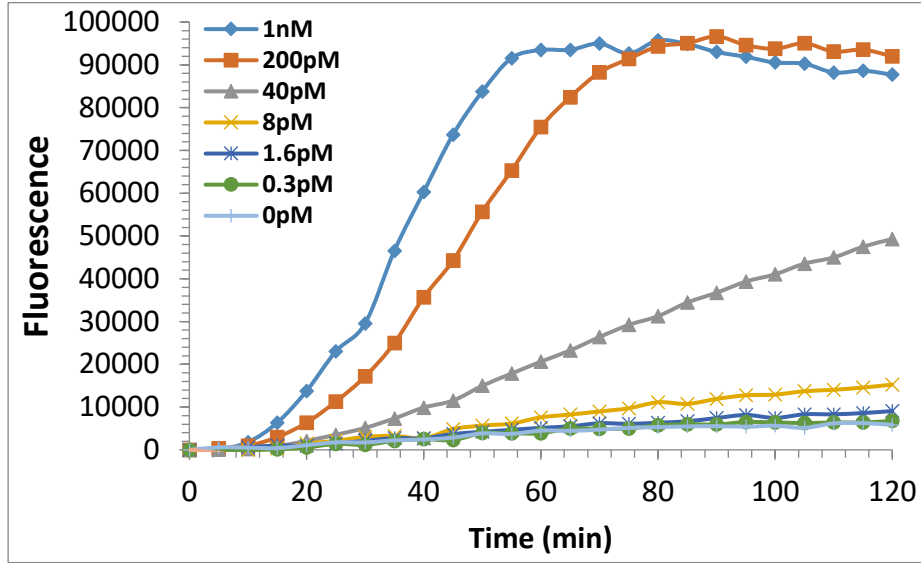


Figure 5-8. Comparison of different diameters of AuNP (from 20 nm to 50 nm). Both the net signal and the signal-to-background ratio were highest when using 30 nm AuNPs. Fluorescence was from the cleaved probes due to the 125 pM ds-DNA AuNP (Y1-FQB) reaction with 20 pM streptavidin and 2.5 nM NB36 with 100 nM Blocker 4 in a 2 unit nicking enzyme at 37 °C. Fluorescence was taken at 60 min.

By using **Y1-FQB** dsDNA conjugated on a 30 nm size AuNP, 200 pM streptavidin reached a signal plateau at 90 min, indicating that a maximum amount of **Y1-F** output DNA on 125 pM of dsDNA-AuNP was cleaved (Figure 5-9A). Increasing the concentration of target streptavidin showed that the fluorescence intensity increased (Figure 5-9B). The LOD of streptavidin (300 fM) was calculated by adding three times standard deviation of the blank signals to the average of blank signal.

(A)



(B)

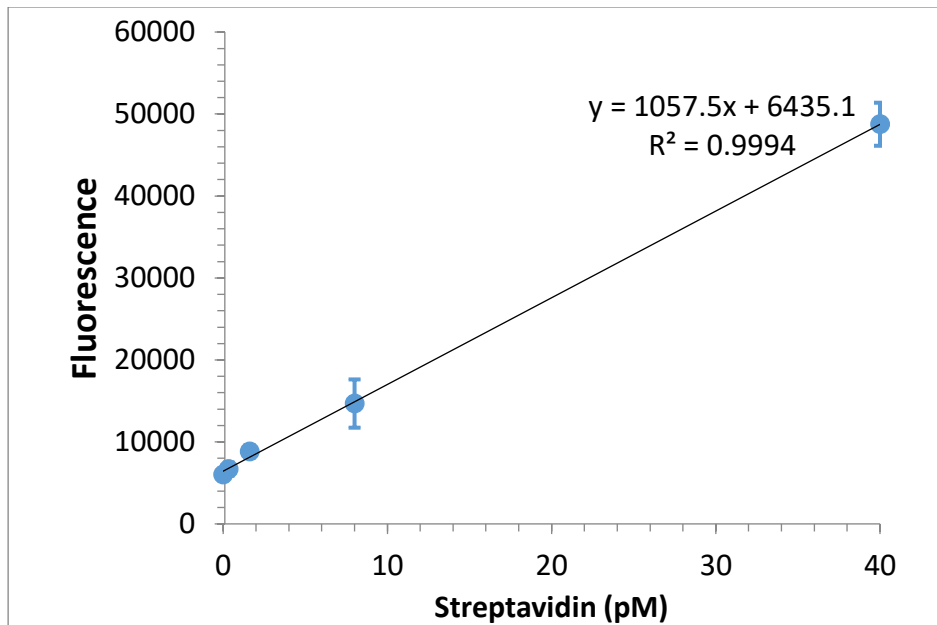


Figure 5-9. Evaluation of the streptavidin–binding system using 30 nm AuNP. (A) Kinetic cleavage of Y1-F output DNA from 30 nm Y1-FQB dsDNA-AuNP with different target streptavidin concentrations (from 300 fM to 1 nM). (B) Fitting the streptavidin value to a linear regression model. Fluorescence was taken at 120 min.

5.3.5 Application of the DNA binding-induced molecular amplifier to the detection of thrombin

Our dsDNA assembly-enhanced binding-induced amplifier performed well under streptavidin–biotin conditions. To demonstrate the application of this strategy, a thrombin and thrombin-binding-aptamer (TBA) system was designed (Figure 5-10). Two different TBA can bind to two different epitopes on one thrombin molecule. The binding affinity of the 29-nucleotide TBA is stronger than that of the 15-nucleotide TBA. Considering that the local concentration of labeled dsDNA on AuNP was relatively higher than the concentration of free arm-swing probe DNA in solution, the 15-nucleotide TBA was modified on the supporting DNA that was functionalized to the AuNP (**Y1-15A**), and 29-nucleotide TBA was modified on the **NB** probe (**Y1-29A**) to capture low concentrations of thrombin. In addition, compared to the length of 15 n.t., the 29 n.t. TBA was longer and increased the flexibility of the **NB**. All reaction conditions were the same as the biotin-streptavidin system.

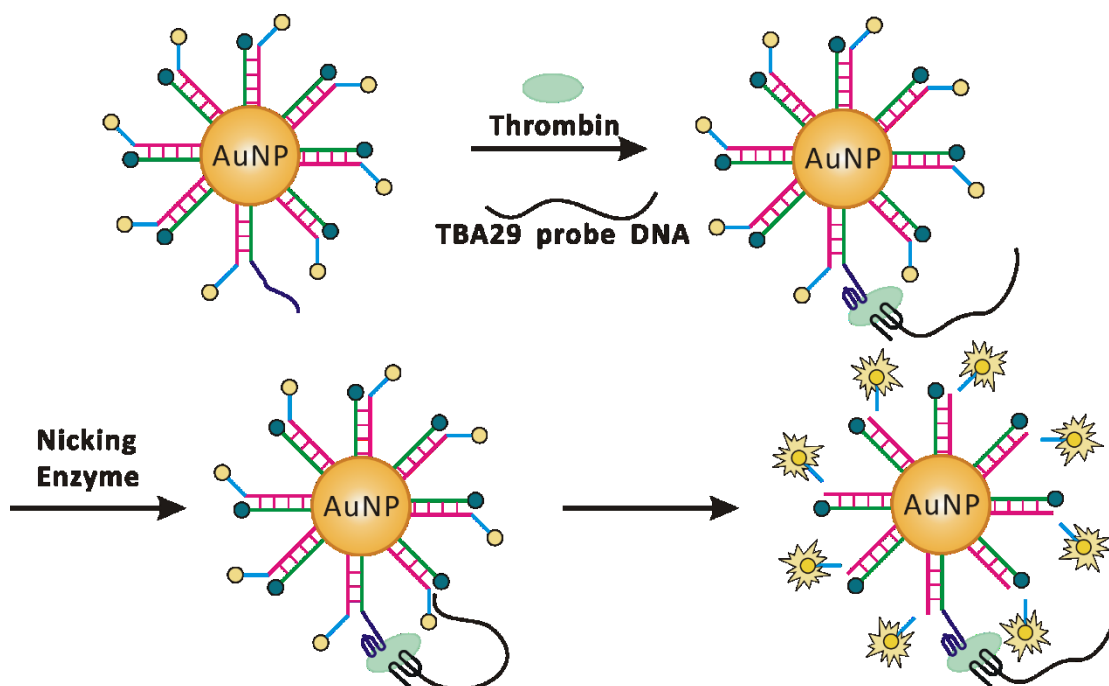


Figure 5-10. Schematic illustration of a thrombin-TBA binding-induced molecular amplifier. In the presence of thrombin, both TBA 15 on dsDNA and TBA 29 on NB probe formed a G-quadruplex structure that bonded on two sites of thrombin and brought the NB tail very close to Y1-F DNA. The local concentration of Y1-F increased and brought a complementary sequence on the Y1-29A NB probe and Y1-F together. This double-strand hybrid recognized by nicking enzyme and Y1-F was cleaved on the nicking site. Fluorescence was released in the solution and, without a Y1-Q or AuNP quenching effect, it was detected by the microplate reader and was a turn-on assay. The same NB probe dissociated and hybridized with another Y1-F output DNA. By cleavage of multiple Y1-F, the sample signal was amplified.

We further studied the effects of salt concentration on the system. Potassium is involved in TBA folding into G-quadruplex structure and improves the stability in the complex state¹⁷²⁻¹⁷³. A 1 mM KCl was added to the nicking endonuclease reaction buffer (Figure 5-11) and the net signal was larger than in the absence of KCl. A stable G-quadruplex structure increased intermolecular binding and reduced the possibility of self-dimers or hetero-dimers between the two probes. Therefore, we generated a calibration curve of thrombin from 500 pM to 1.6 pM (Figure 5-12). The limit of detection was 8 pM.

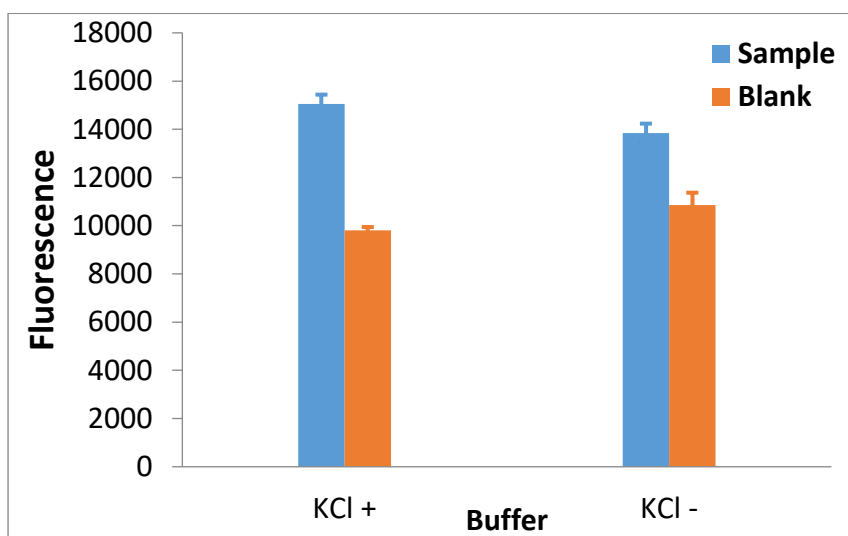


Figure 5-11. Potassium effects on the TBA reaction. 1 mM KCl was added to the reaction buffer. Fluorescence was measured at 120 min. Fluorescence was from the cleaved probes due to the 125 pM Y1-FQB dsDNA-AuNP reaction with 100 pM thrombin and the 2.5 nM Y1-29A NB probe with 100 nM Blocker 4 in a 2 unit nicking enzyme at 37 °C.

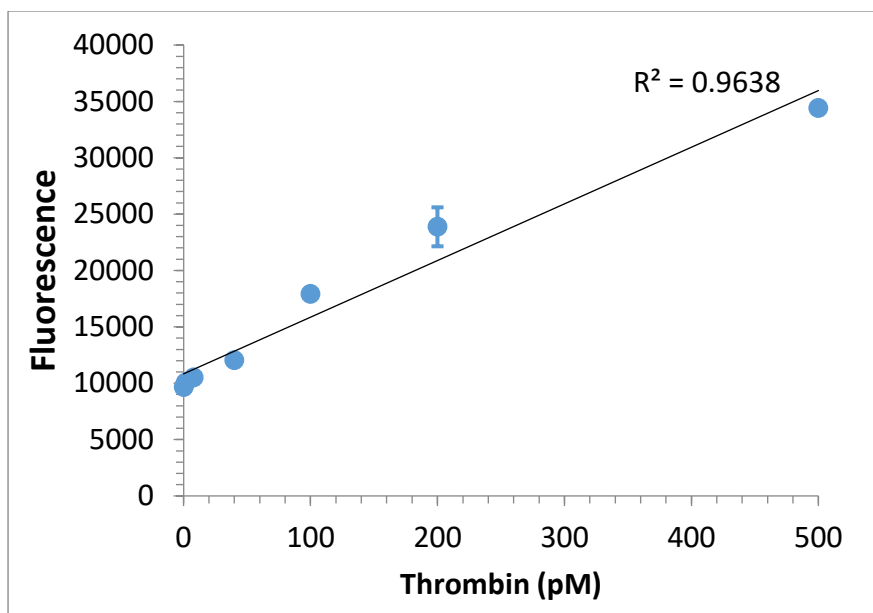


Figure 5-12. Detection of thrombin dynamic range. Fluorescence was measured at 120 min, from the 125 pM quencher-labeled Y1-FQB dsDNA-AuNP reaction with the 5 nM Y1-29A probe and 500 nM Blocker 4 in a 4 unit nicking enzyme at 37°C. The detection limit of thrombin was 8 pM.

After all the performance comparisons, we tested the specificity of thrombin against four other human serum proteins, including human hemoglobin, cytochrome c, transferrin, and prothrombin. As shown in Figure 5-13, the thrombin-TBA dsDNA-AuNP amplifier showed high signal for target protein thrombin. The thrombin signal was significantly higher than other proteins, which gave a signal similar to the blank, even though they had a concentration 10 times higher than the tested thrombin.

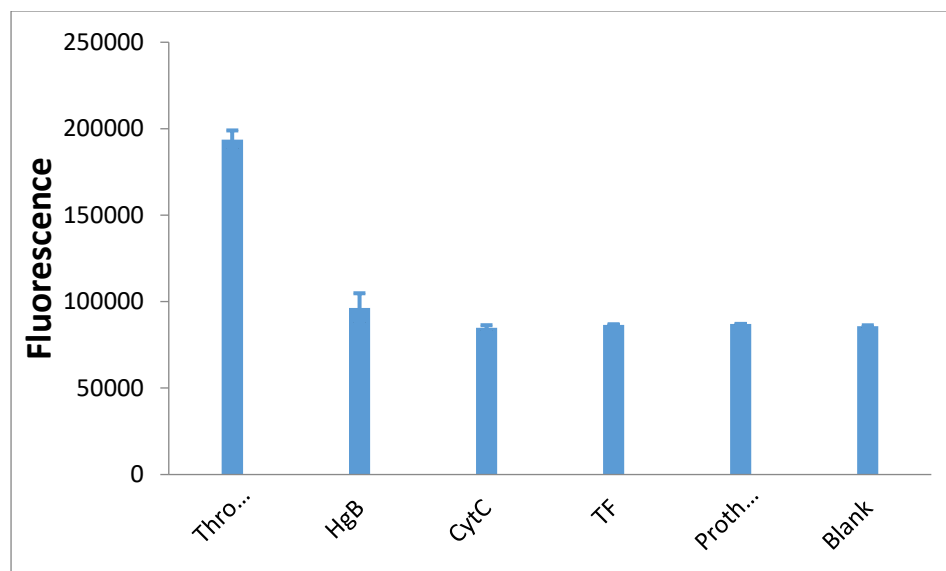


Figure 5-13. Specificity of thrombin with other common serum proteins (human hemoglobin, cytochrome c, transferrin, and prothrombin). 125pM Y1-FQB dsDNA-AuNP reacted with the 10 nM Y1-29A probe, 1 nM thrombin, and 10 nM of other proteins in 500 nM Blocker 4 and in a 6 unit nicking enzyme at 37 °C.

5.4 Conclusions

In conclusion, we have successfully developed a DNA assembly-enhanced binding-induced molecular amplifier. Using dsDNA probes instead of ssDNA increased the overall chemical stability of the DNA-AuNP structure. To form the binding-induced molecular amplifier, one affinity ligand was labeled on dsDNA-AuNP and the other affinity ligand was labeled on the swing arm of **NB** probes. The binding of the two affinity ligands to a specific target protein assembled all substrates to the AuNP. Binding to the target increased the local concentration of the probes, which triggered binding-induced cleavage of a fluorophore. In addition, one input target protein generated multiple output DNA released from AuNP for an amplified signal. Furthermore, the addition of blocker probes to compete with nonspecific hybridization between probes reduced target-independent cleavage. the use of a quencher-labeled support DNA functionalized on the AuNPs, substantially decreased the background signal. This dsDNA-AuNP BIMA has a limit of detection of 300 fM for the detection of streptavidin and 8 pM for the thrombin. This strategy also can be applied to other proteins that can be bound by two affinity probes. DNA or RNA targets with two probes complementary on each end also have the possibility to utilize this molecular amplifier.

Chapter Six: Conclusions and Future Work

I have studied the applications of binding-induced DNA assembly for the detection of biomolecules, including proteins and nucleic acids. Specifically, Chapter 2 and Chapter 3 focused on the formation and utilization of binding-induced three-way junction (TWJ) to construct the DNA assembly for the detection of proteins and microRNA (miRNA). Chapter 4 and Chapter 5 focused on the development and utilization of a binding-induced molecular amplifier (BIMA) for the detection of universal targets. Magnetic beads and nanomaterials, such as gold nanoparticles (AuNPs), were used in these assays. The following paragraphs summarize the main findings and offer future perspective.

In Chapter 2, I focused on the formation of binding-induced DNA TWJ and its applications to the detection of proteins. Prostate specific antigen (PSA) and human α -thrombin were chosen as the target proteins for analyses. Antibody binding to PSA and aptamer binding to human α -thrombin resulted in the formation of the binding-induced TWJs. The key design parameters that influenced the signal intensity and kinetics were studied. Real-time monitoring of fluorescence signals showed that different concentrations of target, reaction temperatures, and nucleotide lengths of the toehold domain affected the reaction rate. Native polyacrylamide gel electrophoresis (PAGE) was used to characterize the oligonucleotides involved in the formation of TWJ and strand displacement. The binding-induced DNA TWJ technique was compared to three other DNA strand-displacement strategies. The binding-induced TWJ exhibited fast kinetics, low background, and high sensitivity. With no need for enzymes or thermal cycling, this new DNA TWJ approach was applied to the development of assays for biomolecules using inductively coupled plasma mass spectrometry (ICP-MS).

In Chapter 3, the binding-induced DNA TWJ approach was used to construct a molecular translator for the detection of various targets, including proteins and miRNAs. The molecular translator was able to translate the input target information to the predesign output DNA, thereby converting the detection of the target to the detection of the output DNA. The generated output DNA was hybridized to a complementary oligonucleotide that was conjugated on the AuNP. Subsequent detection of the corresponding AuNP using ICP-MS provided quantitative information on the target molecule that initiated the formation of the DNA TWJ. Because each 20-nm AuNP was composed of approximately 10^5 Au atoms, ICP-MS detection of Au in the oligonucleotide-functionalized AuNP afforded amplified detection and improved sensitivity. Various oligonucleotides were used in the construction of the TWJs, with their length and toehold domain carefully designed. Experimental conditions, such as the concentrations and ratio of the probes, were optimized. The optimized molecular translator was successfully used for the detection of human α -thrombin, miRNA 10b, and miRNA 128, achieving better detection limit than those with fluorescence detection.

In Chapter 4, a binding-induced molecular amplifier (BIMA) was described as a universal detection platform for multiple classes of biomolecules and biomolecular interactions. AuNPs were used as the scaffold to conjugate multiple oligonucleotide sequences, including DNA tracks, recognition probes, and output DNA barcodes. In response to the binding of a single target molecule to two affinity probes, a nicking endonuclease enzyme cleaved off multiple DNA barcode molecules from the AuNP, achieving a high translation efficiency for translating various biomolecules and interactions into the output DNA barcodes. Then, the output DNA barcode triggered the toehold-

mediated strand displacement reactions that turned on fluorescence. Therefore, the BIMA detection signal was amplified due to the multiple DNA barcodes, which were the cleavage products of the nicking endonuclease in response to target binding. Using the BIMA strategy, I was able to detect streptavidin, PSA, synthetic DNA target, PDGF-BB, and PDGF receptor β . As such, a simple strand displacement beacon that conventionally only detects a single-stranded DNA target has been expanded for the detection of nucleic acids, proteins, and the protein–protein interactions.

In Chapter 5, I described an improvement of the binding-induced molecular amplifier by using double-stranded DNA oligonucleotides conjugated on the surface of AuNPs. Conjugation of the double-stranded DNA oligonucleotides on the surface of AuNPs enhanced the chemical stability and made it easier to control the modification of DNA probes loaded on AuNPs. Several parameters, such as the spacer length on the probe and the addition of a quencher label, were optimized to reduce the background and increase the reaction rate. Because the input target protein generated multiple output DNA molecules that were released from AuNP, the detection signal was amplified. Streptavidin and human α -thrombin at picomolar concentrations could be detected by using the enhanced binding-induced molecular amplifier technique.

The binding-induced DNA assembly strategies designed in this thesis are not limited to the chosen protein and nucleic acid targets; they could potentially be applied to other molecular targets. Several potential issues must be considered when applying our techniques to real-world analyses. For example, many target proteins and nucleic acids are present in a very complicated sample matrix, such as in blood and urine. The sample matrix could interfere with quantitative analyses. It is possible for a background signal to be generated

due to the nonspecific binding. Thus, specific, reliable, and robust affinity ligands are required to trigger the binding-induced dynamic DNA structures. In addition, the concentrations of many important proteins and nucleic acids present in real-life samples are extremely low, e.g., lower than picomolar, demanding for high sensitivity. An efficient and effective signal amplification method is necessary to increase the sensitivity.

Building on the success of the binding-induced TWJs and molecular amplifier DNA strategies, I plan to expand the application of these strategies further with other proteins, nucleic acids, and small molecules in clinically relevant samples, like human serum. Other nanomaterials could be combined with the binding-induced DNA structures. The use of a magnetic separation step could be possible to overcome some problems of matrix effect. Quantum dots (QDs) could be used as fluorescence labels, which emit fluorescence of different colors depending on the size of QDs. They could be used to develop binding-induced molecular amplifiers for multiple target detection. Different QD labels would be used to construct different detection systems. Also, fluorescence labels emitting in the near-IR region could be useful because autofluorescence from the background of sample matrix could be minimized. The fluorescence signal amplification from the binding-induced molecular amplifier has the potential to enhance molecular imaging^{37, 174} as the negligible toxicity of the AuNPs allows them to be used as a scaffold to introduce the DNA nanostructures to *in vivo* systems¹⁷⁵⁻¹⁷⁶.

Reference

1. Seeman, N. C., DNA NANOTECHNOLOGY: Novel DNA Constructions. *Annual Review of Biophysics and Biomolecular Structure* **1998**, 27 (1), 225-248.
2. Watson, J. D.; Crick, F. H. C., THE STRUCTURE OF DNA. *Cold Spring Harbor Symposia on Quantitative Biology* **1953**, 18, 123-131.
3. Carlson, R., The changing economics of DNA synthesis. *Nature Biotechnology* **2009**, 27, 1091.
4. Rangnekar, A.; LaBean, T. H., Building DNA Nanostructures for Molecular Computation, Templated Assembly, and Biological Applications. *Accounts of Chemical Research* **2014**, 47 (6), 1778-1788.
5. Okholm, A. H.; Kjems, J., DNA nanovehicles and the biological barriers. *Advanced Drug Delivery Reviews* **2016**, 106, 183-191.
6. Zhang, D. Y.; Seelig, G., Dynamic DNA nanotechnology using strand-displacement reactions. *Nature Chemistry* **2011**, 3, 103.
7. Pinheiro, A. V.; Han, D.; Shih, W. M.; Yan, H., Challenges and opportunities for structural DNA nanotechnology. *Nature Nanotechnology* **2011**, 6, 763.
8. Rothmund, P. W. K., Folding DNA to create nanoscale shapes and patterns. *Nature* **2006**, 440, 297.
9. Li, F.; Zhang, H.; Wang, Z.; Li, X.; Li, X.-F.; Le, X. C., Dynamic DNA Assemblies Mediated by Binding-Induced DNA Strand Displacement. *Journal of the American*

Chemical Society **2013**, *135* (7), 2443-2446.

10. Yin, P.; Choi, H. M. T.; Calvert, C. R.; Pierce, N. A., Programming biomolecular self-assembly pathways. *Nature* **2008**, *451*, 318.
11. Li, Q.; Luan, G.; Guo, Q.; Liang, J., A new class of homogeneous nucleic acid probes based on specific displacement hybridization. *Nucleic Acids Res* **2002**, *30* (2), E5.
12. Zhang, D. Y.; Winfree, E., Control of DNA Strand Displacement Kinetics Using Toehold Exchange. *Journal of the American Chemical Society* **2009**, *131* (47), 17303-17314.
13. Qian, L.; Winfree, E., Scaling Up Digital Circuit Computation with DNA Strand Displacement Cascades. *Science* **2011**, *332* (6034), 1196-1201.
14. Zhang, D. Y.; Chen, S. X.; Yin, P., Optimizing the specificity of nucleic acid hybridization. *Nature Chemistry* **2012**, *4*, 208.
15. Frezza, B. M.; Cockroft, S. L.; Ghadiri, M. R., Modular Multi-Level Circuits from Immobilized DNA-Based Logic Gates. *Journal of the American Chemical Society* **2007**, *129* (48), 14875-14879.
16. Picuri, J. M.; Frezza, B. M.; Ghadiri, M. R., Universal Translators for Nucleic Acid Diagnosis. *Journal of the American Chemical Society* **2009**, *131* (26), 9368-9377.
17. Ellington, A. D.; Szostak, J. W., In vitro selection of RNA molecules that bind specific ligands. *Nature* **1990**, *346*, 818.

18. Klug, S. J.; Famulok, M., All you wanted to know about SELEX. *Molecular Biology Reports* **1994**, *20* (2), 97-107.
19. Seeman, N. C., Nucleic acid junctions and lattices. *Journal of Theoretical Biology* **1982**, *99* (2), 237-247.
20. D.R., D.; D.M., L., The three-way DNA junction is a Y-shaped molecule in which there is no helix-helix stacking. *The EMBO Journal* **1990**, *9* (5), 1659-1664.
21. Chen, X., Expanding the Rule Set of DNA Circuitry with Associative Toehold Activation. *Journal of the American Chemical Society* **2012**, *134* (1), 263-271.
22. Genot, A. J.; Fujii, T.; Rondelez, Y., Scaling down DNA circuits with competitive neural networks. *Journal of The Royal Society Interface* **2013**, *10* (85).
23. Li, F.; Lin, Y.; Le, X. C., Binding-Induced Formation of DNA Three-Way Junctions and Its Application to Protein Detection and DNA Strand Displacement. *Analytical Chemistry* **2013**, *85* (22), 10835-10841.
24. Heyduk, E.; Heyduk, T., Nucleic Acid-Based Fluorescence Sensors for Detecting Proteins. *Analytical Chemistry* **2005**, *77* (4), 1147-1156.
25. Heyduk, E.; Dummit, B.; Chang, Y.-H.; Heyduk, T., Molecular Pincers: Antibody-Based Homogeneous Protein Sensors. *Analytical Chemistry* **2008**, *80* (13), 5152-5159.
26. Ha, T.; Enderle, T.; Ogletree, D. F.; Chemla, D. S.; Selvin, P. R.; Weiss, S., Probing the interaction between two single molecules: fluorescence resonance energy

- transfer between a single donor and a single acceptor. *Proceedings of the National Academy of Sciences* **1996**, *93* (13), 6264-6268.
27. Di Giusto, D. A.; Wlassoff, W. A.; Gooding, J. J.; Messerle, B. A.; King, G. C., Proximity extension of circular DNA aptamers with real-time protein detection. *Nucleic Acids Research* **2005**, *33* (6), e64-e64.
 28. Li, J.; Zhong, X.; Zhang, H.; Le, X. C.; Zhu, J.-J., Binding-Induced Fluorescence Turn-On Assay Using Aptamer-Functionalized Silver Nanocluster DNA Probes. *Analytical Chemistry* **2012**, *84* (12), 5170-5174.
 29. Yeh, H.-C.; Sharma, J.; Han, J. J.; Martinez, J. S.; Werner, J. H., A DNA–Silver Nanocluster Probe That Fluoresces upon Hybridization. *Nano Letters* **2010**, *10* (8), 3106-3110.
 30. Cui, L.; Ke, G.; Wang, C.; Yang, C. J., A cyclic enzymatic amplification method for sensitive and selective detection of nucleic acids. *Analyst* **2010**, *135* (8), 2069-2073.
 31. Liu, X.; Freeman, R.; Willner, I., Amplified Fluorescence Aptamer-Based Sensors Using Exonuclease III for the Regeneration of the Analyte. *Chemistry – A European Journal* **2012**, *18* (8), 2207-2211.
 32. Fredriksson, S.; Gullberg, M.; Jarvius, J.; Olsson, C.; Pietras, K.; Gústafsdóttir, S. M.; Östman, A.; Landegren, U., Protein detection using proximity-dependent DNA ligation assays. *Nature Biotechnology* **2002**, *20*, 473.
 33. Le, X.; Zhang, H.; Li, X.-F., Binding-induced hairpin detection system. Google

Patents: 2015.

34. Zhang, H.; Li, X.-F.; Le, X. C., Binding-Induced DNA Assembly and Its Application to Yoctomole Detection of Proteins. *Analytical Chemistry* **2012**, *84* (2), 877-884.
35. Li, F.; Zhang, H.; Lai, C.; Li, X. F.; Le, X. C., A Molecular Translator that Acts by Binding - Induced DNA Strand Displacement for a Homogeneous Protein Assay. *Angewandte Chemie International Edition* **2012**, *51* (37), 9317-9320.
36. Hongquan, Z.; Maode, L.; Albert, Z.; Hanyong, P.; Xing-Fang, L.; Chris, L. X., Binding-Induced DNA Nanomachines Triggered by Proteins and Nucleic Acids. *Angewandte Chemie International Edition* **2015**, *54* (48), 14326-14330.
37. Peng, H.; Li, X.-F.; Zhang, H.; Le, X. C., A microRNA-initiated DNAzyme motor operating in living cells. *Nature Communications* **2017**, *8*, 14378.
38. Li, F.; Zhang, H.; Lai, C.; Li, X.-F.; Le, X. C., A Molecular Translator that Acts by Binding-Induced DNA Strand Displacement for a Homogeneous Protein Assay. *Angewandte Chemie International Edition* **2012**, *51* (37), 9317-9320.
39. Zeng, S.; Yong, K.-T.; Roy, I.; Dinh, X.-Q.; Yu, X.; Luan, F., A Review on Functionalized Gold Nanoparticles for Biosensing Applications. *Plasmonics* **2011**, *6* (3), 491.
40. Saha, K.; Agasti, S. S.; Kim, C.; Li, X.; Rotello, V. M., Gold Nanoparticles in Chemical and Biological Sensing. *Chemical Reviews* **2012**, *112* (5), 2739-2779.

41. Elghanian, R.; Storhoff, J. J.; Mucic, R. C.; Letsinger, R. L.; Mirkin, C. A., Selective Colorimetric Detection of Polynucleotides Based on the Distance-Dependent Optical Properties of Gold Nanoparticles. *Science* **1997**, *277* (5329), 1078-1081.
42. Giljohann, D. A.; Seferos, D. S.; Daniel, W. L.; Massich, M. D.; Patel, P. C.; Mirkin, C. A., Gold Nanoparticles for Biology and Medicine. *Angewandte Chemie International Edition* **2010**, *49* (19), 3280-3294.
43. Li, J.; Fu, H.-E.; Wu, L.-J.; Zheng, A.-X.; Chen, G.-N.; Yang, H.-H., General Colorimetric Detection of Proteins and Small Molecules Based on Cyclic Enzymatic Signal Amplification and Hairpin Aptamer Probe. *Analytical Chemistry* **2012**, *84* (12), 5309-5315.
44. Wang, W.; Chen, C.; Qian, M.; Zhao, X. S., Aptamer biosensor for protein detection using gold nanoparticles. *Analytical Biochemistry* **2008**, *373* (2), 213-219.
45. Levy, M.; Cater, S. F.; Ellington, A. D., Quantum-Dot Aptamer Beacons for the Detection of Proteins. *ChemBioChem* **2005**, *6* (12), 2163-2166.
46. Carthew, R. W.; Sontheimer, E. J., Origins and Mechanisms of miRNAs and siRNAs. *Cell* **2009**, *136* (4), 642-655.
47. Cai, Y.; Yu, X.; Hu, S.; Yu, J., A Brief Review on the Mechanisms of miRNA Regulation. *Genomics, Proteomics & Bioinformatics* **2009**, *7* (4), 147-154.
48. Bartel, D. P., MicroRNAs: Target Recognition and Regulatory Functions. *Cell* **2009**, *136* (2), 215-233.

49. Seferos, D. S.; Giljohann, D. A.; Hill, H. D.; Prigodich, A. E.; Mirkin, C. A., Nano-Flares: Probes for Transfection and mRNA Detection in Living Cells. *Journal of the American Chemical Society* **2007**, *129* (50), 15477-15479.
50. Prigodich, A. E.; Randeria, P. S.; Briley, W. E.; Kim, N. J.; Daniel, W. L.; Giljohann, D. A.; Mirkin, C. A., Multiplexed Nanoflares: mRNA Detection in Live Cells. *Analytical Chemistry* **2012**, *84* (4), 2062-2066.
51. Alhasan, A. H.; Kim, D. Y.; Daniel, W. L.; Watson, E.; Meeks, J. J.; Thaxton, C. S.; Mirkin, C. A., Scanometric MicroRNA Array Profiling of Prostate Cancer Markers Using Spherical Nucleic Acid–Gold Nanoparticle Conjugates. *Analytical Chemistry* **2012**, *84* (9), 4153-4160.
52. Zheng, D.; Seferos, D. S.; Giljohann, D. A.; Patel, P. C.; Mirkin, C. A., Aptamer Nano-flares for Molecular Detection in Living Cells. *Nano Letters* **2009**, *9* (9), 3258-3261.
53. Halo, T. L.; McMahon, K. M.; Angeloni, N. L.; Xu, Y.; Wang, W.; Chinen, A. B.; Malin, D.; Strekalova, E.; Cryns, V. L.; Cheng, C.; Mirkin, C. A.; Thaxton, C. S., NanoFlares for the detection, isolation, and culture of live tumor cells from human blood. *Proceedings of the National Academy of Sciences* **2014**.
54. Degueldre, C.; Favarger, P. Y., Colloid analysis by single particle inductively coupled plasma-mass spectroscopy: a feasibility study. *Colloids and Surfaces A: Physicochemical and Engineering Aspects* **2003**, *217* (1), 137-142.
55. Degueldre, C.; Favarger, P. Y.; Bitea, C., Zirconia colloid analysis by single particle

- inductively coupled plasma–mass spectrometry. *Analytica Chimica Acta* **2004**, *518* (1), 137-142.
56. Degueldre, C.; Favarger, P. Y., Thorium colloid analysis by single particle inductively coupled plasma-mass spectrometry. *Talanta* **2004**, *62* (5), 1051-1054.
57. Degueldre, C.; Favarger, P. Y.; Wold, S., Gold colloid analysis by inductively coupled plasma-mass spectrometry in a single particle mode. *Analytica Chimica Acta* **2006**, *555* (2), 263-268.
58. Tuoriniemi, J.; Cornelis, G.; Hassellöv, M., Size Discrimination and Detection Capabilities of Single-Particle ICPMS for Environmental Analysis of Silver Nanoparticles. *Analytical Chemistry* **2012**, *84* (9), 3965-3972.
59. Zhao, Q.; Lu, X.; Yuan, C.-G.; Li, X.-F.; Le, X. C., Aptamer-Linked Assay for Thrombin Using Gold Nanoparticle Amplification and Inductively Coupled Plasma–Mass Spectrometry Detection. *Analytical Chemistry* **2009**, *81* (17), 7484-7489.
60. Li, F.; Zhao, Q.; Wang, C.; Lu, X.; Li, X.-F.; Le, X. C., Detection of Escherichia coli O157:H7 Using Gold Nanoparticle Labeling and Inductively Coupled Plasma Mass Spectrometry. *Analytical Chemistry* **2010**, *82* (8), 3399-3403.
61. Li, W.; Li, J.; Qiang, W.; Xu, J.; Xu, D., Enzyme-free colorimetric bioassay based on gold nanoparticle-catalyzed dye decolorization. *Analyst* **2013**, *138* (3), 760-766.
62. Szymanski, M.; Noble, J.; Knight, A.; Porter, R.; Worsley, G., Aptamer-mediated

- detection of thrombin using silver nanoparticle signal enhancement. *Analytical Methods* **2013**, 5 (1), 187-191.
63. Wang, X.; Zhao, Q., A fluorescent sandwich assay for thrombin using aptamer modified magnetic beads and quantum dots. *Microchimica Acta* **2012**, 178 (3), 349-355.
64. Tennico, Y. H.; Hutanu, D.; Koesdjojo, M. T.; Bartel, C. M.; Remcho, V. T., On-Chip Aptamer-Based Sandwich Assay for Thrombin Detection Employing Magnetic Beads and Quantum Dots. *Analytical Chemistry* **2010**, 82 (13), 5591-5597.
65. Centi, S.; Tombelli, S.; Minunni, M.; Mascini, M., Aptamer-Based Detection of Plasma Proteins by an Electrochemical Assay Coupled to Magnetic Beads. *Analytical Chemistry* **2007**, 79 (4), 1466-1473.
66. Wang, Y.; He, X.; Wang, K.; Ni, X.; Su, J.; Chen, Z., Electrochemical detection of thrombin based on aptamer and ferrocenylhexanethiol loaded silica nanocapsules. *Biosensors and Bioelectronics* **2011**, 26 (8), 3536-3541.
67. Zhao, Q.; Wang, X., An aptamer-capture based chromogenic assay for thrombin. *Biosensors and Bioelectronics* **2012**, 34 (1), 232-237.
68. Zhao, Q.; Li, X.-F.; Le, X. C., Aptamer Capturing of Enzymes on Magnetic Beads to Enhance Assay Specificity and Sensitivity. *Analytical Chemistry* **2011**, 83 (24), 9234-9236.

69. Centi, S.; Messina, G.; Tombelli, S.; Palchetti, I.; Mascini, M., Different approaches for the detection of thrombin by an electrochemical aptamer-based assay coupled to magnetic beads. *Biosensors and Bioelectronics* **2008**, *23* (11), 1602-1609.
70. Hecht, A.; Kumar, A. A.; Kopelman, R., Label-Acquired Magnetorotation As a Signal Transduction Method for Protein Detection: Aptamer-Based Detection of Thrombin. *Analytical Chemistry* **2011**, *83* (18), 7123-7128.
71. N C Seeman, a.; Kallenbach, N. R., DNA Branched Junctions. *Annual Review of Biophysics and Biomolecular Structure* **1994**, *23* (1), 53-86.
72. Goodman, R. P.; Schaap, I. A. T.; Tardin, C. F.; Erben, C. M.; Berry, R. M.; Schmidt, C. F.; Turberfield, A. J., Rapid Chiral Assembly of Rigid DNA Building Blocks for Molecular Nanofabrication. *Science* **2005**, *310* (5754), 1661-1665.
73. Yang, H.; Sleiman, H. F., Templated Synthesis of Highly Stable, Electroactive, and Dynamic Metal–DNA Branched Junctions. *Angewandte Chemie International Edition* **2008**, *47* (13), 2443-2446.
74. Boer, D. R.; Kerckhoffs, J. M. C. A.; Parajo, Y.; Pascu, M.; Usón, I.; Lincoln, P.; Hannon, M. J.; Coll, M., Self-Assembly of Functionalizable Two-Component 3D DNA Arrays through the Induced Formation of DNA Three-Way-Junction Branch Points by Supramolecular Cylinders. *Angewandte Chemie International Edition* **2010**, *49* (13), 2336-2339.
75. He, Y.; Chen, Y.; Liu, H.; Ribbe, A. E.; Mao, C., Self-Assembly of Hexagonal DNA Two-Dimensional (2D) Arrays. *Journal of the American Chemical Society* **2005**,

127 (35), 12202-12203.

76. Shu, D.; Shu, Y.; Haque, F.; Abdelmawla, S.; Guo, P., Thermodynamically stable RNA three-way junction for constructing multifunctional nanoparticles for delivery of therapeutics. *Nature Nanotechnology* **2011**, *6*, 658.
77. Müller, J.; Lippert, B., Imposing a Three-Way Junction on DNA or Recognizing One: A Metal Triple Helicate Meets Double Helix. *Angewandte Chemie International Edition* **2006**, *45* (16), 2503-2505.
78. Hamada, S.; Murata, S., Substrate-Assisted Assembly of Interconnected Single-Duplex DNA Nanostructures. *Angewandte Chemie International Edition* **2009**, *48* (37), 6820-6823.
79. Thomas, J. M.; Chakraborty, B.; Sen, D.; Yu, H.-Z., Analyte-Driven Switching of DNA Charge Transport: De Novo Creation of Electronic Sensors for an Early Lung Cancer Biomarker. *Journal of the American Chemical Society* **2012**, *134* (33), 13823-13833.
80. Seemann, I. T.; Singh, V.; Azarkh, M.; Drescher, M.; Hartig, J. S., Small-Molecule-Triggered Manipulation of DNA Three-Way Junctions. *Journal of the American Chemical Society* **2011**, *133* (13), 4706-4709.
81. Thomas, J. M.; Yu, H.-Z.; Sen, D., A Mechano-Electronic DNA Switch. *Journal of the American Chemical Society* **2012**, *134* (33), 13738-13748.
82. Ge, B.; Huang, Y. C.; Sen, D.; Yu, H.-Z., A Robust Electronic Switch Made of

- Immobilized Duplex/Quadruplex DNA. *Angewandte Chemie International Edition* **2010**, *49* (51), 9965-9967.
83. Nutiu, R.; Li, Y., Structure-Switching Signaling Aptamers. *Journal of the American Chemical Society* **2003**, *125* (16), 4771-4778.
84. Li, B.; Jiang, Y.; Chen, X.; Ellington, A. D., Probing Spatial Organization of DNA Strands Using Enzyme-Free Hairpin Assembly Circuits. *Journal of the American Chemical Society* **2012**, *134* (34), 13918-13921.
85. Genot, A. J.; Bath, J.; Turberfield, A. J., Combinatorial Displacement of DNA Strands: Application to Matrix Multiplication and Weighted Sums. *Angewandte Chemie International Edition* **2013**, *52* (4), 1189-1192.
86. Seelig, G.; Soloveichik, D.; Zhang, D. Y.; Winfree, E., Enzyme-Free Nucleic Acid Logic Circuits. *Science* **2006**, *314* (5805), 1585-1588.
87. Liao, S.; Seeman, N. C., Translation of DNA Signals into Polymer Assembly Instructions. *Science* **2004**, *306* (5704), 2072-2074.
88. Shin, J.-S.; Pierce, N. A., A Synthetic DNA Walker for Molecular Transport. *Journal of the American Chemical Society* **2004**, *126* (35), 10834-10835.
89. Gu, H.; Chao, J.; Xiao, S.-J.; Seeman, N. C., A proximity-based programmable DNA nanoscale assembly line. *Nature* **2010**, *465*, 202.
90. He, Y.; Liu, D. R., Autonomous multistep organic synthesis in a single isothermal solution mediated by a DNA walker. *Nature Nanotechnology* **2010**, *5*, 778.

91. Bath, J.; Turberfield, A. J., DNA nanomachines. *Nature Nanotechnology* **2007**, *2*, 275.
92. Le, X. C.; Li, F., Binding-induced formation of dna three-way junctions from non-dna targets. Google Patents: 2015.
93. Rocci, A.; Hofmeister, C. C.; Pichiorri, F., The potential of miRNAs as biomarkers for multiple myeloma. *Expert Review of Molecular Diagnostics* **2014**, *14* (8), 947-959.
94. Vrijens, K.; Bollati, V.; Nawrot, T. S., MicroRNAs as potential signatures of environmental exposure or effect: a systematic review. *Environ Health Perspect* **2015**, *123* (5), 399-411.
95. Cheng, L.; Sharples, R. A.; Scicluna, B. J.; Hill, A. F., Exosomes provide a protective and enriched source of miRNA for biomarker profiling compared to intracellular and cell-free blood. *Journal of Extracellular Vesicles* **2014**, *3* (1), 23743.
96. Croce, C. M., Causes and consequences of microRNA dysregulation in cancer. *Nature Reviews Genetics* **2009**, *10*, 704.
97. Di Leva, G.; Croce, C. M., miRNA profiling of cancer. *Current Opinion in Genetics & Development* **2013**, *23* (1), 3-11.
98. Rifai, N.; Gillette, M. A.; Carr, S. A., Protein biomarker discovery and validation: the long and uncertain path to clinical utility. *Nature Biotechnology* **2006**, *24*, 971.

99. Zhang, C.; Zhang, Z.; Yu, B.; Shi, J.; Zhang, X., Application of the Biological Conjugate between Antibody and Colloid Au Nanoparticles as Analyte to Inductively Coupled Plasma Mass Spectrometry. *Analytical Chemistry* **2002**, *74* (1), 96-99.
100. Baranov, V. I.; Quinn, Z.; Bandura, D. R.; Tanner, S. D., A Sensitive and Quantitative Element-Tagged Immunoassay with ICPMS Detection. *Analytical Chemistry* **2002**, *74* (7), 1629-1636.
101. Quinn, Z. A.; Baranov, V. I.; Tanner, S. D.; Wrana, J. L., Simultaneous determination of proteins using an element-tagged immunoassay coupled with ICP-MS detection. *Journal of Analytical Atomic Spectrometry* **2002**, *17* (8), 892-896.
102. Liu, J.-M.; Yan, X.-P., Ultrasensitive, selective and simultaneous detection of cytochrome c and insulin based on immunoassay and aptamer-based bioassay in combination with Au/Ag nanoparticle tagging and ICP-MS detection. *Journal of Analytical Atomic Spectrometry* **2011**, *26* (6), 1191-1197.
103. Ornatsky, O. I.; Baranov, V. I.; Bandura, D. R.; Tanner, S. D.; Dick, J., Messenger RNA detection in leukemia cell lines by novel metal-tagged in situ hybridization using inductively coupled plasma mass spectrometry. *Translational Oncogenomics* **2006**, *1*, 1-9.
104. Dequaire, M.; Degrand, C.; Limoges, B., An Electrochemical Metalloimmunoassay Based on a Colloidal Gold Label. *Analytical Chemistry* **2000**, *72* (22), 5521-5528.
105. Ornatsky, O.; Baranov, V. I.; Bandura, D. R.; Tanner, S. D.; Dick, J., Multiple

- cellular antigen detection by ICP-MS. *Journal of Immunological Methods* **2006**, *308* (1), 68-76.
106. Scheffer, A.; Engelhard, C.; Sperling, M.; Buscher, W., ICP-MS as a new tool for the determination of gold nanoparticles in bioanalytical applications. *Analytical and Bioanalytical Chemistry* **2008**, *390* (1), 249-252.
107. Merkoçi, A.; Aldavert, M.; Tarrasón, G.; Eritja, R.; Alegret, S., Toward an ICPMS-Linked DNA Assay Based on Gold Nanoparticles Immunocconnected through Peptide Sequences. *Analytical Chemistry* **2005**, *77* (19), 6500-6503.
108. Zoorob, G. K.; McKiernan, J. W.; Caruso, J. A., ICP-MS for elemental speciation studies. *Microchimica Acta* **1998**, *128* (3), 145-168.
109. Lagos-Quintana, M.; Rauhut, R.; Lendeckel, W.; Tuschl, T., Identification of Novel Genes Coding for Small Expressed RNAs. *Science* **2001**, *294* (5543), 853-858.
110. Lau, N. C.; Lim, L. P.; Weinstein, E. G.; Bartel, D. P., An Abundant Class of Tiny RNAs with Probable Regulatory Roles in *Caenorhabditis elegans*. *Science* **2001**, *294* (5543), 858-862.
111. Lee, R. C.; Ambros, V., An Extensive Class of Small RNAs in *Caenorhabditis elegans*. *Science* **2001**, *294* (5543), 862-864.
112. Rhoades, M. W.; Reinhart, B. J.; Lim, L. P.; Burge, C. B.; Bartel, B.; Bartel, D. P., Prediction of Plant MicroRNA Targets. *Cell* **2002**, *110* (4), 513-520.
113. Tang, G.; Reinhart, B. J.; Bartel, D. P.; Zamore, P. D., A biochemical framework for

- RNA silencing in plants. *Genes & Development* **2003**, *17* (1), 49-63.
114. Ambros, V., The functions of animal microRNAs. *Nature* **2004**, *431*, 350.
115. Rajewsky, N., microRNA target predictions in animals. *Nature Genetics* **2006**, *38*, S8.
116. Lewis, B. P.; Burge, C. B.; Bartel, D. P., Conserved Seed Pairing, Often Flanked by Adenosines, Indicates that Thousands of Human Genes are MicroRNA Targets. *Cell* **2005**, *120* (1), 15-20.
117. Bartel, D. P., MicroRNAs: Genomics, Biogenesis, Mechanism, and Function. *Cell* **2004**, *116* (2), 281-297.
118. Mitchell, P. S.; Parkin, R. K.; Kroh, E. M.; Fritz, B. R.; Wyman, S. K.; Pogosova-Agadjanyan, E. L.; Peterson, A.; Noteboom, J.; O'Briant, K. C.; Allen, A.; Lin, D. W.; Urban, N.; Drescher, C. W.; Knudsen, B. S.; Stirewalt, D. L.; Gentleman, R.; Vessella, R. L.; Nelson, P. S.; Martin, D. B.; Tewari, M., Circulating microRNAs as stable blood-based markers for cancer detection. *Proceedings of the National Academy of Sciences* **2008**, *105* (30), 10513-10518.
119. Chen, X.; Ba, Y.; Ma, L.; Cai, X.; Yin, Y.; Wang, K.; Guo, J.; Zhang, Y.; Chen, J.; Guo, X.; Li, Q.; Li, X.; Wang, W.; Zhang, Y.; Wang, J.; Jiang, X.; Xiang, Y.; Xu, C.; Zheng, P.; Zhang, J.; Li, R.; Zhang, H.; Shang, X.; Gong, T.; Ning, G.; Wang, J.; Zen, K.; Zhang, J.; Zhang, C.-Y., Characterization of microRNAs in serum: a novel class of biomarkers for diagnosis of cancer and other diseases. *Cell Research* **2008**, *18*, 997.

120. Lu, J.; Getz, G.; Miska, E. A.; Alvarez-Saavedra, E.; Lamb, J.; Peck, D.; Sweet-Cordero, A.; Ebert, B. L.; Mak, R. H.; Ferrando, A. A.; Downing, J. R.; Jacks, T.; Horvitz, H. R.; Golub, T. R., MicroRNA expression profiles classify human cancers. *Nature* **2005**, *435*, 834.
121. Rosi, N. L.; Mirkin, C. A., Nanostructures in Biodiagnostics. *Chemical Reviews* **2005**, *105* (4), 1547-1562.
122. Burke, A. M.; Gorodetsky, A. A., Taking charge of detection. *Nature Chemistry* **2012**, *4*, 595.
123. Das, J.; Cederquist, K. B.; Zaragoza, A. A.; Lee, P. E.; Sargent, E. H.; Kelley, S. O., An ultrasensitive universal detector based on neutralizer displacement. *Nature Chemistry* **2012**, *4*, 642.
124. Xia, F.; Zuo, X.; Yang, R.; Xiao, Y.; Kang, D.; Vallée-Bélisle, A.; Gong, X.; Yuen, J. D.; Hsu, B. B. Y.; Heeger, A. J.; Plaxco, K. W., Colorimetric detection of DNA, small molecules, proteins, and ions using unmodified gold nanoparticles and conjugated polyelectrolytes. *Proceedings of the National Academy of Sciences* **2010**, *107* (24), 10837-10841.
125. Xiang, Y.; Lu, Y., Using personal glucose meters and functional DNA sensors to quantify a variety of analytical targets. *Nature Chemistry* **2011**, *3*, 697-703.
126. Zhang, J.; Xiang, Y.; Wang, M.; Basu, A.; Lu, Y., Dose-Dependent Response of Personal Glucose Meters to Nicotinamide Coenzymes: Applications to Point-of-Care Diagnostics of Many Non-Glucose Targets in a Single Step. *Angewandte*

Chemie International Edition **2016**, 55 (2), 732-736.

127. Xiang, Y.; Lu, Y., An invasive DNA approach toward a general method for portable quantification of metal ions using a personal glucose meter. *Chemical Communications* **2013**, 49 (6), 585-587.
128. Xiang, Y.; Lu, Y., Portable and Quantitative Detection of Protein Biomarkers and Small Molecular Toxins Using Antibodies and Ubiquitous Personal Glucose Meters. *Analytical Chemistry* **2012**, 84 (9), 4174-4178.
129. Tram, K.; Kanda, P.; Salena, B. J.; Huan, S.; Li, Y., Translating Bacterial Detection by DNazymes into a Litmus Test. *Angewandte Chemie International Edition* **2014**, 53 (47), 12799-12802.
130. Du, Y.; Pothukuchy, A.; Gollihar, J. D.; Nourani, A.; Li, B.; Ellington, A. D., Coupling Sensitive Nucleic Acid Amplification with Commercial Pregnancy Test Strips. *Angewandte Chemie International Edition* **2017**, 56 (4), 992-996.
131. Zhu, Z.; Guan, Z.; Liu, D.; Jia, S.; Li, J.; Lei, Z.; Lin, S.; Ji, T.; Tian, Z.; Yang, C. J., Translating Molecular Recognition into a Pressure Signal to enable Rapid, Sensitive, and Portable Biomedical Analysis. *Angewandte Chemie International Edition* **2015**, 54 (36), 10448-10453.
132. Paliwoda, R. E.; Li, F.; Reid, M. S.; Lin, Y.; Le, X. C., Sequential Strand Displacement Beacon for Detection of DNA Coverage on Functionalized Gold Nanoparticles. *Analytical Chemistry* **2014**, 86 (12), 6138-6143.

133. Tang, Y.; Lin, Y.; Yang, X.; Wang, Z.; Le, X. C.; Li, F., Universal Strategy To Engineer Catalytic DNA Hairpin Assemblies for Protein Analysis. *Analytical Chemistry* **2015**, *87* (16), 8063-8066.
134. Tang, Y.; Wang, Z.; Yang, X.; Chen, J.; Liu, L.; Zhao, W.; Le, X. C.; Li, F., Constructing real-time, wash-free, and reiterative sensors for cell surface proteins using binding-induced dynamic DNA assembly. *Chemical Science* **2015**, *6* (10), 5729-5733.
135. Li, F.; Tang, Y.; Traynor, S. M.; Li, X.-F.; Le, X. C., Kinetics of Proximity-Induced Intramolecular DNA Strand Displacement. *Analytical Chemistry* **2016**, *88* (16), 8152-8157.
136. Yang, X.; Tang, Y.; Mason, S. D.; Chen, J.; Li, F., Enzyme-Powered Three-Dimensional DNA Nanomachine for DNA Walking, Payload Release, and Biosensing. *ACS Nano* **2016**, *10* (2), 2324-2330.
137. Zhang, H.; Lai, M.; Zuehlke, A.; Peng, H.; Li, X.-F.; Le, X. C., Binding-Induced DNA Nanomachines Triggered by Proteins and Nucleic Acids. *Angewandte Chemie* **2015**, *127* (48), 14534-14538.
138. Jung, C.; Ellington, A. D., Diagnostic Applications of Nucleic Acid Circuits. *Accounts of Chemical Research* **2014**, *47* (6), 1825-1835.
139. Lilja, H.; Ulmert, D.; Vickers, A. J., Prostate-specific antigen and prostate cancer: prediction, detection and monitoring. *Nature Reviews Cancer* **2008**, *8*, 268.

140. Green, L. S.; Jellinek, D.; Jenison, R.; Östman, A.; Heldin, C.-H.; Janjic, N., Inhibitory DNA Ligands to Platelet-Derived Growth Factor B-Chain. *Biochemistry* **1996**, *35* (45), 14413-14424.
141. Floege, J.; Ostendorf, T.; Janssen, U.; Burg, M.; Radeke, H. H.; Vargese, C.; Gill, S. C.; Green, L. S.; Janjic, N., Novel Approach to Specific Growth Factor Inhibition in Vivo: Antagonism of Platelet-Derived Growth Factor in Glomerulonephritis by Aptamers. *The American Journal of Pathology* **1999**, *154* (1), 169-179.
142. Zhang, H.; Li, X.-F.; Le, X. C., Differentiation and Detection of PDGF Isomers and Their Receptors by Tunable Aptamer Capillary Electrophoresis. *Analytical Chemistry* **2009**, *81* (18), 7795-7800.
143. Dirks, R. M.; Pierce, N. A., Triggered amplification by hybridization chain reaction. *Proceedings of the National Academy of Sciences of the United States of America* **2004**, *101* (43), 15275-15278.
144. Li, B.; Ellington, A. D.; Chen, X., Rational, modular adaptation of enzyme-free DNA circuits to multiple detection methods. *Nucleic Acids Research* **2011**, *39* (16), e110-e110.
145. Wang, C.; Bae, J. H.; Zhang, D. Y., Native characterization of nucleic acid motif thermodynamics via non-covalent catalysis. *Nature Communications* **2016**, *7*, 10319.
146. Zhang, D. Y.; Turberfield, A. J.; Yurke, B.; Winfree, E., Engineering Entropy-Driven Reactions and Networks Catalyzed by DNA. *Science* **2007**, *318* (5853),

1121-1125.

147. Wagner, V.; Dullaart, A.; Bock, A.-K.; Zweck, A., The emerging nanomedicine landscape. *Nature biotechnology* **2006**, *24* (10), 1211.
148. Bertrand, N.; Wu, J.; Xu, X.; Kamaly, N.; Farokhzad, O. C., Cancer nanotechnology: The impact of passive and active targeting in the era of modern cancer biology. *Advanced Drug Delivery Reviews* **2014**, *66*, 2-25.
149. Bath, J.; Green, S. J.; Allen, K. E.; Turberfield, A. J., Mechanism for a Directional, Processive, and Reversible DNA Motor. *Small* **2009**, *5* (13), 1513-1516.
150. Bath, J.; Green, S. J.; Turberfield, A. J., A Free-Running DNA Motor Powered by a Nicking Enzyme. *Angewandte Chemie* **2005**, *117* (28), 4432-4435.
151. Wickham, S. F. J.; Bath, J.; Katsuda, Y.; Endo, M.; Hidaka, K.; Sugiyama, H.; Turberfield, A. J., A DNA-based molecular motor that can navigate a network of tracks. *Nature Nanotechnology* **2012**, *7*, 169.
152. Hess, H., Toward Devices Powered by Biomolecular Motors. *Science* **2006**, *312* (5775), 860-861.
153. Venkataraman, S.; Dirks, R. M.; Rothmund, P. W. K.; Winfree, E.; Pierce, N. A., An autonomous polymerization motor powered by DNA hybridization. *Nature Nanotechnology* **2007**, *2*, 490.
154. Liber, M.; Tomov, T. E.; Tsukanov, R.; Berger, Y.; Nir, E., A Bipedal DNA Motor that Travels Back and Forth between Two DNA Origami Tiles. *Small* **2015**, *11* (5),

568-575.

155. Tian, Y.; He, Y.; Chen, Y.; Yin, P.; Mao, C., A DNzyme That Walks Processively and Autonomously along a One-Dimensional Track. *Angewandte Chemie* **2005**, *117* (28), 4429-4432.
156. Yin, P.; Yan, H.; Daniell, X. G.; Turberfield, A. J.; Reif, J. H., A Unidirectional DNA Walker That Moves Autonomously along a Track. *Angewandte Chemie* **2004**, *116* (37), 5014-5019.
157. Muscat, R. A.; Bath, J.; Turberfield, A. J., Small Molecule Signals that Direct the Route of a Molecular Cargo. *Small* **2012**, *8* (23), 3593-3597.
158. Sherman, W. B.; Seeman, N. C., A Precisely Controlled DNA Biped Walking Device. *Nano Letters* **2004**, *4* (7), 1203-1207.
159. Wang, F.; Liu, X.; Willner, I., DNA Switches: From Principles to Applications. *Angewandte Chemie International Edition* **2015**, *54* (4), 1098-1129.
160. Yang, Y.; Liu, G.; Liu, H.; Li, D.; Fan, C.; Liu, D., An Electrochemically Actuated Reversible DNA Switch. *Nano Letters* **2010**, *10* (4), 1393-1397.
161. Liedl, T.; Olapinski, M.; Simmel, F. C., A Surface-Bound DNA Switch Driven by a Chemical Oscillator. *Angewandte Chemie International Edition* **2006**, *45* (30), 5007-5010.
162. Zhang, Y.; Tang, Z.; Wang, J.; Wu, H.; Maham, A.; Lin, Y., Hairpin DNA Switch for Ultrasensitive Spectrophotometric Detection of DNA Hybridization Based on

- Gold Nanoparticles and Enzyme Signal Amplification. *Analytical Chemistry* **2010**, 82 (15), 6440-6446.
163. Yurke, B.; Turberfield, A. J.; Mills Jr, A. P.; Simmel, F. C.; Neumann, J. L., A DNA-fuelled molecular machine made of DNA. *Nature* **2000**, 406, 605.
164. Lund, K.; Manzo, A. J.; Dabby, N.; Michelotti, N.; Johnson-Buck, A.; Nangreave, J.; Taylor, S.; Pei, R.; Stojanovic, M. N.; Walter, N. G.; Winfree, E.; Yan, H., Molecular robots guided by prescriptive landscapes. *Nature* **2010**, 465, 206.
165. Amir, Y.; Ben-Ishay, E.; Levner, D.; Ittah, S.; Abu-Horowitz, A.; Bachelet, I., Universal computing by DNA origami robots in a living animal. *Nature Nanotechnology* **2014**, 9, 353.
166. Wang, Z.-G.; Elbaz, J.; Willner, I., DNA Machines: Bipedal Walker and Stepper. *Nano Letters* **2011**, 11 (1), 304-309.
167. Song, C.; Wang, Z.-G.; Ding, B., Smart Nanomachines Based on DNA Self-Assembly. *Small* **2013**, 9 (14), 2382-2392.
168. Daniel, M.-C.; Astruc, D., Gold nanoparticles: assembly, supramolecular chemistry, quantum-size-related properties, and applications toward biology, catalysis, and nanotechnology. *Chemical reviews* **2004**, 104 (1), 293-346.
169. Li, F.; Lin, Y.; Lau, A.; Tang, Y.; Chen, J.; Le, X. C., Binding-Induced Molecular Amplifier as a Universal Detection Platform for Biomolecules and Biomolecular Interaction. *Analytical Chemistry* **2018**, 90 (14), 8651-8657.

170. Storhoff, J. J.; Elghanian, R.; Mirkin, C. A.; Letsinger, R. L., Sequence-Dependent Stability of DNA-Modified Gold Nanoparticles. *Langmuir* **2002**, *18* (17), 6666-6670.
171. Chilkoti, A.; Stayton, P. S., Molecular Origins of the Slow Streptavidin-Biotin Dissociation Kinetics. *Journal of the American Chemical Society* **1995**, *117* (43), 10622-10628.
172. Macaya, R. F.; Schultze, P.; Smith, F. W.; Roe, J. A.; Feigon, J., Thrombin-binding DNA aptamer forms a unimolecular quadruplex structure in solution. *Proceedings of the National Academy of Sciences* **1993**, *90* (8), 3745-3749.
173. Russo Krauss, I.; Merlino, A.; Randazzo, A.; Novellino, E.; Mazzarella, L.; Sica, F., High-resolution structures of two complexes between thrombin and thrombin-binding aptamer shed light on the role of cations in the aptamer inhibitory activity. *Nucleic Acids Research* **2012**, *40* (16), 8119-8128.
174. Popovtzer, R.; Agrawal, A.; Kotov, N. A.; Popovtzer, A.; Balter, J.; Carey, T. E.; Kopelman, R., Targeted Gold Nanoparticles enable Molecular CT Imaging of Cancer. *Nano letters* **2008**, *8* (12), 4593-4596.
175. Khlebtsov, N.; Dykman, L., Biodistribution and toxicity of engineered gold nanoparticles: a review of in vitro and in vivo studies. *Chemical Society Reviews* **2011**, *40* (3), 1647-1671.
176. Lasagna-Reeves, C.; Gonzalez-Romero, D.; Barria, M. A.; Olmedo, I.; Clos, A.; Sadagopa Ramanujam, V. M.; Urayama, A.; Vergara, L.; Kogan, M. J.; Soto, C.,

Bioaccumulation and toxicity of gold nanoparticles after repeated administration in mice. *Biochemical and Biophysical Research Communications* **2010**, 393 (4), 649-655.

Appendix A: List of publications from the PhD program

1. Li, F.; **Lin, Y.**; Lau, A.; Tang, Y.; Chen, J.; Le, X. C., Binding-Induced Molecular Amplifier as a Universal Detection Platform for Biomolecules and Biomolecular Interaction. *Analytical Chemistry* **2018**, *90* (14), 8651-8657.
2. Tang, Y.; **Lin, Y.**; Yang, X.; Wang, Z.; Le, X. C.; Li, F., Universal Strategy To Engineer Catalytic DNA Hairpin Assemblies for Protein Analysis. *Analytical Chemistry* **2015**, *87* (16), 8063-8066.
3. Deng, B.*; **Lin, Y.***; Wang, C.; Li, F.; Wang, Z.; Zhang, H.; Li, X.-F.; Le, X. C., Aptamer binding assays for proteins: The thrombin example—A review. *Analytica Chimica Acta* **2014**, *837*, 1-15. (*These authors contributed equally to the publication)
4. Paliwoda, R. E.; Li, F.; Reid, M. S.; **Lin, Y.**; Le, X. C., Sequential Strand Displacement Beacon for Detection of DNA Coverage on Functionalized Gold Nanoparticles. *Analytical Chemistry* **2014**, *86* (12), 6138-6143.
5. Li, F.; **Lin, Y.**; Le, X. C., Binding-Induced Formation of DNA Three-Way Junctions and Its Application to Protein Detection and DNA Strand Displacement. *Analytical Chemistry* **2013**, *85* (22), 10835-10841